Investigation of lung mechanics using CT scan analysis, a mathematical model and the static pressure volume curve

By Mads Holm Andersen
Health Science and Technology
Aalborg University
September 2007 - June 2008

Aalborg University

Department of Health Science and Technology, Fredrik Bajers Vej 7D, 9220 Aalborg Ø

Title:
    Investigation of lung mechanics using CT scan analysis, a mathematical model and the static pressure volume curve.

Theme:
    Biomedical Engineering and Informatics

Group:
    1087g

Group members:
    Mads Holm Andersen

Supervisor:
    Dan Stieper Karbing

Numbers of copies: 6

Numbers of pages: 114

Project period:
    September 2nd- June 2nd, 2008

Abstract:

Patients with Acute Lung Injury and Acute Respiratory Distress Syndrome depend on ventilator therapy to survive. Finding correct ventilator settings for these patients is complicated as a balance must be obtained between ensuring sufficient gas exchange whilst preventing Ventilator Induced Lung Injury. The static PV curve and CT scanning can offer information about the evolution of the disease. However, the shape of the PV curve is poorly understood and CT scanning cannot be performed repeatedly under clinical conditions to gain a better understanding. Several approaches have been taken to model the static PV curve. Amongst them a model based on alveoli compartments that is able to simulate the distribution of open, collapsed and overdistended alveoli when fitted to PV data. The purpose of this project is to investigate the relationship between the alveolar states extracted from CT scans and simulated alveolar states from the model. Both CT scans and PV curves are obtained from different pigs, with and without OA damaged lungs and with different applied PEEP levels. An image segmentation algorithm which extracts information regarding the alveolar states from CT scans is developed and presented. Results show that there is no relationship between the optimal pressure range identified by the model and extracted from the CT scans. Results furthermore show that there is no relationship between the progression of collapsed alveoli along the entire static PV curve identified by the model and extracted from the CT scans. It has furthermore been shown that not all of the obtained values of the parameters used to obtain the best fit of the model to PV data were within the normal physiological range. It has also been shown that the model has a lack of ability to simulate the true shape of the static PV curve which may be considered as a major limitation. It can be concluded that there is no relationship between the simulated alveolar states and the extracted alveolar states from the algorithm.

Preface

This report is the documentation of the 9th and 10th semester project carried out by Mads Holm Andersen during the autumn and spring 2007/2008 at Department of Health Science and Technology at Aalborg University. The theme of the semesters is *Biomedical Engineering and Informatics*. The report is written in the period from 2nd September to 2nd of June, 2008.

The project primarily aims at fellow students and others who share interests. The chosen project proposal deals with investigation of lung mechanics with CT scan analysis, the static respiratory pressure volume curve and a mathematical model. It is anticipated that the reader has a fundamental knowledge of the respiratory system.

The author would like to thank the following persons:

Gaetano Perchiazzi, MD, PhD, Assistant Professor at Intensive Care Medicine Department of Emergency and Organ Transplant University of Bari, for providing the author with data materials.

Charlotte Allerød, MD, Anesthesiologist, 1st department, Anaestesia and Intensive Care, Region North jutland, Aalborg Hospital, Aarhus University, for assistance during the test of the image segmentation algorithm.

Supervisor of this project, Dan Stieper Karbing, M.Sc.

Reading instructions

The report is divided into the following seven parts and is intended to be read chronologically:

- Introduction and Analysis.

- Materials.

- Image Analysis and Processing.

- Modelling the alveolar states based on static PV curves.

- Relationship between CT scans and the model.

- Closure.

- Appendix.

Citations are noted according to Harvard style and the list of the citations is located at the end of the report starting at page 102. The author's name and year of publishing are noted in squared brackets for example [Lumb, 2005]. In cases of publications with more than one author the citation is written as follows [Amato et al., 1998b].

When a citation is written after a full stop then the citation refers to the entire section. If the citation is written before a full stop then the citation is only valid for the respective sentence.

Figures, tables etc. are numerated by two numbers; the first states the current chapter and the second is forthcoming for the chapter.

Mads Holm Andersen

Contents

Part I

Introduction and Analysis

Chapter 1

Background

Intensive care therapy comprises continuous and sufficient observation, diagnosis, treatment and caring of patients with potential reversible failure of one or more organ systems with the aim of effectively maintain, stabilize and re-establish normal organ function. Almost all patients admitted to intensive care units suffer from respiratory failure due to a variety of causes. For instance disease in and trauma to the airways, heart attack, neurological diseases, trauma to and paralysis of the respiratory musculature. The patients with respiratory failure need mechanical ventilatory support, applied either by way of an endotracheal tube or noninvasively. The primary goals of mechanical ventilation are to secure sufficient oxygenation, unload the respiratory muscles and buy time for other therapies to treat the causes of respiratory failure. Normally, finding the most appropriate settings of the ventilatior is a simple task, however in especially two specific patientgroups, Acute Lung Injury (ALI) and Acute Respiratory Distress Syndrome (ARDS) finding these settings is more complex. Lung regions of these patients are often collapsed or overdistended and are not participating in gas exchange. In order to improve gas exchange, prevent further overdistension and recruit the collapsed alveoli, correct pressure and volume settings of the ventilator must be selected. Unappropriate settings of the ventilator which is either too low or high pressure and volume as well as repetitive opening and closing of the alveoli may at worst lead to Ventilator Induced Lung Injury (VILI). The main concern regarding ventilator treatment of these patient groups are therefore to find an accurate balance between appropriate gas exchange and preventing VILI. Common ways of obtaining information regarding how to find the most appropriate ventilator settings is by evaluating the pressure volume relationship of the lungs and Computed Tomography (CT) scans of the chest. In the following chapter problems regarding how to find the appropriate ventilator settings in ALI/ARDS patients will be introduced. In order to do this ALI/ARDS will be described in order to give a more general understanding of the pathophysiology of the syndrome. Secondly, mechanical ventilation, hypoxemia and VILI will be described. In this context, pressure volume curves and CT scans which are the two primary tools used in research to understand mechanical properties of the respiratory system will be described. Finally the problems associated with, and the controversy that exists regarding optimization of the ventilator settings will be discussed which at the end of the chapter will lead to the initial problem statement for this report.

1.1 ALI and ARDS

Acute Lung Injury (ALI) is a distinct form of acute respiratory failure characterized by diffuse pulmonary infiltrates, progressive hypoxemia, reduced lung compliance. Acute Respiratory Distress Syndrome (ARDS) is an acute, severe injury to the lungs. and is the most severe form of ALI. Both ALI and ARDS may arise due to a variety of causes. [Harman and Walia, 2006] In

most cases a person who develops ARDS is already hospitalized being treated for other medical problems. Some of the causes that can lead to ARDS are: sepsis, severe bleeding that requires blood transfusions, severe pneumonia, breathing in smoke or harmful gases and fumes, injury to the chest from trauma that causes bruising of the lungs, nearly drowning and drug overdoses [National-Heart-Lung-Institute, 2007; Lumb, 2005].

ALI/ARDS continues to cause substantial morbidity and mortality in the USA and worldwide [Heart and Lung Institute, 1972; Villar and Slutsky, 1989]. The National Heart and Lung Institute Task Force on Respiratory Distress Syndromes estimated the incidence of ARDS in the USA at 150.000 new cases per year [Heart and Lung Institute, 1972]. In 1989 Villar et al. calculated the incidence of ARDS in a limited British population to 4.5 per 100.000 people [Villar and Slutsky, 1989]. A survey of both USA and European respiratory ICUs determined that the survival rate was 33% (mortality 67%) over a 1-year period. Survival was higher in patients with acute respiratory failure secondary to pneumonia (63%) or postshock lung injury (67%), compared with respiratory failure resulting from sepsis (46%) [Evans et al., 1988].

The definition of ALI/ARDS was clarified by a 1994 American European Consensus Conference [Bernard et al., 1994] and was characterized by the following definition:

- Acute onset of respiratory failure

- Bilateral diffuse pulmonary infiltrates on chest radiograph

- 200 mmHg < (arterial oxygen tension / inspired oxygen fraction) < 300 mmHg, irrespective of the level of Positive End Expiratory Pressure (ALI)

- (Arterial oxygen tension / inspired oxygen fraction) < 200 mmHg, irrespective of the level of Positive End Expiratory Pressure (ARDS)

- No clinical evidence of elevated left atrial pressure or pulmonary capillary wedge pressure <18 mmHg

The acute onset of respiratory failure often occurs within 24 to 48 hours of the initial injury or illness. The duration and intensity of the condition can vary considerably from patient to patient. At the onset of ARDS, lung injury may first appear in one lung, but then quickly spreads to affect most of both lungs. Damaged lungs as seen in ALI/ARDS patients are often characterized as heterogeneous distributed lungs, which means that three different types of alveoli can be distinguished: [Funk et al., 2004]

- **Open alveoli susceptible to overdistension.** These alveoli are open throughout the respiratory cycle and are predominantly located in the non-dependent lung areas.

- **Open alveoli susceptible to collapse.** These alveoli are closed, at least at end-expiration. They can be recruited by applying a positive pressure but are susceptible to atelectrauma.

- **Collapsed alveoli.** These alveoli can be filled with cellular material and are difficult if not impossible to recruit even with very high pressure. Theese alveoli are often termed consolidated tissue.

Figure 1.1 illustrates how healthier lung regions versus heterogeneous lungs as seen in ALI/ARDS are effected by applying a positive pressure. [MacIntyre, 2000] When alveoli are damaged, some collapse or fills with fluid which causes the affected alveoli of the lung to become stiff and difficult
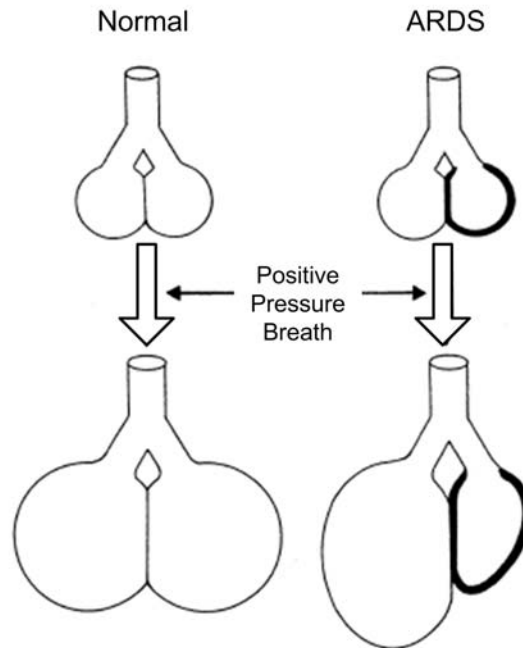
Figure 1.1: *The figure illustrates how healthier lung regions vs heterogeneous lungs are effected by positive pressure. By applying a positive pressure in the lungs illustrated in the left part of the figure all lung areas are effected equally. This is not the case in the heterogeneous distributed lungs illustrated in the right part of the figure. The positive pressure does not effect the lung regions equally and thereby leads to an overdistension of some of the lung regions. The figure is modified from [MacIntyre, 2000].*

to open. However, not all alveoli are collapsed which means that a high pressure applied in order to recruit the collapsed alveoli may overdistend the remaining alveoli. Once the alveoli collapses, gas exchange ceases, and the body becomes starved of O_2. Therefore patients with ARDS experience severe shortness of breath and often require mechanical ventilation. Because of hypoxemia the mechanical ventilation treatment of ARDS reguires high inspired O_2 concentrations to maintain adequate tissue oxygenation and life. O_2 toxicity may unfurtunately promote further lung injury. Generally, O_2 concentrations greater than 65% for prolonged periods result in diffuse alveolar damage, hyaline membrane formation and eventually fibrosis. [Bernard et al., 1994; Harman and Walia, 2006]

As mentioned ARDS often occurs quickly after the initial injury or illness. The ability to identify patients with these potentially lethal syndromes is therefore critically important. The first step in identifying these patients is to obtain a chest X-ray and an arterial blood gas analysis.

1.2   X-rays and CT scans

Chest X-rays is normally obtained in ALI/ARDS patients to allow formal diagnosis by inference using the aforementioned criteria. Figure 1.2 illustrates the presence and the progression of ARDS in chest X-rays from a case study with a 41 year old caucasian female who went to the emergency room for dehydration, coughing and fever.

Figure 1.2A illustrates day one examination which demonstrated a large right upper lobe infiltrate. The right lower lobe and left lung remain clear and heart size and pulmonary vasculature
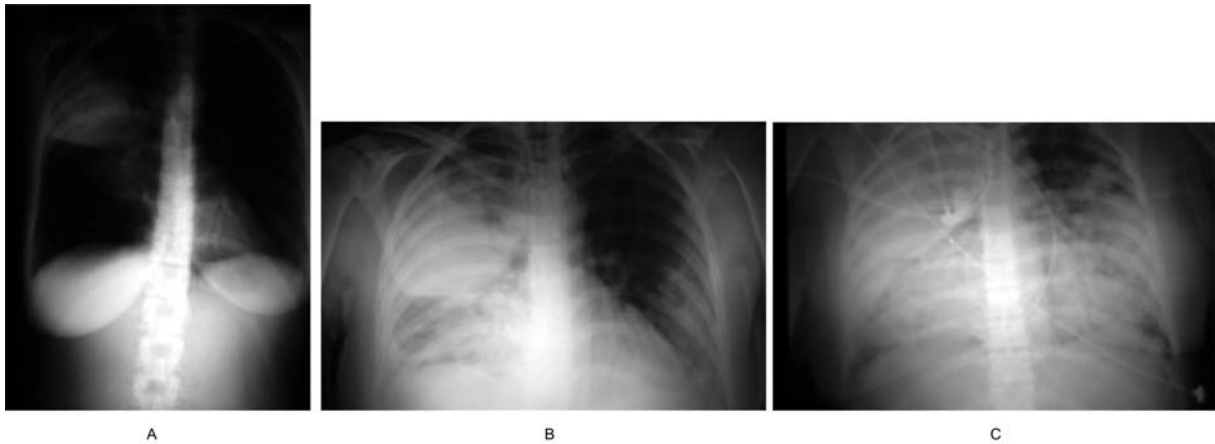
Figure 1.2: *The figure illustrates the progression of ARDS in a chest X-ray from a case study with a 41 year old female/Caucasion who went to the emergency room for dehydration, cough and fever. See text for further description. [The ARDS foundation, 2007]*

was within normal limits. Inspection of the chest X-ray indicates pneumonia and the patient was admitted to the hospital.

At day two examination, figure 1.2B, there was still dense infiltrate involving the right upper lobe particularly the anterior and posterior segments with less damage of the apical segment. In the interval, however, there has been development of a parenchymal infiltrate at the right base most likely involving right middle and lower loves with evidence of bilateral diffuse infiltrates. As mentioned in the definition of ALI/ARDS bilateral diffuse infiltrates is one of the character trait of the syndrome.

At day three, figure 1.2C, there is a worsening in the right lung showing opacity. The left lung showed new multifocal infiltrates and increasing effusion as well. [The ARDS foundation, 2007]

As visualized in the example with the case study chest X-ray can provide detailed information concerning the progress of the disease. In most Intensive Care Units (ICU) obtaining a chest X-ray each day is the current practice. The chest X-ray remains the most commonly used diagnostic tool for following the evolution of lung diseases. [Pelosi et al., 1999a]

Several recent studies consider the Computed Tomography scan (CT) to be part of the routine management of ALI/ARDS, and it has become a very popular tool. [Hall et al., 1998; Vieira et al., 1999a] CT scans can offer clinicians detailed information on ARDS patients such as morphological descriptions, recognizing specific lesions, quantitative analysis of lung tissue, and the evolution of the disease. [Puybasset et al., 1998; Payán et al., 2001]. The superimposition of differing pathologies, such as pleural effusion, pneumothorax, and lung consolidation, can be undetectable in conventional X-rays. [Pasenti et al., 2001]. As mentioned previously ALI/ARDS is normally a heterogeneous distributed lung disease. Compared to conventionel X-rays the CT scans can provide a more detailed information regarding the heterogeneous distributed issue which can be seen in figure 1.3. The accurate and detailed images provided by CT scanners have encouraged clincans to use CT more frequently to improve the description of the pathological process [Tagliabue et al., 1998].

Several anatomic descriptors have varied greatly in the past years so it is worthwhile to precisely define the CT terminology. [Austin et al., 1996]

- Ground-glass opacification: A hazy increase in lung attenuation, meaning more white than black with preservation of bronchial and vascular margins

- Consolidation: A homogeneous increase in lung attenuation that obscures bronchovascular margins in which an airbronchogram may be present

- Reticular pattern: Innumerable interlacing line shadows that may be fine, intermediate, or coarse.

During the early phases of ALI/ARDS CT scans can reveal ground glass opacities and heterogeneous consolidation distributed peripherally and mainly in the dependent portions of the lung, but it can also include patchy infiltrates with lung areas of normal appearance. [Goodman, 2000]. Figure 1.3 illustrates three different examples of the aforementioned anatomic CT descriptors.
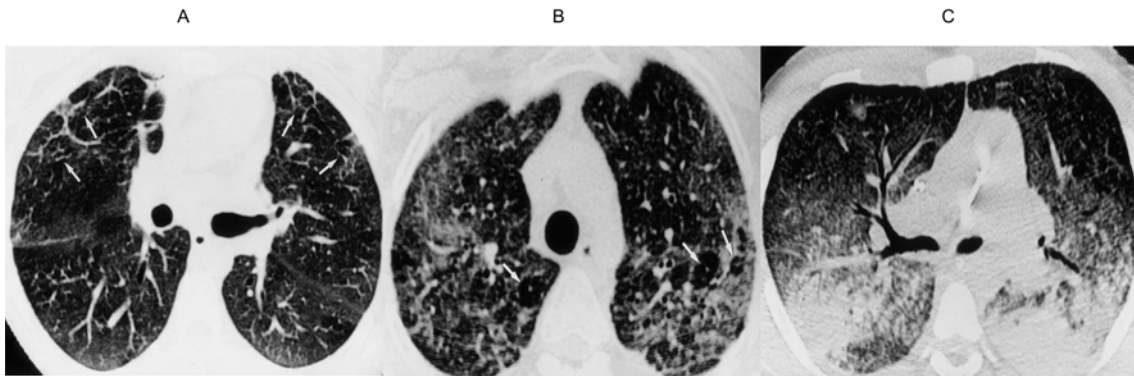
Figure 1.3: *The figure illustrates ARDS in 3 different CT patients. As above mentioned in the definition of CT terminology all three definitions are visualized. Figure A illustrates an example of reticular patterns and irregular interfaces which indicates the presence of ARDS. Figure B shows a marked increase in ground glass opacity. Figure C illustrates consolidation with air bronchograms in the posterior dependent areas of the lung. [Desai et al., 1999]*

In spite of the powerful and useful tool, CT scans do however carry some disadvantages. They are not always available, relatively costly and they expose patients to a higher amount of radiation than standard chest Xray do. [Pasenti et al., 2001]

1.3 Mechanical ventilation

One of the most important parts of treating ALI/ARDS patients is mechanical ventilation which is to secure sufficient oxygenation, unload the respiratory muscles and to protect the airways. However, mechanical ventilation may constitute a risk factor for both the development or the worsening of ALI/ARDS. Thus, a balance between avoiding Ventilator Induced Lung Injury (VILI) and achieving sufficient oxygenation must be obtained. In order to understand this balance one must have knowledge of the mechanism of both hypoxemia and VILI.

Hypoxemia

Hypoxemia is an abnormal deficiency in the concentration of oxygen in arterial blood [Martini, 2004]. One of the most common causes of hypoxemia is ventilation perfusion inequality, which means that ventilation and blood flow are mismatched in various regions of the lung, with the result that all gas transfer becomes inefficient [West, 2003]. In an ideal lung the perfusion ventilation ratio is equal to 1, which means that the amount of air reaching the alveolus divided with the amount of blood reaching the alveolus is equal to 1. However, all lungs have some ventilation perfusion inequality. In the normal upright lung, this takes the form of a regional pattern, with the ventilation perfusion ratio decreasing from apex to base. This means that the lower regions receive more perfusion compared to ventilation than the higher regions. This distribution is significant affected in ALI/ARDS patients, due to the heterogenous character of the lungs. [Martini, 2004; Lumb, 2005]

Five different ventilation perfusion mismatch can be defined: [Lumb, 2005]

- Ventilation/Perfusion = 0, No ventilation reaches perfused alveoli which means atelectic and consolidated lung regions.

- Ventilation/Perfusion = 1. Match between perfusion and ventilation, which means healthy ventilated alveoli.

- Ventilation/Perfusion < 1. Increased perfusion, but with healty ventilation.

- Ventilation/Perfusion > 1. Increased ventilation, but with limited perfusion.

- Ventilation/Perfusion = ∞. Increased ventilation but with allmost none perfusion, which results in alveolar overdistension.

These mismatches of ventilation perfusion ratio often occur in ALI/ARDS patients because of the heterogenous character of the lungs. [Lumb, 2005] If the ventilation perfusion mismatch causes atelectic and consolidated lung regions a high positive pressure may be applied in order to recruit the collapsed lung area. However, excessive pressure may cause Ventilator Induced Lung Injury which at the same time must be avoided.

Ventilator Induced Lung Injury

Ventilator Induced Lung Injury (VILI) is a term used to describe injury to the lungs caused by mechanical ventilation. Under normal circumstances high pressure and high volume mechanical ventilation may not harm patients with normal lungs and is therefore rarely a problem in clinical practice. [Lumb, 2005] This is not the case in heterogenous lungs as seen in ALI/ARDS patients. In these patients the high pressure and high volume mechanical ventilation may potentially both generate, perpetuate or worsen lesions of the alveolar-capillary membrane. Much attention has been addressed this issue in the past years. [Webb and Tierney, 1974; Dreyfuss et al., 1985, 1988; Sandhar et al., 1988; Hickling, 1997; Dreyfuss and Saumon, 1998; Slutsky, 1999]

VILI is often identified in four different types: [Dreyfuss et al., 1988; Slutsky, 1999; Lumb, 2005; Santos et al., 2005; Rotta, 2006]

- **Barotrauma** is a physical rupture and damage to body tissues caused by extreme pressures. The rupture of alveoli caused by barotrauma may lead to leakage of air into the interstitiel space. The manifestations of this injury includes pneumothorax, subcutaneous emphysema, pneumomediastinum, tension lung, cysts and hyperinflation.

- **Volutrauma** is similar to barotrauma and is characterized by physical rupture and damage to body tissues. However, the cause is high lung volume. This form of VILI is most commonly manifested as interstitial or alveolar oedema.

- **Atelectrauma** is an injury associated with repeated opening and closing (recruitment and collapse) of collapsed alveoli during mechanical ventilation. Atelectrauma is commonly caused by ventilation at low lung volumes and is manifested as pulmonary oedema and atelectasis.

- **Biotrauma** is an increase in pulmonary and systemic inflammatory mediators. Biotrauma is a possible cause of baro-, volu- and atelectrauma. This is the major cause of death in ARDS patients since spreading of these inflammatory mediators may eventually lead to multi organ failure.

To open collapsed alveoli securing gas exchange and avoiding atelectrauma high volume and pressure may be necesary. However high volume and pressure may cause overdistension which may result in barotrauma, volutrauma and biotrauma. [Slutsky, 1999; MacIntyre, 2000; Piacentini et al., 2003; Lumb, 2005; Rotta, 2006] In clinical practice much attention has to be paid to avoid VILI. Thus, accurate and optimal settings of the ventilator is very important.

1.4   Optimization of ventilator settings

Identification of a ventilator setting that in a particular patient is both optimal with respect to desired physiological effects and minimizing the risk of VILI is very difficult. Several studies has investigated how the most appropriate pressure/volume ventilator settings should be in order to fit the need of ARDS/ALI patients [Matamis et al., 1984b; Amato et al., 1998b; MacIntyre, 2000]. One of the most important goal is obtaining sufficient gas exchange in order to secure properly oxygenation. This implies that the "full" lung should contribute to the gas exchange which means that all collapsed alveoli should be recruited. In order to recruit the collapsed alveoli a Positive End Expiratory Pressure (PEEP) may be applied. However, finding appropriate settings of PEEP is often considered very complex because of the heterogeneous distributed lungs.

Postive End Expiratory Pressure

Numerous studies has been trying to identify the optimal PEEP level when adjusting the ventilator. This issue is still very controversial and under heavy debate. In the past years several studies have tried to find an appropriate PEEP level which have given rise to numerous terms such as: [Carroll et al., 1988; Peruzzi et al., 1997]

- *Optimal* PEEP level which is related to the lowest physiological shunt fraction.

- *Best* PEEP level which is related to optimal lung compliance.

- *Preferred* PEEP level which is related to best oxygen delivery.

- *Least* PEEP level which is related to "acceptable" values of P_aO_2, F_iO_2 and cardiac output.

The numerous terms described in the litterature indicates that there is no consensus on what the most appropriate PEEP setting is. In clinical practice it is commonly known that a PEEP value as low as 5 cmH$_2$O is beneficial, but PEEP as high as 20 cmH$_2$O or more are sometimes used in order to make considerable improvement in the arterial PO$_2$ [Bond and Froese, 1993; Bond et al., 1994; Cakar et al., 2000; Grasso et al., 2002]. Another common approach in clinical

practice is the use of recruitment manoeuvres. Recruitment manoeuvres have been repeatedly proposed for alveolar recruitment and lung protection [Bond and Froese, 1993; Bond et al., 1994; Cakar et al., 2000; Grasso et al., 2002; Hess and Bigatello, 2002]. Many different methods of recruitment manoeuvres have been proposed in the literature. In 2004, Piacentini and coworkers identified the most recent proposed recruitment manoeuvre which can be seen in table 1.1 [Piacentini et al., 2003].

One of the mentioned recruitment manoevres in table 1.1 were proposed by Amato et al. who were the first to use a lung recruitment maneuver in a randomized controlled trial. They recruited the lung with continuous positive airway pressure of 40 cm H_2O for 30 to 40 s, followed by an appropriate PEEP setting where alveoli were kept open [Amato et al., 1998b]. As to my knowledgde, the study by Amato and coworkers is the only study showing an improving in mortality. Since the publication of the study from Amato and coworkers the application of recruitment manoevres in patients with ALI/ARDS has gained acceptance among clinicians. However, the numerous studies listed in table 1.1 and the approaches that has been trying to identify the optimal PEEP level indicates that controvery exists in the litterature of how to use recruitment manoevres and how to find the ideal PEEP value. These controversy indicates a lack of understanding of the underlying physiology related to the effect of PEEP and recruitment manoevres. One very important step in clinical practice regarding appropriate PEEP setting is obtaining information of the relationship between flows, pressures and volumes. This information can be gained from the static or dynamic Pressure Volume (PV) curve of the lungs.

Methods	Study	References
Continuous positive airway pressure at 30 to 60 cmH$_2$O for 15 to 60 seconds	*Saline lavage, oleic acid, and pneumonia in animals*	*[Bond et al., 1994; Rimensberger et al., 1999; Kloot et al., 2000; Takeuchi et al., 2002; Cakar et al., 2000; Fujino et al., 2001; Cakar et al., 2002]*
Pressure controlled mode: peak inspiratory pressure at 60 cmH$_2$O and end-expiratory pressure at 40 cmH$_2$O for 2 min	*Saline lavage in animals*	*[Takeuchi et al., 2002; Fujino et al., 2001]*
Volume controlled mode: 20 breaths at tidal volume of 20 ml/kg	*Anesthetized healthy animals*	*[Lu et al., 2000]*
Continuous positive airway pressure at 30 to 45 cmH$_2$O for 15 to 20 seconds	*Anesthetized healthy patients*	*[Rothen et al., 1995; Dyhr et al., 2002]*
Pressure controlled mode: peak inspiratory pressure at 30 to 40 cmH$_2$O and end-expiratory pressure at 10 to 20 cmH$_2$O for 1 min	*Anesthetized healthy patients*	*[Tusman et al., 1999, 2002; Claxton et al., 2003]*
Sighs with a tidal volume to reach 45 cmH$_2$O plateau pressure	*ARDS patients*	*[Pelosi et al., 1999b; Broccard et al., 2000]*

Methods	Study	References
Continuous positive airway pressure at 30 to 40 cmH$_2$O for 30 to 40 seconds	*ALI/ARDS patients*	*[Amato et al., 1998b; Lapinsky et al., 1999; Richard et al., 2001; Grasso et al., 2002; Patroniti et al., 2002]*
Extended sigh with a tidal volume to reach 40 cmH$_2$O and end-expiratory pressure at 35 cmH$_2$O for 1 min	*ARDS patients*	*[Lim et al., 2003]*
Pressure controlled mode: peak inspiratory pressure at 40 to 60 cmH$_2$O and end-expiratory pressure at 10 to 30 cmH$_2$O for 30 to 120 seconds	*ARDS/brain injury patients*	*[Villagrá et al., 2002; Bein et al., 2002; Johannigman et al., 2003]*
Pressure support mode: peak inspiratory pressure at 40 cmH$_2$O and end-expiratory pressure for 30 seconds	*ALI/ARDS patients*	*[Maggiore et al., 2003a]*

Table 1.1: The table lists different methods used in experimental and human studies to perform recruitment maneuvers. [Piacentini et al., 2003]

Pressure Volume curves

The PV curve is a classical physiological method used since late 1940s to describe the mechanical properties of the respiratory system [Rahn et al., 1946]. An early study has shown the PV curve's usefulness in the diagnosis of ALI/ARDS in mechanically ventilated patients [Bone, 1976]. Later studies described the role of the PV curve as a monitoring tool in the management of ALI/ARDS [Matamis et al., 1984a]. Recently it has been shown how it can improve the survival of these patients because it has the potential to be used to guide adjustment and optimization of the mechanical ventilation settings [Amato et al., 1998b].

Dynamic and static PV curves

Two different PV curves exist: the dynamic and the static. Both dynamic and static PV curve are based on a measurement of the pressure obtained at the mouth. The dynamic PV curve is measured under dynamic conditions which means that flow is present. The dynamic measurement therefore includes the pressure contributions from airway resistance. The static PV curve is measured at static conditions (no flow, or allmost no flow = quasi static) where there is no pressure contribution from the resistive components of the respiratory system, which therefore represents the pressures in the lungs. In ALI/ARDS patients the impairment of the respiratory mechanics involves mainly the elastic component of the respiratory system. As a consequence, the measurement of respiratory PV curves should be done under static conditions in order to eliminate the resistive component. [Lu and Rouby, 2000]

Interpretation of static PV curves

The static PV curve illustrated in figure 1.4 shows two different curves, representing a healthy subject and a ARDS patient. The static PV curve can be considered as consisting of three different segments separated by two different inflection points. The first segment with a low

compliance is separated from the intermediate linear segment with a greater compliance (CLIN) by a lower inflection point (LIP). The steeper part of the curve is followed by an upper inflection point (UIP) beyond which the curve flattens again. [Maggiore et al., 2003b]
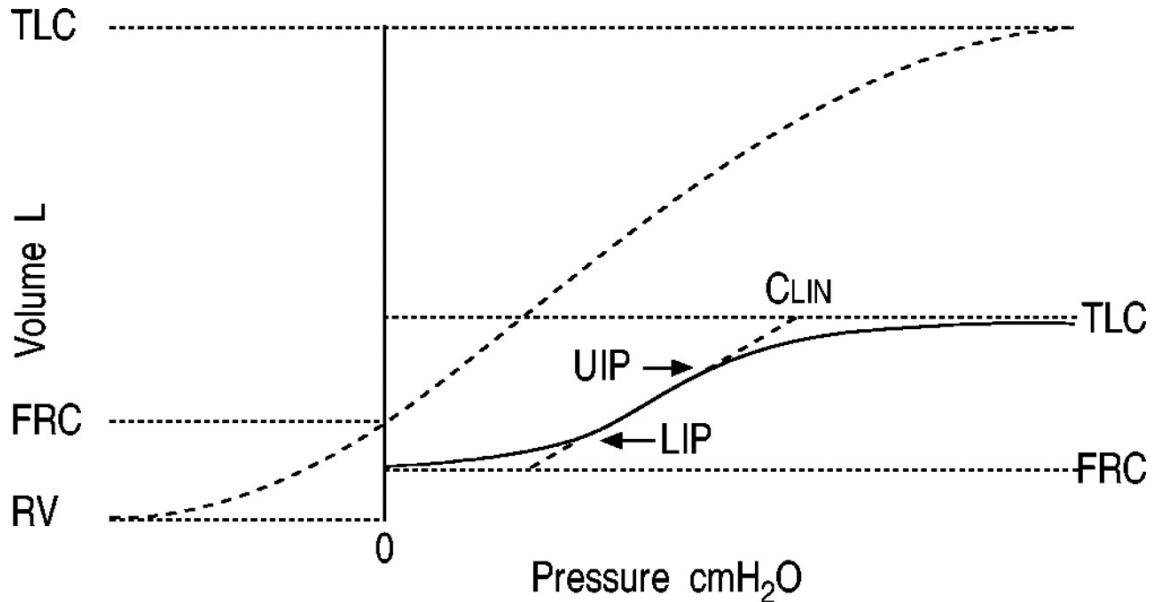

Figure 1.4: *The figure illustrates a PV curve of the respiratory system in a healthy subject (- - -) and in a patient with ARDS (-). [Maggiore et al., 2003b]*

The interpretation of the PV curve often consists of the two mentioned components: compliance and inflection points. The compliance is the change in volume per unit pressure change of the respiratory system at different volumes and pressures. The respiratory compliance therefore reflects the elastic properties of the respiratory system. A stiff lung as seen in ARDS has a low compliance. The first low compliance segment indicates that some lung compartments do not receive insufflated gas because airway closure and/or alveolar collapse prevent their inflation. Above the lower inflection point the slope of the curve, i.e., compliance, increases over a nearly linear segment. This often sudden change has been interpreted as a reopening of alveoli and as a marker of recruitment [Maggiore et al., 2003b]. A number of studies including ALI/ARDS patients, have tried to clarify the meaning of the inflection points, in the belief that this could be helpful for the ventilatory management of the syndrome. The studies suggested that the upper inflection point conceptually determines the pressure level that is not to be exceeded in order to avoid barotrauma and volutrauma due to overdistension [Gattiononi et al., 1987; Gattinoni et al., 1995; Dambrosio and Servillo, 1995]. A marked lower inflection point is often interpreted as an indication of a pressure at which many collapsed alveoli are opening at the same time. In clinical practice, the two inflection points of maximum curvature are often determined by eye from a plot of the PV curve which is a method that is not only highly subjective but also relatively imprecise [Venegas et al., 1998; Harris et al., 2000].

Measurement of static PV curve

Several methods and techniques exist for acquiring the static or quasi static PV curves, among them the supersyringe technique, the constant flow technique, the multiple occlusion technique

and the automated single inflation occlusion technique.

The supersyringe technique is normally considered to be the reference technique for measuring the static PV curve of the respiratory system in patients with acute respiratory failure [Matamis et al., 1984a; Mergoni et al., 1997]. The technique consists of connecting a supersyringe to the end of the endotracheal tube and inflating the lungs in steps of 50 to 100 ml up to 1.5 or 3.0 l starting from the Functionel Residual Volume (FRC). [Matamis et al., 1984a; Harris, 2005] The plunger of the syringe is moved in regular steps with 2 to 3 second pauses to allow for static conditions. [Harris, 2005]. The pressures and the volumes are recorded simultaneously and the PV curve is constructed from the obtained data. Normally, the inflation is stopped and deflation is performed in the same way when airway pressure reaches 40 cm H_2O. The supersyringe technique is a simple technique that allows the construction of both inflation and deflation curves. However, it also has several disadvantages: it requires additional equipment and the patient has to be disconnected from the ventilator and sedated. Furthermore, the technique is relatively time consuming [Matamis et al., 1984a; Harris, 2005].

The constant flow technique is a simple quasi static technique that can be performed by some conventional ventilators [Harris, 2005]. The quasi static technique does not eliminate, but minimizes flow and thereby the effect of respiratory resistance. The technique consists of a single inflation and deflation of the lungs at a constant flow. During inflation and deflation volumes and pressures are measured continously. Because the technique does not require disconnection from the ventilator, it can preserve some changes in volume history that are lost with the supersyringe technique. Several studies has shown that higher constant flow than 3 L/min produces a right shift of the quasi static PV curve compared to the static PV curve. But the higher constant flow gave similar slopes [Lu et al., 1999; Servillo et al., 1997].

The multiple occlusion technique consists of measurement of plateau pressures that correspond to different tidal volumes during successive end inspiratory occlusions [Harris, 2005]. The technique is performed using a mechanical ventilator equipped with facilities for end inspiratory and end expiratory occlusions. Ventilation is performed in a volume controlled mode with a constant flow. The deflation static PV curve is obtained by performing exiratory occlusions at different expiration volumes. As with the constant flow technique it is not necessary to disconnect the patient from the ventilator, and the loss of volume due to lung oxygen uptake is negligible because each measurement lasts only 3 seconds. However, the multiple occlusion technique still requires sedation and/or paralysis to prevent spontaneous breaths during the measurements. [Lu et al., 1999; Harris, 2005] The multiple occlusion technique are often impractical to use in clinical practice because they are time-consuming, requiring about 5 to 10 min for measuring one static PV curve. However, faster techniques have been developed, based on occlusions on a single long inflation and/or deflation. [Ingimarsson et al., 2001a,b; Zhao et al., 2007]

The automated single inflation occlusion technique is a computer controlled technique for obtaining the inspiratory and expiratory limbs of the static PV curve. [Ingimarsson et al., 2001a,b; Zhao et al., 2007] The technique by Zhao et al., which is relatively fast (approximately 20 seconds), uses 1 second occlusions duration in order to obtain one static PV curve. The automated single inflation occlusion technique uses a ventilator routinely used in the intensive care unit. The technique was reproducible when obtaining inspiratory and expiratory limbs of the static PV curve in pigs with healthy lungs and in lung damaged by oleic acid infusion. [Zhao et al., 2007]

1.5   Initial problem

As described in this chapter, measurement and interpretation of the static PV curve is a way of evaluating ALI/ARDS patients' respiratory status when adjusting and optimizing the ventilator settings. The static PV curve can provide information regarding how to find the optimal PEEP setting which is crucial in ALI/ARDS patients. That is how to find a "minimum" PEEP level in order to avoid atelectasis, shunt and VILI but also to "limit" PEEP in order to avoid overdistension which also can lead to VILI, alveolar dead spaces and ventilation/perfusion mismatch. It is commonly known that finding the optimal PEEP setting is complex and has led to several controversies in the litterature. In clinical practice mechanical ventilation settings, including PEEP, are often determined by trial and error using different rules due to difficulty in understanding the interaction between ventilator and the specific patients' lung mechanics. Hence, ventilator support may often be influenced by the intuition and experience of the clinical staff as seen by the wide variety of different published protocols [Amato et al., 1998a; Takeuchi et al., 2002; Funk et al., 2004]. In spite of the valuable information the static PV curve can provide regarding how to find the optimal PEEP setting it is still a common issue that there is no consensus of how the curve should be interpreted and applied. CT scans can offer clinicans detailed information about ARDS patients such as morphological descriptions, recognizing specific lesions, quantitative analysis of lung tissue, and the evolution of the disease. Several recent studies consider the CT scanning to be part of the routine management of ARDS, and it has become a very popular tool. The accurate and detailed images provided by CT scanners have encouraged clinicans to use CT more frequently to improve the description of the pathological process. CT scans are also a useful tool for measuring lung recruitment. The lung recruitment can be quantified by measuring how much nonaerated tissue becomes aerated by the application of different levels of PEEP. Alternative approaches include computing changes in the weight of normally aerated tissue or computing the weight of consolidated tissue has also been suggested. There is no doubt that CT scans can provide valuable and detailed information about the progression of ARDS and thereby lead to a better adjustment of the ventilator settings. However, as mentioned previously CT scans do carry several disadvantages. They cannot be performed repeatedly under clinical conditions whenever a new PEEP level is applied because they are not always available, relatively costly and they expose patients to a higher amount of radiation than standard chest X-rays do. [Pasenti et al., 2001]

One could summarize the two methods: static PV curves are, compared to CT scans, the most easily obtained method at the bedside and can provide information regarding how to adjust and optimize the ventilator related to PEEP setting. However, the interpretation of the curve is still the main issue when using this method and the curve is often evaluated by eye which is very subjective and relatively unprecise. The controversy described in the litterature also indicates that there is still a lack of understanding of the pressure volume curves related to the mechanisms of PEEP, alveolar states and gas exchange. CT scans can provide a more detailed and accurate description of the status and progression of the syndrome than PV curves can. For that reason it would in the following be interesting to investigate what approaches have been made to model and gain a better understanding of the static PV curve and how they are used in clinical practice. It would furthermore be interesting to investigate if analysis of CT scans has contributed to gain a better understanding of the static PV curve. One of the main concerns regarding optimal ventilator setting is choosing the optimal PEEP level which also has been described during the previous sections. Due to that it would be natural to gain focus on this issue when analyzing and describing the models. Based on this introduction and the summation the following questions can be formulated:

- *What approaches has been made to model and understand the underlying physiology behind the static PV curves?*

- *How has image based analysis i.e CT scans been used in the context of these approaches*

In order to investigate these questions, existingc PV models are reviewed. The models will be divided into different categories and both advantages and disadvantages of the models will be described. Approaches regarding image based analysis will also be described. Both static PV models and the image based analysis are reviewed with focus on identifying "appropriate" and "best" PEEP settings and also whether they are capable of identifying open, collapsed and overdistended alveoli.

Chapter 2

Pressure volume models and CT scans

The purpose of this chapter is to answer the questions formulated in the initial problem which are to review what approches has been made to model and understand the static PV curve and how CT scans have been used in the quantification and modelling context. The main focus in this review will be how the models are able to simulate the effect of adjusting the PEEP level and how they are able to explain/describe how lung areas are effected i.e. whether alveoli are open, overdistended or collapsed. The different reviewed PV models encompass: Model based on finite element analysis, models based on the sigmoid function, models based on opening and closing pressures and models based on alveoli compartments.

2.1 Models of the static PV curve

Interpretation of the static PV curve has commonly been done by eye from a graph, a method that may be affected by large interobserver and intraobserver variability [Harris et al., 2000]. In the past years several techniques and mathematical methods has been proposed to model and quantify the static pressure-volume curve of the respiratory system to overcome the variability derived from eye fitting and to gain a better understanding of the underlying physiology.

Models based on finite element analysis

In order to obtain a deeper understanding of the underlying physiology behind the mechanical behaviour of the lung several detailed models of the microscopic behaviour of lung tissue have been proposed. Many of theese models have applied finite element displacement analysis to describe both a single alveolus and clusters of alveoli [Matthews and West, 1972; Dale et al., 1980; Kowe and Schroter, 1986]. Finite element analysis is used to describe structures as divided into sub elements. The process starts with the creation of a geometric model, which is then divided into smaller shapes connected at specific nodal points, which can be seen in figure 2.1. Simulation of the displacement and volume change of the complete structure can be performed by applying a pressure at the nodal points of the elements. By applying finite element analysis when modelling the elastic mechanical behaviour of the lung it is possible to obtain a better understanding of stress strain relationships. [Matthews and West, 1972; Dale et al., 1980; Kowe and Schroter, 1986] However, none of these relatively complex models are able to simulate and quantify the amount of collapsed and overdistended alveoli.
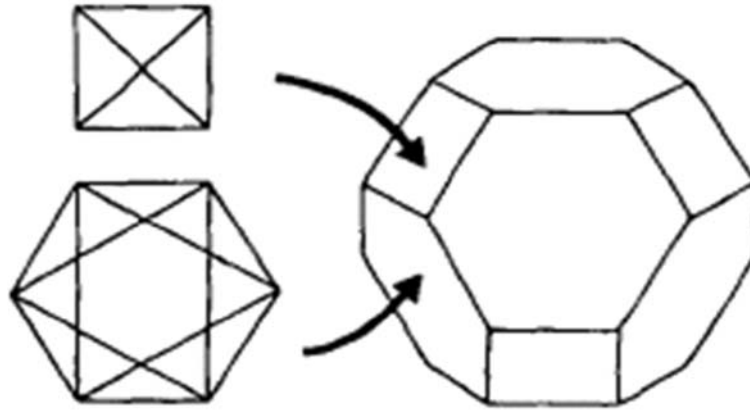
Figure 2.1: *The structure of a geometric model used to represent an alveolus. The distribution of fibres on the faces of the structure is represented in the figures. [Kowe and Schroter, 1986]*

Models based on the sigmoid function

Curve fitting of the PV relationship based on sigmoid functions is one way of determining more accurate inflection points of the PV curve. Various PV equations based on sigmoid functions have been proposed [Gibson et al., 1979; Bogaard et al., 1995; Venegas et al., 1998; Pelosi et al., 2001; Heller et al., 2002; Henzler et al., 2003]. One of the most accurate and comprehensive equations was proposed by Venegas et al. in 1998. The equation can with good accuracy fit the inflation and deflation limbs of PV curves obtained under a variety of experimental and pathological conditions and yields physiologically useful parameters.

The sigmoidal equation is formulated as:

$$V = a + \frac{b}{1 + \exp^{(-1(P-c)/d)}} \tag{2.1}$$

Where V is inflation or absolute lung volume. P is transpulmonary pressure. a, b, c, and d are four different fitting parameters which have a physiological correlate illustrated in figure 2.2. a corresponds to the lower asymptote volume, which approximates residual volume. b corresponds to the total change in volume between the lower and the upper asymptotes. c is the pressure at the "true" inflection point of the sigmoidal curve. d is proportional to the pressure range within which most of the volume change takes place. The equation also allows calculation of the inflection points of the PV curve as: LIP = c - 1.317d and UIP = c + 1.317d.. By using the four different fitting parameters it is possible to resize the curve horizontally and vertically to fit a given set of patient data [Venegas et al., 1998].

The symmetric equation with the four parameters has proven to be in very good agreement with data from both dogs, healthy humans and patients with lung injury [Venegas et al., 1998]. A more recent report based on analysis of 24 sets of inflation and deflation PV curves from patients with ARDS shows that the equation by Venegas et al. fits the data remarkably well and furthermore that it was possible to determine lower and upper inflection points. The study also shows that the application of the sigmoidal equation reduces inter- and intraobserver variability in the clinical evaluation of the PV curves. [Harris et al., 2000]

Despite these encouraging results the model by Venegas et al. does not provide information

regarding gas exchange ie. open, collapsed and overdistended alveoli. the model uses the normal clinical values which characterizes the pressure volume relationship, but does not provide any physiological interpretation of the curve. A previous review has questioned the use of the symmetric shape of the upper and the lower segments in the model. In 2002 Heller et al. showed how the model of Venegas et al. can be improved by adding one more coefficient to allow nonsymmetrical upper and lower segments. [Heller et al., 2002]
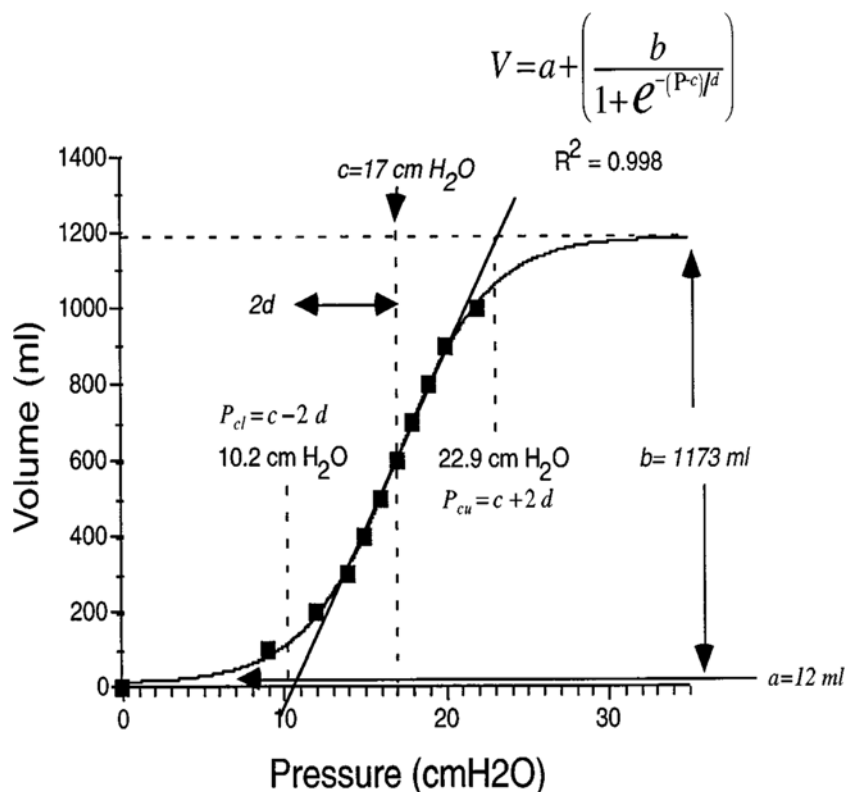

Figure 2.2: *The figure illustrates inflation static PV data measured in a patient with ARDS and fitted to a sigmoidal equation. See text for further description. [Venegas et al., 1998]*

Models based on opening and closing pressures

Several mathematical models of the static PV curve have been based on the alveolar opening and closing pressure thresholds. [Hickling, 1998, 2001; Markhorst et al., 2004; Frazer et al., 2004; Chase et al., 2006] In 1998 Hickling proposed a simple mathematical model in order to facilitate an understanding of the shape of the PV curve in ARDS. The model was used to evaluate the effect of varying alveolar opening pressures and PEEP on the slope of the pressure volume curve between the upper and lower inflection points, the pressures at the upper and lower inflection points, and the relationship between the upper and lower inflection points and ideal ventilator settings. The model was based on dividing the lung into alveoli compartments with equal opening and closing pressure. When the pressure across the alveolar wall, during inflation, exceeds the opening pressure of the alveoli it opens to a certain volume. Conversely, during deflation, the alveoli collapses when going below the closing pressure. Different levels of opening and closing pressures were applied in this model in order to simulate the dissimilarity of the lung recruitment which characterizes ALI/ARDS lungs. The shape of the different PV curves obtained with the simulation, as illustrated in figure 2.3, proved to be very close to those curves obtained in
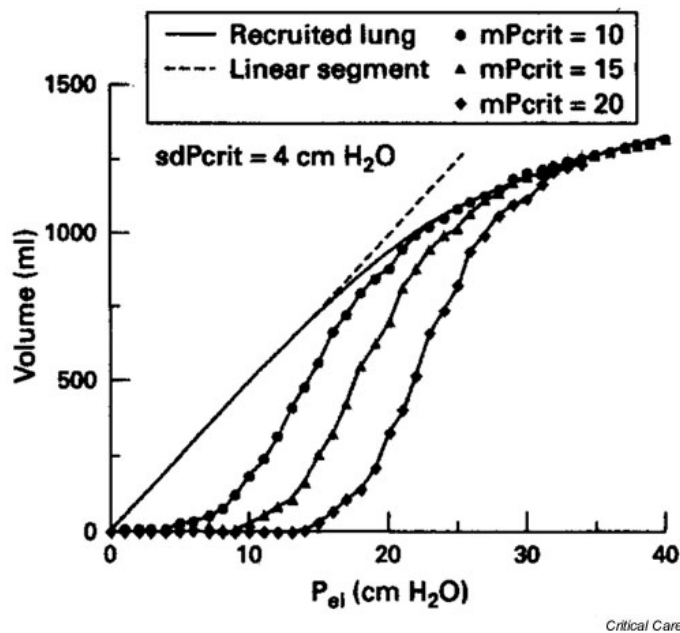
Figure 2.3: *The figure illustrates PV curves obtained with simulations using a multicompartmental mathematical lung model. The continuous PV curve reflects elastic properties of a completely recruited lung. The other curves represent the behavior of the simulated models according to different mean opening pressure (10 cmH2O, 15 cmH2O and 20 cmH2O) The figure is modified from [Hickling, 1998].*

patients. Most interestingly was the authors' suggestion that the absence of an upper inflexion point not necessarilly indicates the lack of overdistension since continuous recruitment may mask the flattening upper part of the curve. [Hickling, 1998]

In 2004 Markhorst et al. developed a mathematical lung model based on the Hickling model. The model was modified and extended to include air trapping, degree of alveolar recruitability, degree of ARDS severity, and chest wall characteristics. [Markhorst et al., 2004] The model encompasses 30 compartments, representing horizontal slices of lung. Each compartment consists of 9.000 alveoli, which encounter a gravitational superimposed pressure from zero in the ventral compartment to a maximum value in the dorsal compartment. Each lung unit, as in the model by Hickling et al., was assigned an individual threshold closing pressure to simulate either alveolar or small airway collapse and a threshold opening pressure to simulate reopening. [Markhorst et al., 2004]

In 2006 Chase et al. developed a comprehensive mechanical lung model especially developed for teaching of clinical staff. The model is intended to capture the Threshold Opening Pressure (TOP) and the Threshold Closing Pressure (TCP) in a visible and accurately way. TOP and TCP for the alveoli units are the critical pressures at which lung units open and collapse [Chase et al., 2006]. The study presented a complete mechanical model of the human lung to identify and verify the fundamental mechanics of any mechanically ventilated lungs and the effect of PEEP on recruitment. The lung was modelled with several units represented by rubber bellows. Adjustable weights were placed on bellows to simulate compartments of different superimposed pressure and compliance, as well as different levels of lung disease, such as ARDS. The model was directly connected to a ventilator and the resulting PV curves recorded. The schematic drawing of the model by Chase and coworkers can be seen in figure 2.4.
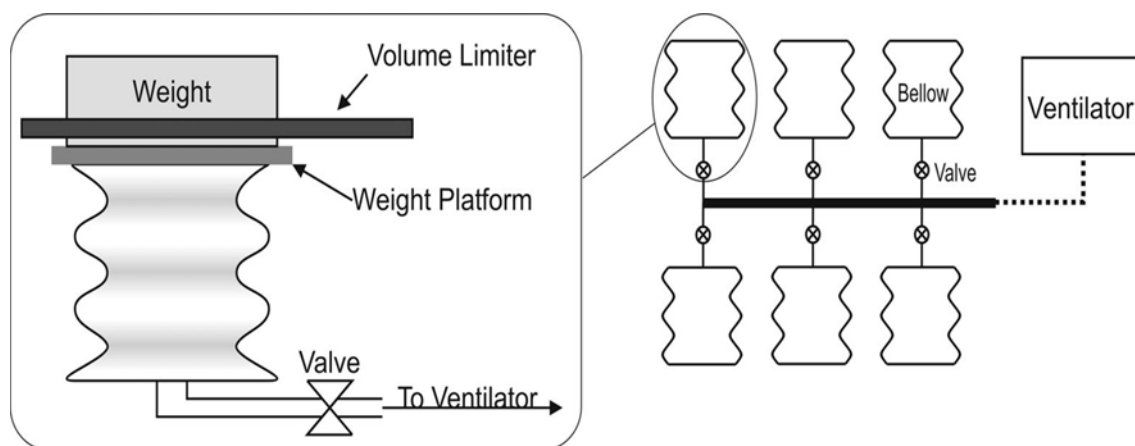
Figure 2.4: *The figure illustrates a schematic draw of the model. 6 bellows connected to the ventilator is used to represent the lung. A platform is placed on top of rubber bellow which is used to vary the driving pressure of the bellow. A volume limiter sets the maximum height of the platform, thus limiting the height which the bellow is allowed to expand vertically. Each bellow is connected to the larger common tube through an adjustable valve. [Chase et al., 2006].*

Results of the model show that it was capable of capturing the fundamental lung dynamics for a variety of conditions. The model could be used for teaching and thereby provide a better understanding of the lung mechanics [Chase et al., 2006].

Model based on alveoli compartments

In 2005 Smith et al. presented a compartment model of the lungs based on a physiological interpretation of lung function. The model, which is intended for use in clinical practice, was built on the assumption of alveoli beeing in three different states open, collapsed or overdistended. In the model a PV relationship was assigned to the individual alveoli compartments which allowed the volume and state of each to be determined depending on the trans alveolaer pressure across the alveoli wall. Total volume of all alveoli at a certain pressure was calculated and a static PV curve was determined. A curve fitting technique was applied in order to adjust parameters of the model to fit the static PV curves from patients. [Smith et al., 2005]

The result of fitting the sigmoid function and alveoli model, which can be seen in figure 2.5, shows that the model achieved an almost equivalent fit to the experimental data from an ARDS patient. In contrast to other previous studies the alveoli model is based on the interpretation of physiological parameters. The model couples gas exchange and lung mechanics, witch makes it possible to simulate the percentile of overdistended, open and collapsed alveoli at a given pressure. This can be considered advantageous in clinical practice when adjusting and optimizing ventilator settings. [Smith et al., 2005]
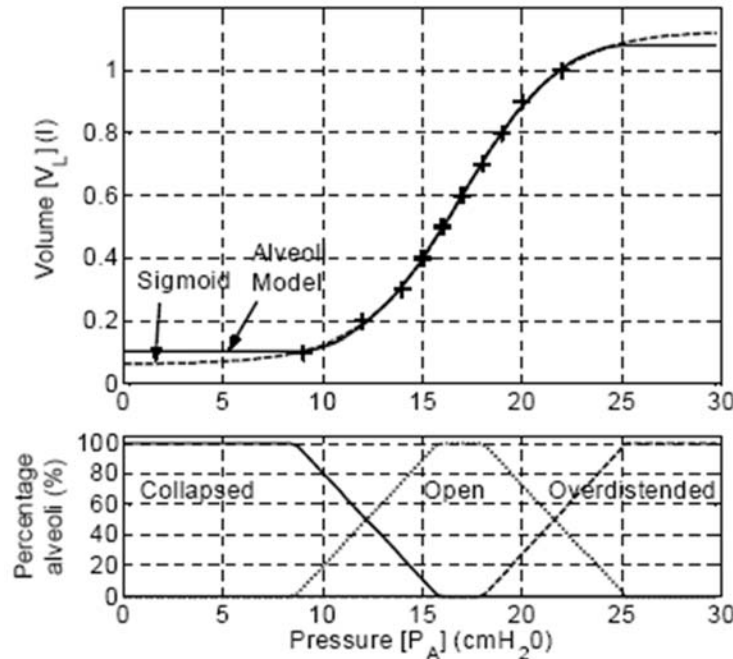
Figure 2.5: *The figure illustrates fitting of the sigmoid function (dashed line) and the alveoli model (solid line) to experimentally measured patient data (+) from Venegas et al. (top). The distribution of alveoli in the three states is calculated by the alveoli model and illustrated in the bottom figure [Smith et al., 2005]*

Application in clinical practice

In spite of the increased understanding of lung mechanics the presented models provide, only a few of them have been developed with the aim of application in clinical practice. Some of the models have proved very effective in simulating the effect of different ventilator settings including the impact of PEEP on lung recruitment. Some of the models also permit a more objective estimate of the lower and upper inflection points than done by eye, which can be useful when adjusting the PEEP level. However, one of the main concerns when treating ALI/ARDS patients is to find the "best" PEEP level. That is to find a PEEP level that recruit the recruitable alveoli and at the same time not overdistend other alveoli. Only the models based on distribution of opening and closing pressures and the model based on alveoli compartments may simulate changes regarding open, collapsed and overdistended alveoli.

2.2 CT scans analysis

CT analysis have largely contributed to gain a better understanding of the physiological mechanisms regarding the heterogeneously distributed tissue damage, gas exchange problems, recruitment and derecruitment in ARDS patients. In conjunction with that effort, several mathematical models of the lung airways, vascular tree, and parenchymal mechanics based on individual subject anatomy determined from CT scans have been developed. [Takishima and Mead, 1972; Venegas et al., 1993; Tawhai et al., 2004, 2005],

To my knowledge, no study has aimed at modelling and simulating the pulmonary pressure volume relationship based on image analysis of CT scans. However several studies have evaluated CT findings with PV curves and suggested that the morphology in CT scans correlates well

with parameters derived from the PV curves.

The goal of a study by Vieira et al. in 1999 was to test the hypothesis that the presence or the absence of a lower inflection point on the PV curve corresponds to differences in lung morphology. Eight patients with a lower inflection point in the PV curve and six without underwent a spiral thoracic CT scan performed at zero end-expiratory pressure and at two levels of PEEP: 10 cmH$_2$O and 15 cmH$_2$O The volumes of air and tissue in the lungs were measured and the volumes of overdistended and normally, poorly, and nonaerated lung areas were determined by frequency histogram distribution of the densities in Hounsfield units (HU). (The sum of normally and poorly lung area are normally refered to as open alveoli, which is the term used in the Introduction chapter. The nonaerated lung are is refered to as collapsed alveoli.) The HU scale is used to assign a numerical value from -1000 to 1000 to body tissue, water, air etc represented in a CT scan. (Hounsfield Units is further described in chapter 5.1). The study showed that the percentage of normally aerated lung are lower in patients with a lower inflection point than in patients without. It also showed that patients with a lower inflection point yield a unimodal distribution in the density histograms and patients without a lower inflection point yield a bimodal distribution which is illustrated in figure 2.6 The applied PEEP level in both patient groups induced an alveolar recruitment. However, in patients without a lower inflection point it was only associated with lung overdistension. [Vieira et al., 1999b]

Another study regarding the correlation between CT findings and the physiological mechanisms of ARDS was carried out in 2000 by Ichikado and coworkers. The study showed that thin section CT findings in juvenile pigs correlated well with pathologic phases of diffuse alveolar damage and that assessment with thin section CT was helpful in predicting prognosis in individuals with acute interstitial pneumonia which is an idiopathic form of ARDS. [Ichikado et al., 1997, 2000]

Several studies in the past years have aimed at describing the correlation between PEEP induced alveolar recruitment and morphological findings in CT scans. In a study in 2000 by Malbouisson and coworkers, a new CT method was proposed for assessing PEEP induced alveolar recruitment in patients with ARDS. The primary aim in this study was to separate PEEP-induced lung overdistension from alveolar recruitment. They suggested that alveolar recruitment should be defined as the volume of gas penetrating in poorly and nonaerating lung units when PEEP is applied. [Malbouisson et al., 2001] This approach of identifying alveolar recruitment was in a later study suggested to be one of the most accurate ways of determining increased recruitment. [Gattinoni et al., 2001]

In 2001 Pelosi and coworkers demonstrated in an experimental animal study where lung damage was performed by inducing oleic acid that recruitment is a continuous process that occurs along the entire inspiratory limb of the PV curve of the respiratory system. [Pelosi et al., 2001] The study compared different applied PEEP levels and obtained CT scans at end-inspiration and end-expiration. The morpholgical findings in the CT scan which include the frequency distribution (HU) obtained from the CT scans were compared to the PV relationship. The relationship between the recruitment obtained from CT scans and the PV relationship is illustrated in figure 2.7. "R" in the figure indicates the percentage of recruitment occurring at the corresponding airway pressure. The result from this study was later confirmed in a study in patients with ALI/ARDS [Crotti et al., 2001].
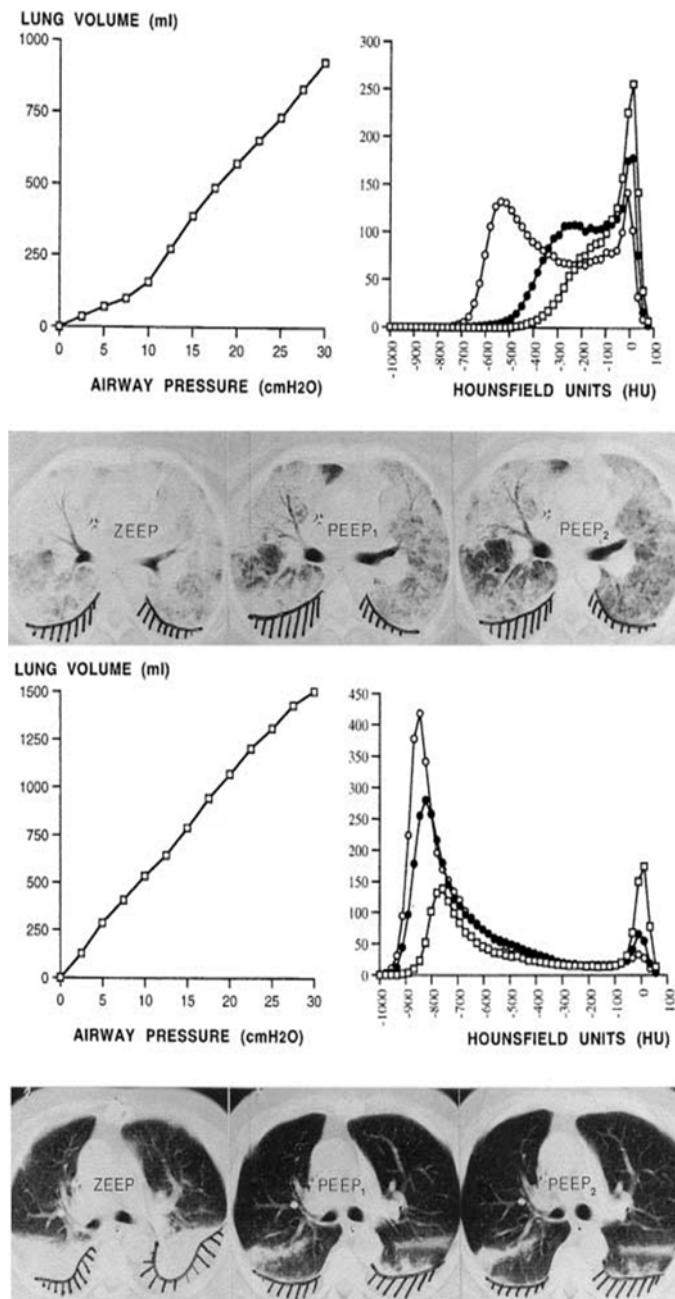
Figure 2.6: *The figure illustrates PV curves and volume distribution of lung aeration in Hounsfield Units (HU) of the entire lung measured at Zero End Expiratory Pressure (ZEEP) [open squares] and two PEEP levels [PEEP1 and PEEP2, solid and open circles] in two patients with ARDS characterized by different lung morphology patterns. Dashed areas in the CT scans indicate pleural effusion, which was not taken into consideration for the CT analysis. The upper part of the figure, illustrates CT section of a patient with diffuse CT attenuations and loss of aeration represented at ZEEP, PEEP 12 cm H2O (PEEP1), and 17 cm H2O (PEEP2). In the conditions with ZEEP there are no normally ventilated lung regions, characterized by CT attenuations ranging from -500 to -900 HU. After increasing levels of PEEP the nonaerated lung regions progressively decrease, whereas a good part of the lung parenchyma becomes normally aerated which is an indication of alveolar recruitment. The threshold of overdistension at which is defined as -900 HU is never reached. The lower part of the figure illustrates a patient with loss of aeration represented at ZEEP, PEEP 10 cm H2O (PEEP1), and 15 cm H2O (PEEP2). Half of the lung is normally aerated in ZEEP (upper lobes), whereas the other half (lower lobes) is either poorly aerated (CT attenuations ranging from -500 to -100 HU) or nonaerated (CT attenuations greater than -100 HU). After increasing the PEEP level, lower lobes are recruited, as evidenced by the decrease in nonaerated lung volume, whereas upper lobes are either distended or overdistended, as evidenced by the appearance of 250 ml of lung parenchyma characterized by CT attenuations less than -900 HU. [Vieira et al., 1999b]*
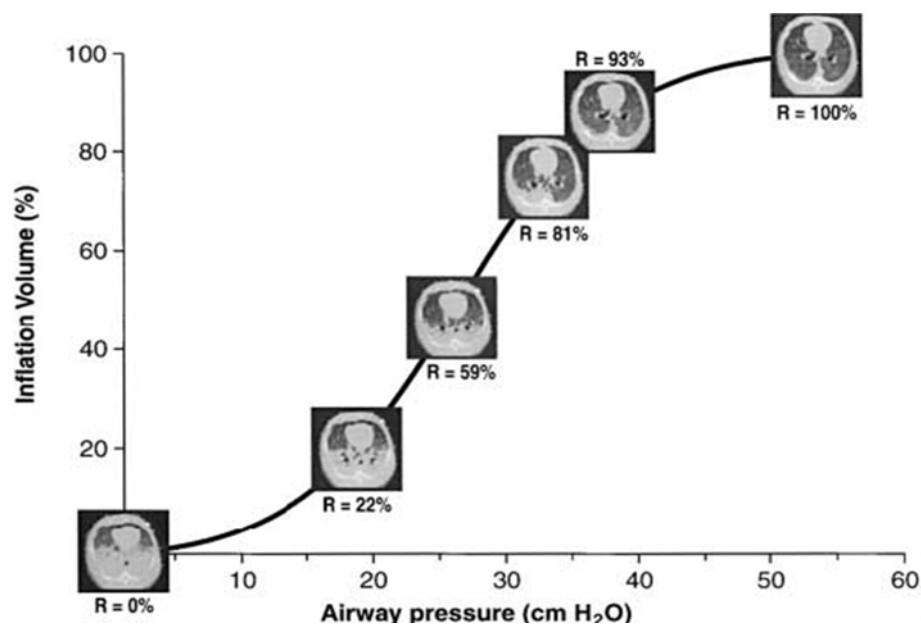
22

Figure 2.7: *Pelosi and coworkers showed in a study with oleic acid injuried dogs and a study with patients with ALI/ARDS that recruitment occurs along the entire PV curve. Each subject was applied different PEEP levels and an end-inspiration and end-expiration CT scan was obtained. The morphological findings in the CT scans were compared to the obtained PV relationship. A the figure illustrates "R" is an indication of the percentage of recruitment occurring at the corresponding airway pressure [Pelosi et al., 2001]*

2.3 Conclusion

In this chapter existing static PV models, and approaches of CT scan analysis have been rewieved and analyzed in order to answer the questions formulated in the initial problem statement. Mathematical modelling of the static PV curve has contributed to a better understanding of lung mechanics and some of the modelling approaches has furthermore helped direct therapy in patients with ARDS. All the reviewed imaging aproaches also show that CT scans in numerous studies have been used successfully to provide insight into the pathophysiology of ALI/ARDS particularly with respect to recruitment and ventilator management. As mentioned in Chapter 1 the static PV curve can provide valuable information regarding how to find the optimal PEEP setting which is crucial in ALI/ARDS patients. That is how to find a "minimum" PEEP level in order to recruit the recruitable alveoli and avoiding VILI but also to "limit" PEEP in order to avoid overdistension which also can lead to VILI. In clinical practice the PV curve is often evaluated by eye which is both unprecise and also highly subjective. So one could argue that if a model based on the static PV curve could simulate the effect of different PEEP settings and thereby find the level which will recruit most alveoli and not overdistend the others would be highly usable in clinical practice. However, only the models based on distribution of opening and closing pressures and the model based on alveoli compartments permits simulations of the distribution of open, closed and overdistened alveoli.

Chapter 3

Problem statement

In this chapter all the revealed problems related to optimization of the ventilator settings in ALI/ARDS patients described in the two previous chapters are summarized and discussed. This will lead to a problem statement for the remainder of the report.

Finding the most appropriate settings for the ventilatior is normally a simple task. However, in ALI and ARDS finding these settings is a more complex task. Lung regions of these patients are often collapsed or overdistended and are therefore not participating in gas exchange. In order to improve gas exchange, prevent further overdistension and recruit the collapsed alveoli, a correct PEEP setting of the ventilator must be selected. Much attention must therefore be paid to avoid inappropriate settings on the ventilator which is excessive pressure and volume. Inappropriate ventilator settings may at worst lead to VILI which in worst case can lead to multiple organ failure and death. A common way of obtaining information regarding how to find the most appropriate ventilator settings is by evaluating the PV curve. The evaluation is very often performed by eye which is both unprecise and highly subjective. Another common issue is that there is no consensus of how to interpret the static PV curve, i.e use the curve to gain information regarding the amount of open, collapsed and overdistended alveoli.

CT scans can compared to the static PV curve provide a more detailed and accurate description and information of the status and progression of the syndrome. However, CT scans do carry several disadvantages whereas the most important is that the CT scanning cannot be performed repeatedly under clinical conditions whenever a new PEEP level is applied.

Several approaches have been taken to model the static PV curve in order to understand the curve and the effect of PEEP. However, only a few of these models which are the model based on alveoli compartments and the models based on opening and closing pressures can simulate changes in open, collapsed and overdistended alvoli which could be considered of major concern when trying to avoid VILI and optimize gas exchange. Of these models only the model based on alveoli compartments has been developed with the aim of application in clinical practice and is based on physiological parameters. To My knowledge, no study has been trying to investigate whether the model based on alveoli compartments correlates with the number of open, collapsed and overdistended alveoli from CT scans when applying different PEEP levels. If such morphological findings of open, collapsed and overdistended alveoli in the CT scans correlates well with this model the model could potentially be used in clinical practice when adjusting and optimizing PEEP. Thus, a problem statement can be formulated:

- How is the relationship between model simulations from the model based on alveoli compartments and the number of open, collapsed and overdistended alveoli from CT scans?

3.1   Solution strategy

In order to answer the formulated problem statement several different tasks can be defined, which can be divided into two main categories: CT scans- and model analysis.

The application of CT scans

- Formulate criteria of the image segmentation algorithm that should be capable of extracting information from CT scans regarding the open, collapsed and overdistended alveoli.

- Design the algorithm.

- Validate the algorithm.

- Extract information regarding the open, collapsed and overdistended alveoli from CT scans.

The application of the model

- Describe the model based on alveoli compartments and investigate the sensitivity of the model parameters.

- Investigate how the model should be applied to fit static PV curves

- Fit the model to static PV curves and simulate the corresponding alveolar states

Comparing simulations and CT scans

- Investigate whether there is a relationship between the simulated alveolar states from the model and the number of open, collapsed and overdistended alveoli from CT scans.

The abovementioned defined tasks can be divided into the following parts for the remaining report:

Part II - Materials

In order to investigate whether there is a relationship between the simulated alveolar states from the model and the number of open, collapsed and overdistended alveoli from CT scans a large amount of materials that includes CT scans and PV curves, are needed. The materials used in this study are described in chapter 4 in Part II.

Part III - Image Analysis and Processing

In order to extract information from the CT scans an image segmentation algorithm must be developed. Both analysis, design and validation of the algorithm are described in chapter 5, 6 and 7 in part III.

Part IV - Model based on alveoli compartments

Chapter 8 contains a detailed describtion of the physiological and mathematical terms used in the model based on alveoli compartments which leads to a parameter sensitivity analysis in

chapter 9. This sensitivity analysis forms the basis of how fit the model to the PV data available for this study.

Part V - Relationship between the model and CT scans

During this part the simulated alveolar states from the model and the extracted alveolar states from the CT scans are compared.

Part VI - Closure

Part VI contains the closure of the project. This encompasses both summation, discussion, perspectives and conclusion.

Part VII - Appendix

Part VII contains the appendix for the report. Appendix A contains the complete nomenclature used in this report. Appendix B contains all plots of the model simulations of alveolar states and the extracted alveolar states from the CT scans.

Part II

Materials

Chapter 4

CT scans and static PV curves

In order to answer the question formulated in the problem statement data materials that encompasses both PV data and CT scans are needed. In the following chapter the materials used in this study is presented.

The materials have been obtained by Gaetano Perchiazzi. The materials encompasses data from three different pigs. Four different sequences of examinations from the two first pigs, and two different sequences of examinations from the last pig. Before the different examinations were carried out the pig was sedated, orally intubated and mechanically ventilated.

The four different sequences from the first two pigs include:

- Measurement with a PEEP setting of 5 cmH2O.

- Measurement with a PEEP setting of 10 cmH2O.

- Measurement with a PEEP setting of 5 cmH2O and with experimental ARDS induced by injection of oleic acid.

- Measurement with a PEEP setting of 10 cmH2O and with experimental ARDS induced by injection of oleic acid.

The two different sequences from the last pig include:

- Measurement with a PEEP setting of 5 cmH2O and with experimental ARDS induced by injection of oleic acid.

- Measurement with a PEEP setting of 10 cmH2O and with experimental ARDS induced by injection of oleic acid.

This means that data from a total of 10 different sequences of examinations is available. In each of the different sequences the following data were obtained:

- 12 different full body spiral thoracic CT scans performed from the apex to the diaphragm using a Siemens Somatom SPI scanner. Each of these 12 different full body scan encompass 50 CT slices. This means that each of the 10 different sequences encompass 600 ($50 \cdot 12$) CT slices. The total number of CT slices from all three pigs are 6000 ($600 \cdot 10$).

- When each full body CT scan was carried out the contemporary peak pressure, plateau pressure, total lung volume and flow at peak pressure were measured.

The relationship between plateau pressure and the total lung volume represents the static pressure volume curve. The materials thereby encompass 10 different full body CT scans with the contemporary pressure volume relationship.

Part III

Image Analysis and Processing

Chapter 5

Analysis and criteria of algorithm

In order to extract information regarding the number of open, collapsed and overdistended alveoli from the CT scans an image segmentation algorithm must be developed. Thus, the first section in this chapter contains a general introduction to morphological analysis of CT images. The three different areas of collapsed, open and overdistended alveoli in CT scans are normally identified based on the CT terminology: Hounsfield Units (HU). Thus the second section describes both Hounsfield Units and how to identify the alveolar states in CT scans. The last section describes the criteria used in the design of the algorithm.

5.1 Morphological analysis of CT images

In ALI/ARDS patients, four different lung compartments are normally considered of interest when a chest CT scan is obtained: collapsed, poorly aerated normally aerated and hyperinflated [Gattinoni et al., 1986, 1987, 1988; Puybasset et al., 1995; Umamaheswara et al., 1997; Dambrosio et al., 1997; Vieira et al., 1998]. However, in some studies poorly aerated and normally aerated tissue are considered as one compartment [Smith et al., 2005]. In this study the latter method is used. The complete contribution of the different compartments is equal to the full lung area in a CT scan.

The lung area is visually represented in different ways depending on what position the CT scan is obtained. Figure 5.1 illustrates a representative selection of the CT scans used in this study. The figure represents different slices from the diaphragm to the apex starting from sub-figure A1, B1 etc. Sub figures A1, B1 and C1 contains no or litle lung area. The next three sub figures contains more lung area. The three last sub figures also contains litle or no lung area. Allmost all of the sub figures contains lung area that are divided into two parts. Only sub figure B2 contains connected lung area. This sub figure also contains several large vessels in contrast to the other sub figures. As the the last three subfigure illustrates, the apex region contains more bone structure than the diaphragm region does. Sub figure B2 and C2 illustrates the heart which can be seen in the midle of the lung area. As demonstrated in these sub figures, the lung area is visually represented in various ways in the different CT scans depending on the position of the CT scan. This encompass both the size of the lung area, whether the lung area is connected or disconnected, whether the actual lung area contains large vessels, whether there are large fractions of bone and whether other organs can be seen. This means that the segmentation algorithm should be capable of segmenting the lung area from all these different CT scans.

In order to quantify the different lung regions with different aeration in CT scans there are

normally two basic approaches available. The first approach is a visual estimate of the consolidation or ground glass opacification as a percentage of the total lung area [Brismar et al., 1985]. The second approach is based on the CT number frequency distribution of the lung. The different lung areas is characterized by a specific range of CT numbers also known as Hounsfield Units (HU).
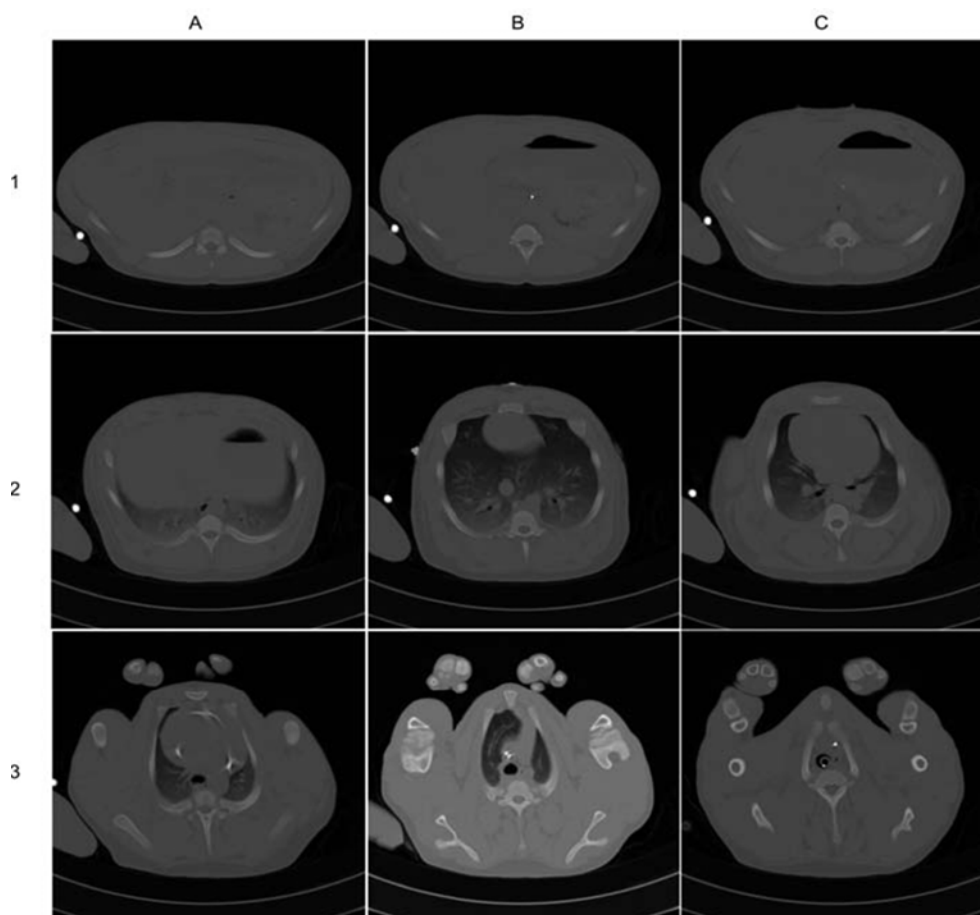

Figure 5.1: *Nine different sub figures that represents the different CT scans used in this study. The CT scans represents different slices from the diaphragm (sub figure A1, B1... to the apex (sub figure ...B3,C3). As the figures indicates the lung area (dark area inside the body) is distributed in several different ways. A2 and B2 illustrates that the lung area in some of the CT scans is connected. However, this is not always the case which is seen in C2 A3 and B3. Furthermore, some of the CT slices, as shown in sub figure A1, B1, C1 and C3, does not contain any lung area.*

Hounsfield units

Pixels of a CT image are proportional to tissue electron density and are usually expressed in HU [Gattinoni et al., 2001; Simon et al., 2005].

HU is obtained, in any given voxel, by determining the percentage of radiation absorbed by that volume of the lung. As with other X-ray techniques, the greater the absorption, the less radiation hitting the X-ray film or CT detector. The attenuation scale roughly cover the numerical range from -1000 to +1000. Each number represents a shade of grey with +1000 (white) and -1000 (black) at either end of the spectrum. Bone is assigned a value of -1,000 HU (complete

absorption), air a value of -1,000 HU (no absorption), and water a value of 0 HU. [Simon et al., 2005; Gattinoni et al., 2001] The spectrum of the HU scale is illustrated in figure 5.2. A quantification of a specific HU range illustrated in the figure indicates the distribution of the specific lung compartment. As the figure shows there are different ways of classifying the different lung compartments. The inserted sub figure divides the lung area in hyperinflated, normally, poorly and non aerated lung tissue. The main figure divides the lung area in overdistended, open and collapsed lung tissue. This means that hyperinflated and overdistended lung tissue covers the same HU range, the total of normally and poorly areated are equal to open lung tissue and non aerated and collapse lung tissue are equal. This study uses the terms of the different lung compartments with coherent HU range illustrated in the main figure, which means that the lung area is divided into the three compartments: open, collapsed and overdistended alveoli.
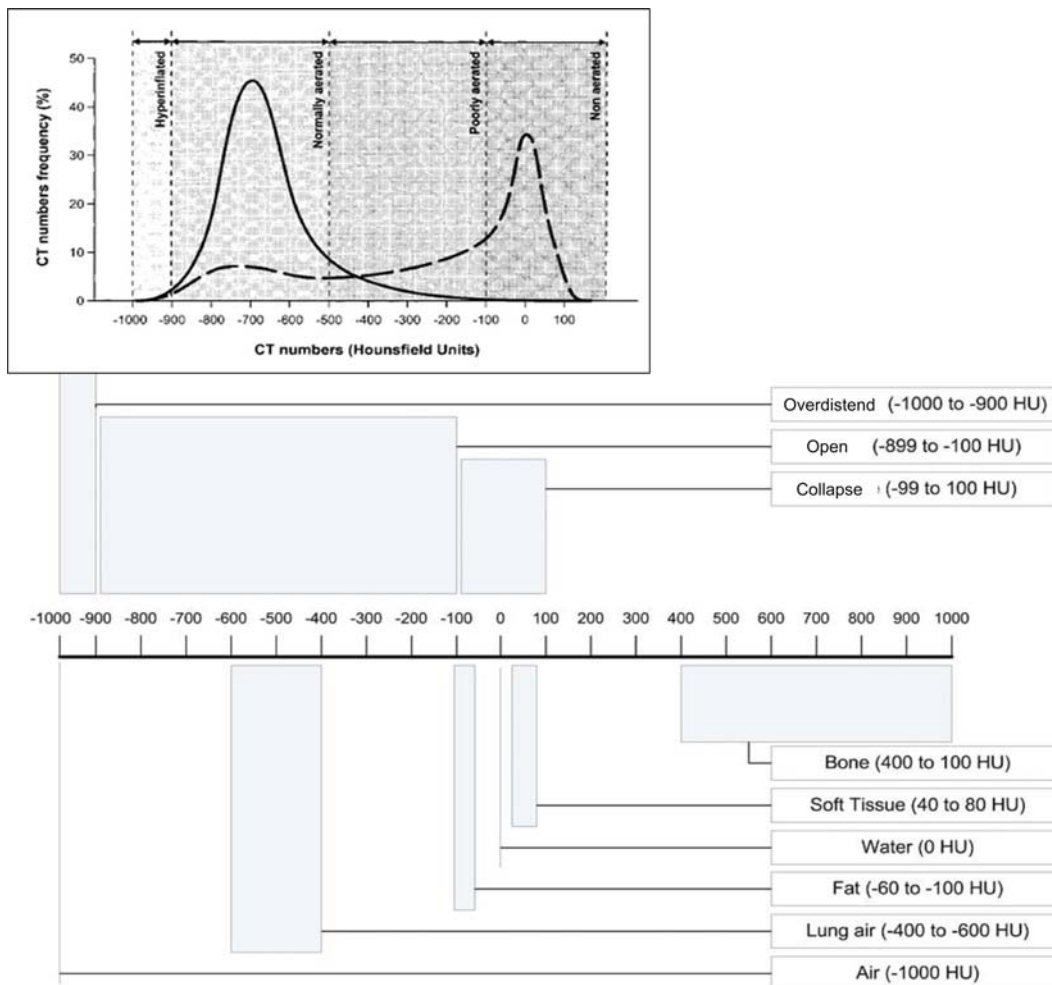
Figure 5.2: *The spectrum of the HU scale covering the numerical range from -1000 to +1000. The distribution of lung compartments is illustrated with dashed areas in the top of the figure. The distribution range from -1000 to 100 HU. In the bottom at the figure the range of bone, soft tissue, water, fat, lung air and air are illustrated. [Gattinoni et al., 2001] The inserted sub figure illustrates a clear difference in the HU between a healthy subject (full line) and a patient with ARDS (dotted line). The ARDS patient shows a peak in the high HU scale which indicates a large number of collapsed alveoli while the healthy subject shows a peak in the normally aerated lung area. [Gattinoni et al., 2001] The total Hu range of normal aerated and poorly aerated lung tissue shown in the inserted sub figure is equal to the open lung area shown in figure. This study uses the range from -900 to -100 HU as the open lung area.*

5.2   Segmentation criteria

In CT scans of normal and healthy lungs it is normally not a complex task to sort out the remaining body from the lungs, since the intensity difference between lung tissue and remaining body is relatively large. The distinct difference between the intensity of the lungs and the remaining body is visualied in the left sub figure in figure 5.3. However, when collapsed lung area is present as seen in ALI/ARDS patients the difference between the intensity of the lungs and the remaining body is less significant, which is visualied in the right sub figure 5.3.
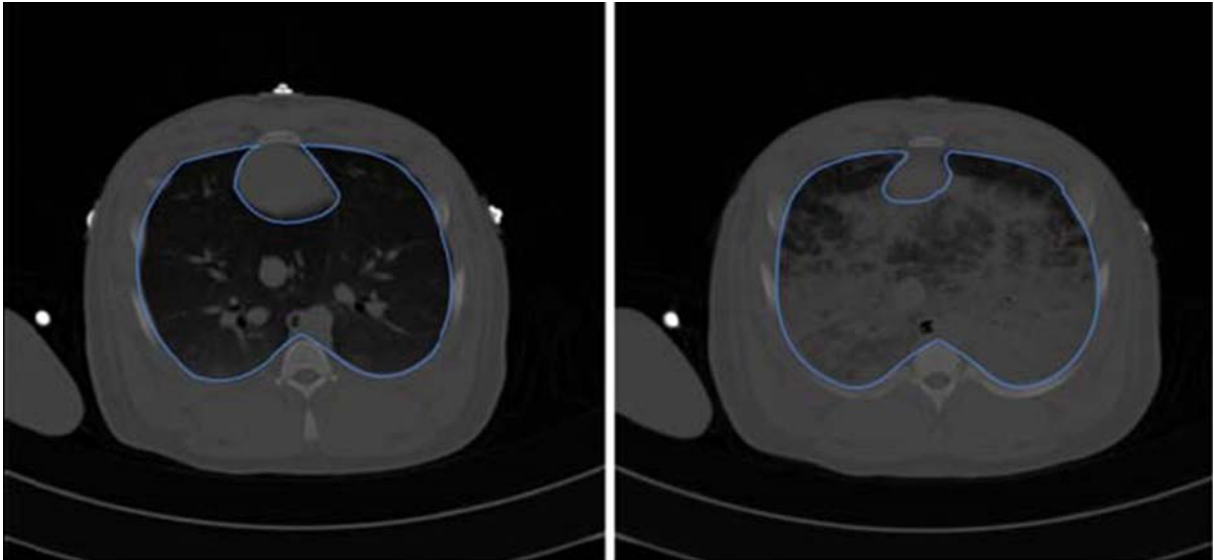

Figure 5.3: *The figure illustrates two different CT scans with the lungs being separated with a blue line. The first CT scan, which is an example of a healthy lung, shows significant intensity difference where the blue line is drawn. This indicates that the segmentation of the full lung area could be a simple process. However, in the second CT scan, which is a typical example of an ALI/ARDS patient with a large amount of collapsed or poorly ventilated tissue, the intensity difference between lung area and remaining body tissue, bone etc. is less significant.*

The main purpose of the algorithm is to identify the different lung compartments defined in the HU scale from -1000 to 100 and to sort out the "the rest" of the image. The HU range of the collapsed lung compartment overlaps the range of both fat, soft tissue and water. This means that collapsed tissue is identified in the same way as fat, soft tissue and water which also is present in the remaining body, surrounding the bones. Consequently, a simple measure of the HU range of the different lung compartment from the entire CT scan, or a simple algorithm with a threshold technique can not be used.

Using semi-automatic segmentation processes is also not an obtion, since these methods rely on manual intervention such as marking of several seed points. When a large numbers of CT scans is segmented, as in this study, semi-automatic methods will be too time consuming. The criteria in the segmentation process used in this study is summarized below and listed in priority order:

- *No need of manual intervention.* When a large amount of CT scans, as used in this study, should be segmented it would be too time consuming to use an algorithm that needs manual interventations.

- *Segmentation of complete lung area.* Segmentation of the "full" lung area, which encompasses the three different lung compartments represented in the lungs: open, collapsed and overdistended alveoli.

- *Distinguish between collapsed tissue in the lungs and fat and soft tissue in the remaining body.* Collapsed lung tissue is defined at the same HU range as the normal soft tissue and fat in the body. Thus, an attempt has to be made in order to preserve the collapsed tissue in the lung but also to remove the remaining normal/healthy tissue in the body.

- *Measurement of the amount of pixels, based on HU of every lung compartment: collapsed, normal and overdistended.* When the segmentation of the "pure" lung area is performed the amount of pixels of every lung compartment should be measured. Thus, the algorithm should be able to recalculate the HU range to the corresponding pixel value.

- *Fast.* When several thousands CT slices has to be segmented the process needs to be relatively fast (few seconds). In the materials chapter the complete amount of CT slices was found to be 6000. If the duration of the segmentation process in each CT slice is one minute, the total amount of time used to segment all of the slices elapse over 4 days (6000 minutes $/ (24 \cdot 60)$).

5.3 Conclusion

During this chapter general morphological analysis of CT images and common CT terminology has been introduced and described. The issues related to the low intensity difference between collapsed tissue and the remaining body in CT scans has also been described. Several examples of CT slices has been shown and how the anatomy of the lung visual can change depending on the position of where the CT slices are obtained. Based on this chapter several criteria were formulated, which forms the basis of the design of the algorithm.

Chapter 6

Design of segmentation algorithm

This chapter is a describtion of the segmentation algorithm used in this study. The algorithm is developed using Matlab and presented stepwise, which means that every step performed, from the original CT slice to the final segmented lung area, are described. Every step will furthermore be visualied with two examples of images: an example with normal lung area and an example with large amount of collapsed tissue. Images with these two types of lung area is chosen in order to show that the algorithm can segment the lungs in both ends of the normal/non normal spectrum. The algorithm includes a generation of three different masks: one that sorts out the artifacts in the image, one that segments the lung area and one that estimates the percentage distribution of the three different lung compartments open, collapsed and overdistended alveoli. The distribution of the different lung compartments are estimated from all 50 obtained CT slices from the full CT scan. A total percentage of the different lung compartments, representing the whole lung, are finally calculated.

6.1 Step 1 - Mask used to remove artifacts

The first step of the algorithm is to remove artifacts from the CT scans. Artifacts are in this study defined as areas outside the remaining body in the CT scan. An example of artifacts can be seen in figure 6.1 (A1) marked with blue arrows. Removal of artifacts can be done by using a mask that extracts the whole body in the CT scan and sorts out the surrounding area.

A threshold teqnique is applied on the original image in order to make the grey area in the image white, and contemporary the black/dark grey area black. A threshold limit at -600 HU, illustrated in figure 4.3 is applied. This means that every part of the image defined at a limit above -600 HU is colored white and below the limit is colored black. By applying this limit almost all the area of the body is turned white. The extracted image with the threshold limit applied can be seen in figure 6.1 (A2) and figure 6.1 (B2). Allmost all the area of the body is colored white with exceptions in the center of the image. These black areas indicates that the lung area also consists of open and overdistended alveoli defined below the threshold at -600 HU that is applied. In order to extract the image at the defined threshold limit measured in HU, the HU range has to be converted to pixel value. The relationship between HU and pixel value is a linear relationship and is defined in the following manner: [Mathworks, 2007]

$$HU = Pixelvalue \cdot RescaleSlope + RescaleIntercept \qquad (6.1)$$

RescaleSlope and RescaleIntercept are values stored in the Dicom header from the CT scan. These values are 1 and -1024 respectively.
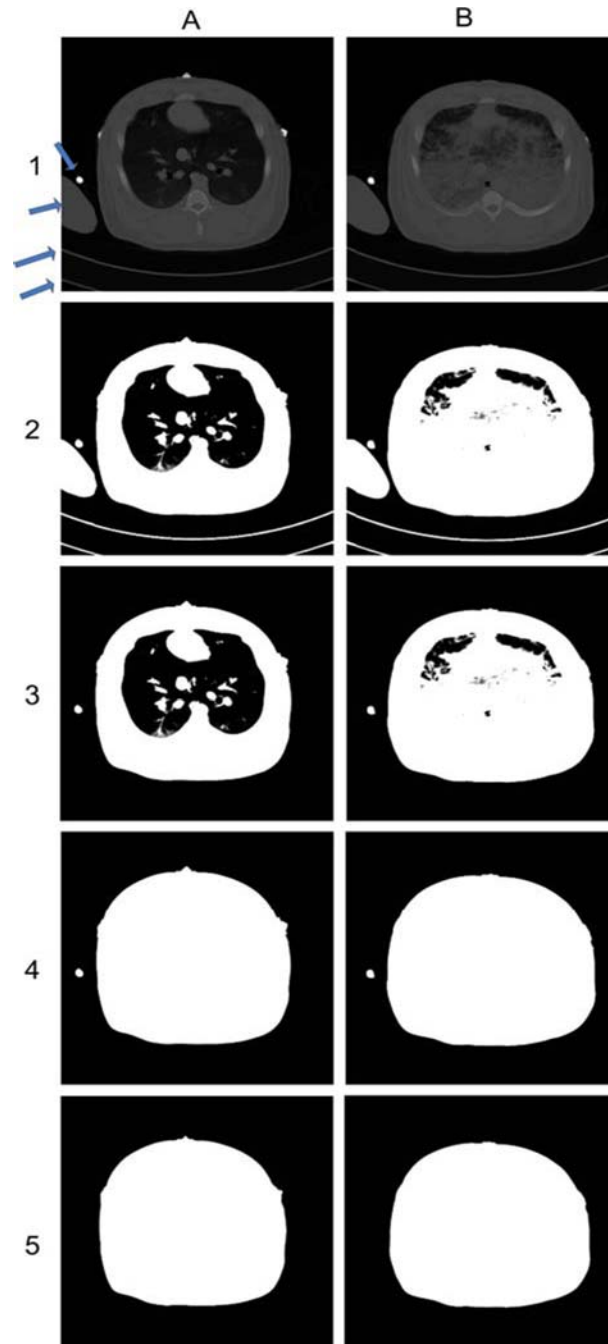
Figure 6.1: *Step 1 in the image segementation process, where the mask used to remove artifact from the image is extracted. Extraction of the mask visualized in sub figure A5 and sub figure B5 consists of four different steps: Threshold of original image, removal of artifacts that is connected with the border, total body area converted to white and removal of small artifacts outside the body. Sub figure A1 and B2 are the original images. A1 is an example of a subject with open lung area. B1 is an example of a subject with large amount of poorly or collapsed tissue, as seen in patients with ALI/ARDS. A2 and B2 shows the image with the applied threshold at -600 HU. A3 and B3 are the images with the removed artifacts connected to the border. A4 and B4 are the images where the total body area is converted to white. The last sub figures A5 and B5 are the final masks where the small artifacts have been removed. See text for further description.*

As seen in figure 6.1 (A1) and figure 6.1 (B1) most of the artifacts marked with blue arrows are connected to the border of the image. These artifacts are removed by using a built-in function in Matlab, called imclearborder, that suppresses structures that are lighter than their surroundings and that are connected to the image border [Gonzales et al., 2004]. Removal of these artifacts is visualized in figure 6.1 (A3) and figure 6.1 (B3).

As mentioned previously, and visualized in figure 6.1 (A3) and figure 6.1 (B3), there are still black areas in the center of the image. The next step in the algoritm is to convert these black areas into white and thereby obtain a full white area of the body. Since the black area can be considered as a "hole" inside the surrounding white area another standard Matlab built-in function, called imfill, is applied. This function fills all sets of background pixels that cannot be reached by filling in the background from the edge of the image. [Gonzales et al., 2004] The result of this operation can be seen in figure 6.1 (A4) and figure 6.1 (B4).

Not all artifacts in the image has been removed by using the aforementioned method, which is seen in figure 6.1 (A4) and figure 6.1 (B4) as a white spot. These spots can be removed by using a teqnique called erosion. The principle of erosion can be seen in figure 6.2.
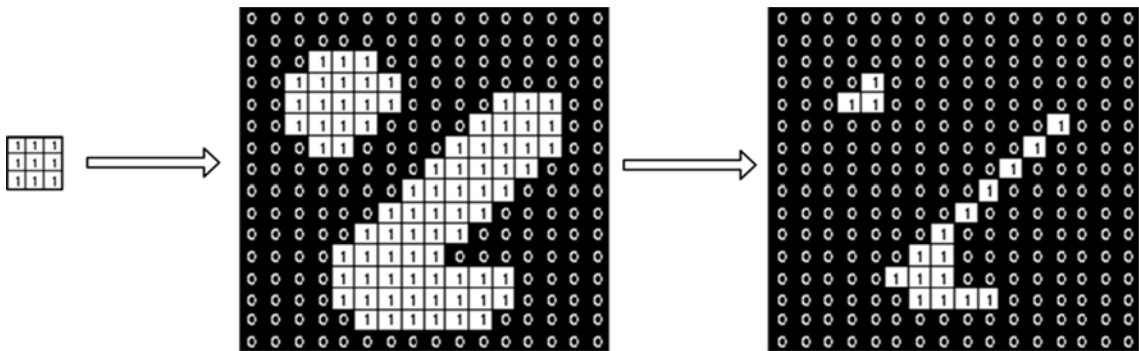

Figure 6.2: *The effect of erosion operation using a 3*3 matrix. [Gonzales et al., 2004]*

Erosion is one of the two basic operators in the area of mathematical morphology, the other being dilation. Erosion "shrinks" the object in the image and dilation "grows" the object. The erosion operator takes two sets of data as inputs. The first is the image which is to be eroded. The second is a set of coordinate points known as a structuring element. It is the structuring element that determines the precise effect of the erosion on the input image. To compute the erosion of a binary input image, the structuring element must be superimposed on top of the input image so that the origin of the structuring element coincides with the input pixel coordinates. If for every pixel in the structuring element, the corresponding pixel in the image underneath is a foreground pixel, then the input pixel is left as it is. If any of the corresponding pixels in the image are background, however, the input pixel is also set to background value. [Gonzales et al., 2004]

An erosion operation with a 8 size disk structuring element is performed on the image. This operation removes the remaining artifacts of the image, as seen in figure 6.1 (A5) and figure 6.1 (B5). However, the large white area that surrounds the body has also been eroded. In order to return this area to normal size, an dilation with the same structuring element is performed. The

result is now a logical mask with white equal to a value of 1 at the body area, and black with a value of 0 outside the body area. The result is seen in figure 6.1 (A5) and figure 6.1 (B5).

6.2   Step 2 - Mask used to extract lung areas

The next step in the segmentation process is to develop a mask that is able to segment the complete lung area, without the surounding body tissue and bone, as shown in figure 5.3 on page 33. The mask used to remove artifacts is applied on the original image, which can be seen in figure 6.3 (A1) and figure 6.3 (B1). A global threshold tecnique named Otsu's method is applied on the image in order to sort out the lung area inside the body. Otsu's method is based on treating the normalized histogram as a discrete probability density function, which can be formulated in the following equation: [Gonzales et al., 2004]

$$Pq_{rq} = \frac{N_q}{n}, q = 0, 1, 2, ..., L - 1 \tag{6.2}$$

where n is the total number of pixels in the image, N_q is the number of pixels that have the intensity level r_q and L is the number of possible intensity levels in the image. A threshold k is chosen such that C_0 is the set of pixels with levels [0,1,...,k - 1] and C_1 is the set of pixels with levels [k,k+ 1,...,L - 1]. The method is based on choosing the threshold value that maximizes the "between class variance" which is defined as: [Gonzales et al., 2004]

$$\sigma_B^2 = \omega_0(\mu_0 - \mu_T)^2 + \omega_1(\mu_1 - \mu_T)^2 \tag{6.3}$$

where:

$$\omega_0 = \sum_{k-1}^{q=0} P_q(r_q) \tag{6.4}$$

$$\omega_1 = \sum_{L-1}^{q=k} P_q(r_q) \tag{6.5}$$

$$\mu_0 = \sum_{L-1}^{q=0} q P_q(r_q)/\omega_0 \tag{6.6}$$

$$\mu_1 = \sum_{L-1}^{q=k} q P_q(r_q)/\omega_1 \tag{6.7}$$

$$\mu_T = \sum_{L-1}^{q=0} q P_q(r_q) \tag{6.8}$$

The returned value from Otsu's method is a normalized value between 0.0 and 1.0 [Gonzales et al., 2004]. However, Otsu's method is not sufficient when using a threshold teqnique in this algorithm. When applying Otsu's method on the CT scans a threshold value close to 0.0078 is measured. By applying this value as a threshold it only distinguishes between the grey and the black area. This is obviously not sufficient when trying to sort out as much as possible of the lung area. Trial and error is then performed based on the measured threshold value from Otsu's method. By picking different threshold values, a multiple of two times the located threshold value of Otsu's method was found as the most acceptable value. Thus the applied threshold value used in this step is the measured threshold from Otsu's method times two. The extracted

image with the applied threshold can be seen in figure 6.3 (A2) and figure 6.3 (B2).

The thresholded image is then inverted, which means that areas of white (value equal to 1) is inverted to black (value equal to 0) and vice versa. The step is performed in order to make the lung area white. The result is seen in figure 6.3 (A3) and figure 6.3 (B3).

As visualized in the previous step, not all of the lung tissue surrounding the lung area is black. This is due to the applied threshold in the first step of the algorithm. In order to sort this area out a smaller version of the final mask from step 1, illustrated in figure 6.1 (A5) and figure 6.1 (B5) is applied. An erosion is performed on this image with a structuring disk element at size 40 in order to obtain a smaller version of the mask. The structuring disk element at size 40 was determined by trial and error. The result can be seen in figure 6.3 (A4) and figure 6.3 (B4).

The last two extracted images are then multiplied. This means that if an area in one of the images is black the resulting color in the final image is also black. Areas in the final image will only be white if the area in both of the images is white. This operation implies a "cut off" of the body tissue and bone that surrounds the lung area. The result is seen in figure 6.3 (A5) and figure 6.3 (B5).

The small artifacts in the remaining image from the removal of body tissue and bone is removed by erosion with a structuring disk element at size 4. In order to resize the image the same structuring element is used in a dilation. The last small "holes" in the segmented lung area is removed by using a dilation with a structuring disk element at size 10. The reverse erosion with the same structuring element is afterwards applied. This operation connects the disconnected area in the anterior region. The result is seen in figure 6.3 (A6) and figure 6.3 (B6).
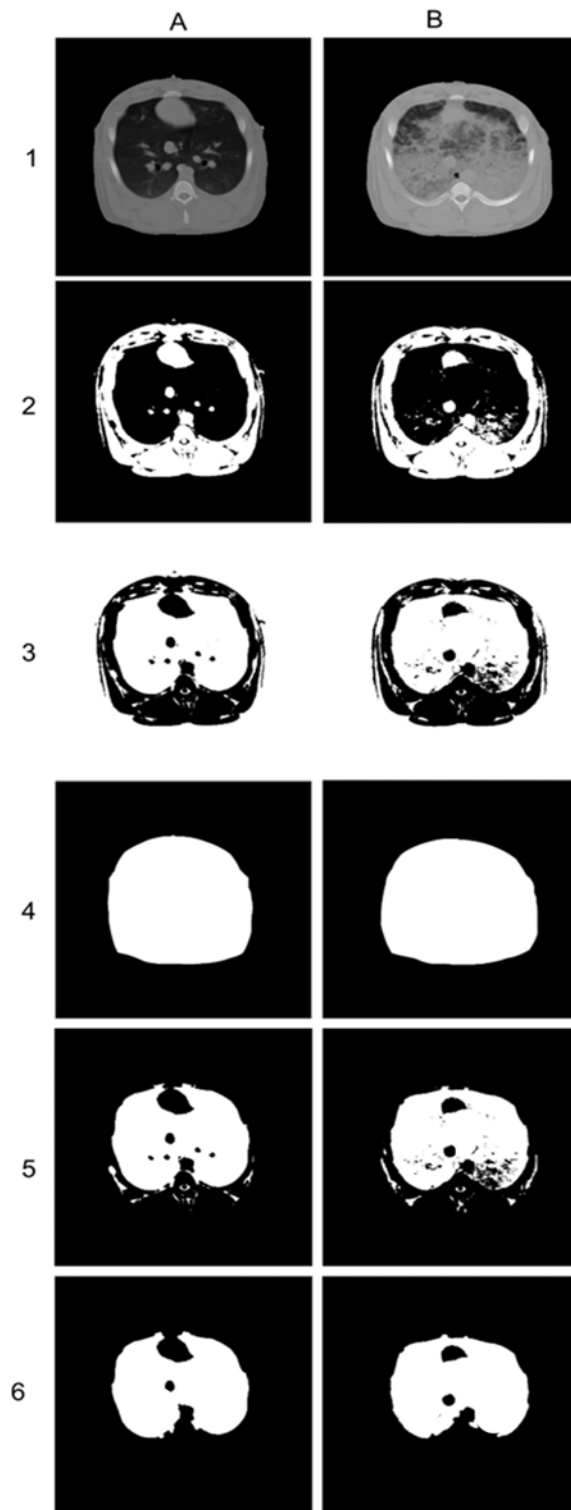
Figure 6.3: *The image segmentation algorithm used to extract "pure" lungs from the rest of the image. The segmentation process encompasses 6 different steps which are illustrated in the subimages. The final mask from step 1 is applied on the original image. This mask extracts the body from the CT scan and sorts out the artifacts, which is seen in sub figure A1 and B1. A threshold teqnique is applied on the images in order to sort out the lung area inside the body (figure A2 and B2). The images are inverted (figure A3 and B3). The mask from step 1, used to remove artifacts, is eroded with a disk structuring element at size 40 (figure A4 and B4). The masks visualized in A3/B3 and A4/B4 are multiplied (figure A5 and B5). Small artifacts have been removed with a disk structuring element at size 4 and a structuring element at size 10 (figure A6 and B6).*

6.3 Step 3 - Extraction of lung compartment values

The final masks from the two previous step is applied on the original image in order to sort out the artifacts and to extract the "pure" lung area. The extracted lung area can be seen in figure 6.4 (A1) and figure 6.4 (B1).
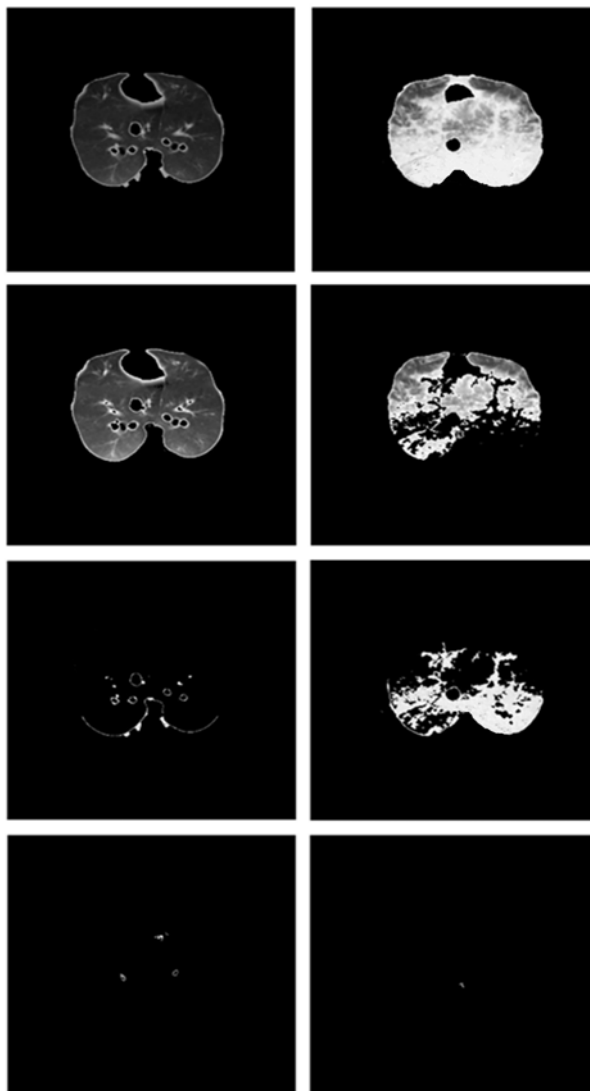
Figure 6.4: *The final mask from step 2 is applied on the original image. Sub figure A1 and B1 represents the extracted lung area. Sub figure A2 and B2 is the extracted area of the open alveoli, A3 and B3 is the collapsed alveoli and A4 and B4 is the overdistended alveoli.*

Before estimating the values of the lung compartments from the image with the segmented lungs, noise has to removed. Noise in this study is defined as unwanted snow in the image, which is almost undetectable with human eye, but can influence the final result when estimating the values from the lung compartments. A common and usefull tool for reducing unwanted snow or "salt and pepper" in images is median filtering. Median filtering is a non linear spatial filtering technique. The response is based on ordering the pixels contained in an image neighborhood

and then replacing the value of the center pixel in the neighorhood with the value determined by the ranking result [Gonzales et al., 2004]. The size of the applied median filter, used on the extracted lungs, is a matrix of 3*3.

Based on the final lung area extraction, values from the three lung compartments overdistended, open and collapsed alveoli can be estimated. The HU range from -1000 to 100 of the lung compartments, shown in figure 5.2 is used. The value from the HU range can be recalculated to pixel value by using equation 4.1 The recalculated value encompass:

- Overdistended alveoli: -1000 to -900 HU equals: 24 to 124

- Open alveoli: -899 to -100 HU equals: 125 to 924

- Collapsed alveoli: -99 to 100 HU equals: 925 to 1124

The abovementioned three different lung compartments are illustrated in figure 6.4 (A2) and figure 6.4 (B2) as the open alveoli, in figure 6.4 (A3) and figure 6.4 (B3) as collapsed alveoli and in figure 6.4 (A4) and figure 6.4 (B4) as overdistended alveoli. The two examples show that the open lung area is the most represented area in the lung. However, in example B there is a large amount of collapsed tissue. This is in full accordance with a visual inspection of the original image and with the knowledge that the CT scan is obtained from a pig with oleic acid damaged lungs.

Table 6.1 shows the percentage distribution of the different lung compartments from the two examples. In order to obtain an expression of the different lung compartments represented in

Calculated % of total area	Example A	Example B
Open	96.1	62.1
Collapsed	3.5	37.8
Overdistended	0.4	0.1

Table 6.1: The calculated values of the three different lung compartments from the two applied examples. The different values from the two examples is in full accordance with both the visual inspection of the images and with the knowledge of the clinical state of the two pigs.

the whole lung, the estimated values for all the 50 CT slices must be summed up and calculated as percentage of the full lung area. The principle of estimating the different lung compartment is visualized in figure 6.5
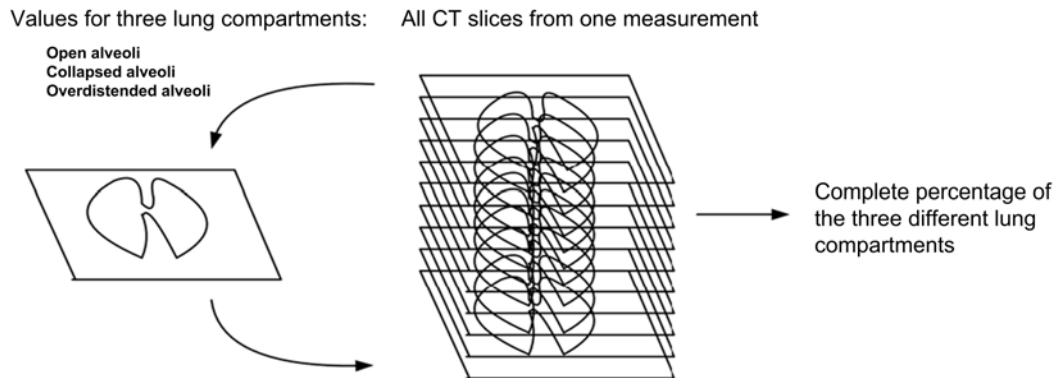
Figure 6.5: *The principle of how the total percentages of the different lung compartments are estimated. Every full CT scan of the subject contains 50 different CT slices. The segmentation algorithm is applied on every CT slice, and the percentage distribution of the different lung compartments is estimated. These estimates are summed up and a complete percentage is obtained.*

6.4 Conclusion

During this chapter the image segmentation algorithm has been developed. The algorithm is now capable of sorting out all artifacts and extract the full lung area. Based on this full lung area the percentage distribution of open, collapsed and overdistended lung area can be calculated. In order to make sure that the algorithm can be made generalizable and thereby applied on all the remaining CT slices the algorithm has to be validated. Thus the next chapter contains the validation of the algorithm.

Chapter 7

Validation of algorithm

To asure that the algorithm can segment the lung area from all the different CT slices, which varies visual depending on what position the CT slice is obtained, it has to be validated. This chapter describes the applied test strategy, the test materials, how the test is carried out and the results obtained from the test.

7.1 Validation strategy

The different masks used to extract the lung area and calculate the percentage distribution of open, collapsed and overdistended lung area were developed based on several different known image processing techniques and methods. How to use these techniques and how to find the optimal settings of the applied methods has mostly been based on trials and errors on several different CT slices. In spite of the visual effective results from those examples applied in the last chapter, the algorithm also has to be validated on CT slices that has not been a part of the development of the algorithm. This is done in order to make sure that the method is generalizable. However, a visual inspection and validation of the algorithm is not sufficient. The calculation of the percentage distribution of collapsed, normal and overdistended lung area also has to be validated. Furthermore, the absolute value of the mask area should be quantified. In order to validate both the visual segmentation process, the calculation of the percentage distribution of the alveolar states and the numerical value of the mask area, the following test strategy will be applied:

- Selection of a pig under two different conditions that has not been a part of the development of the image segmentation algorithm. Both a pig with and without experimental ARDS is selected. This is done in order to validate the algorithm in cases where alveolar states vary significantly.

- Five different CT slices are selected from the pig under the two different conditions. These CT slices are selected from five different positions of the lung where each positions shows different anatomy of the lung. The 5 CT slices also represents different positions where one might expect problems with the algorithm e.g. collapsed alveoli mistaken as tissue.

- Manual extraction of lung area from each of the selected CT slices. The manual extraction is carried out by a medical doctor experienced in using lung CT scans i.e. an expert

- Algorithm applied on each of the selected CT slices.

- Calculation of the percentage distribution of open, collapsed and overdistended lung area from the manually extracted lung area.

- Calculation of the percentage distribution of open, collapsed and overdistended lung area from the algorithm extracted lung area.

- Visual comparison of the manually extracted lung area and the algorithm extracted lung area.

- Statistical comparison of the percentage distribution of collapsed, open and overdistended lung area from the manually extracted lung area and the algorithm extracted lung area.

- Numerical comparison of the total numbers of pixels in the manually extracted lung area and the algorithm extracted lung area and numerical comparison of how the two extracted areas differs from one another.

By applying the abovementioned test strategy the algorithm is both validated visually, statistically and numerically. This makes it possible to investigate whether the algorithm can be made generalizable and thereby applied on the remaining CT slices which is the main purpose of this test.

The visual validation is the most simple method which makes it possible to investigate whether there are large differences in the way the two methods segments the lung area. By using appropriate statistical methods it is possible to investigate whether there are significant differences in the way the two methods segment the lung area. By using a numerical comparison it is possible to determine whether it is the same area that is extracted in both methods.

In order to carry out the test a medical doctor experienced in using lung CT scans will assist in segmenting the CT slices. This is done in order to ensure that the manually extracted lung area is both correctly extracted but also done by a expert that has not been a part of the algorithm design and development. The optimal validation of the algorithm should eventually have included several experienced medical doctor instead of one. By using several experts instead of one it would have been possible to investigate the variance of the manually extracted lung area and thereby have taken this into account when comparing the results. However, this validation strategy is not possible because of the time limit of the project.

7.2 Validation materials

As described in the above mentioned validation strategy, 10 different CT slices are used in the test. These 10 CT slices are selected from the same pig but within two different conditions. The first 5 CT slices are selected from a sequence before the pig is induced with oleic acid and the last 5 CT slices are selected from a sequence after induced oleic acid has been causing experimental ARDS. Both conditions with and without oleic acid are used in order to validate the algorithm in both cases. The 5 CT slices from the pig with induced ARDS is chosen among the examples with a PEEP setting of 5 cmH$_2$O, with low pause pressure and low volume. This is done in order to preserve as much collapsed tissue as possible in the lung area. The 5 CT slices from the pig without ARDS are chosen among the examples with a PEEP setting of 10 cmH$_2$O This is done to make sure that CT slices obtained with both PEEP settings are represented in the validation of the algorithm.

There are two ways of selecting the CT slices from each pig: by doing it randomly or by using manual selection. The advantage of doing it by random selection is that there is no subjective influence on how the 10 CT slices are represented. The disadvantage of random selection is that

there is a risk of selecting 10 CT slices that do not represent the variety in the data, which could lead to an insufficient test of the algorithm. This disadvantage could be avoided by a random selection of a larger sample of CT slices or by a manual selection of the CT slices. A random selection of a larger sample of CT slices is not possible because the circumstances of a segmentation of more than 10 CT slices will be too time consuming. The manual selection is in contrast to the randomly selection under very subjectiv influence. The subjective influence when the CT slices are selected can, however, be given less importance when the result are analysed. This can be done because the lung area from the manually selected CT slices are extracted by an expert that has not been a part of both the algorithm development and by the manual selection of the 10 CT slices. Thus a manual selection of the 10 CT slices is carried out.

The 5 different CT slices are selected from different positions in the body and are chosen from a full CT spiral scan which contains a total of 50 CT slices. Each of the 5 CT slices are numbered from 1 to 5 starting from apex to diaphragm. The position of CT slice number 1 from the pig with ARDS is equal to the position of CT slice number 1 from the pig without ARDS and so on. The first CT slice is the 24th CT slice starting from apex and the last CT slice is number 40. The CT slice at the 24th positon is chosen as the highest position because the first 23 CT slices starting from apex either contains litle or no lung area. The CT slice at position number 40 is also chosen as the last CT slice because the remaining 10 CT slices either contains little or no lung area. A selection of CT slices from the same position of both pig makes it easier to compare and evaluate whether the algorithm segments the lung area accurately in both healthy and damaged lungs. The "distance" between CT slice number one and CT slice number two is selected to be equal to the "distance" between CT slice number two and CT slice number three and so on.

In the following all the 10 CT slices are presented. Furthermore all the coherent values of total lung volumes and pressures are listed in table 7.1

Data from healthy Pig.

Image	Position	Healthy/OA	PEEP	Plateau Pressure	Administered Volume
1	24	Healthy	10 cmH$_2$O	38,3 cmH$_2$O	0.6 L
2	28	Healthy	10 cmH$_2$O	38,3 cmH$_2$O	0.6 L
3	32	Healthy	10 cmH$_2$O	38,3 cmH$_2$O	0.6 L
4	36	Healthy	10 cmH$_2$O	38,3 cmH$_2$O	0.6 L
5	40	Healthy	10 cmH$_2$O	38,3 cmH$_2$O	0.6 L

Data from Pig after induced OA.

Image	Position	Healthy/OA	PEEP	Plateau Pressure	Administered Volume
1	24	OA	5 cmH$_2$O	7,7 cmH$_2$O	0.1 L
2	28	OA	5 cmH$_2$O	7,7 cmH$_2$O	0.1 L
3	32	OA	5 cmH$_2$O	7,7 cmH$_2$O	0.1 L
4	36	OA	5 cmH$_2$O	7,7 cmH$_2$O	0.1 L
5	40	OA	5 cmH$_2$O	7,7 cmH$_2$O	0.1 L

Table 7.1: The 10 different CT slices, from the pig with and without induced OA, with coherent values of PEEP, pressure and volume.
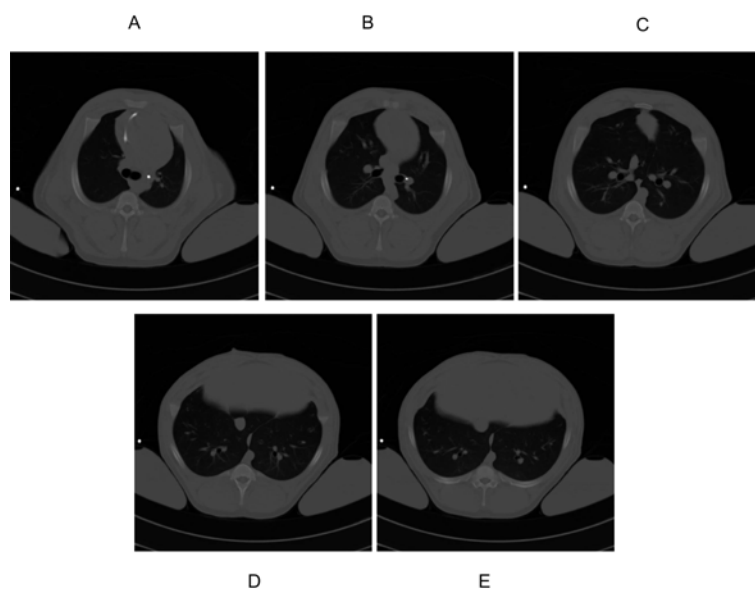
Figure 7.1: *The 5 different CT slices from the healthy pig. The CT slices are obtained from different positions in the body. Image A is equal to position 24, out of a total CT slices of 50, counted from apex to diaphraghm. Image B is equal to position 28. Image C is equal to position 32. Image D is equal to position 36 and image E is equal to position 40. All 5 represented CT slices are obtained from the same full body scan.*

Figure 7.2: *The 5 different CT slices from the pig with experimental ARDS. The CT slices are obtained from different positions in the body. Image A is equal to position 24, out of a total CT slices of 50, counted from apex to diaphraghm. Image B is equal to position 28. Image C is equal to position 32. Image D is equal to position 36 and image E is equal to position 40. All 5 represented CT slices are obtained from the same full body scan.*
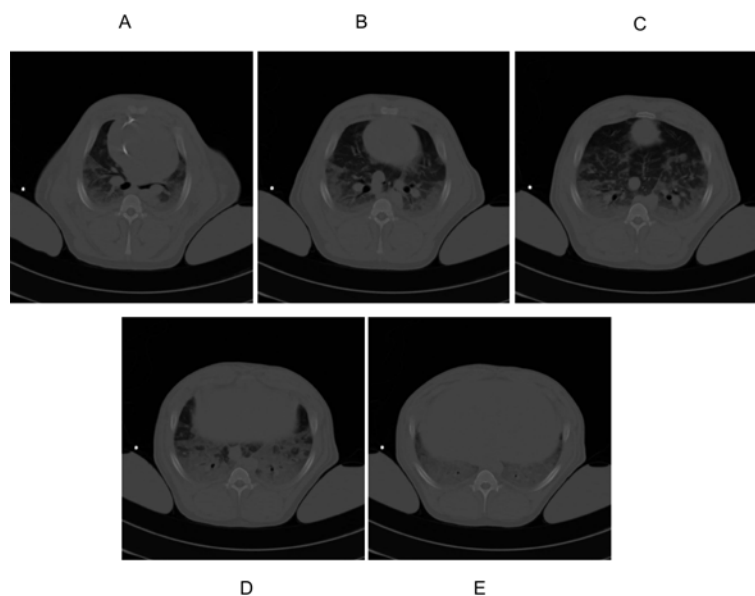
47

7.3 Manual segmentation process

The manual extraction performed by the expert is carried out by using a Matlab function called *Roipoly*. This function allows the expert to interactively mark an innumerable numbers of points on an image. The function generates a logical mask with white (equal to 1) inside the selected region of interest and black (equal to 0) outside the region. This extracted mask is applied on the original CT slice. Based on the extracted lung area the percentage distribution of open, collapsed and overdistended lung areas are calculated. This is done in the same way as with the algorithm extracted areas.

7.4 Results and analysis

As described in the validation strategy, both a visual, statistical and numerical comparison of the algorithm has to be performed. The next three sub sections describes the results and analysis of these three comparisons.

Visual comparison of extracted lung area

In the following sub section all the extracted lung areas from the algorithm and the manual segmentation are visually compared. Figure 7.3 and figure 7.4 illustrate the 10 different CT slices and the manually and algorithm extracted area. The first column in the two figures is the original CT slices. The second column is the manually extracted area and the last column is the algorithm extracted area. Figure 7.3 is the five CT slices from the healthy pig. Figure 7.4 is the five CT slices from the pig with induced OA.

When comparing the manually and algorithm extracted areas it can be seen that there is a difference in the way the top of the lung area is segmented. Two examples of this issue can be seen in figure 7.5. In the manually segmented CT slices the border in the top of the lung area is more like a clear cut with a sharp edge. This is not the case in the CT slices segmented by the algorithm. This can be due to the erosion technique applied when the final mask was developed. The erosion teqhnique always tend towards softening sharp edges. This difference in the segmention proces is only an issue in the top of the lung area. In order to investigate whether this last erosion teqnique applied in the algorithm causes a larger source of error than if it was left out, the following sub test will be applied: The original algorithm is applied on CT slice number 1, which is the CT slice that seems to be mostly affected by this softening sharp edges. Furthermore, the original algorithm is modified with the last erosion technique left out and afterwords applied on CT slice number 1. The two different masks used to extract the lung area from the same CT slice are compared and visualized in figure 7.6. An inspection of the image shows that the mask without the last erosion technique applied seems to keep a large amount of small artifacts surrounding the lung area. This is not the case in the mask extracted by the original algorithm. However, the mask without the last erosion technique applied, also seems to avoid the softening of the sharp edges in the top of the lung. It is however, considered that the mask from the original algorithm extracts the lung area in a more accurate way than by leaving out the last erosion technique.

Another dissimilarity between the algorithm and the manual segmentation is how to leave out the large vessels. In figure 7.7 an example of one of the CT slices illustrates how the difference in the segmentation process looks like.

Figure 7.3: *The figure compares the manual extraction of the lung area with the extraction from the algorithm of the five CT slices from the healthy pig. The column of sub figures in A is the original images, column B is the manual extracted lung areas and column C is the algorithm extracted lung areas.*
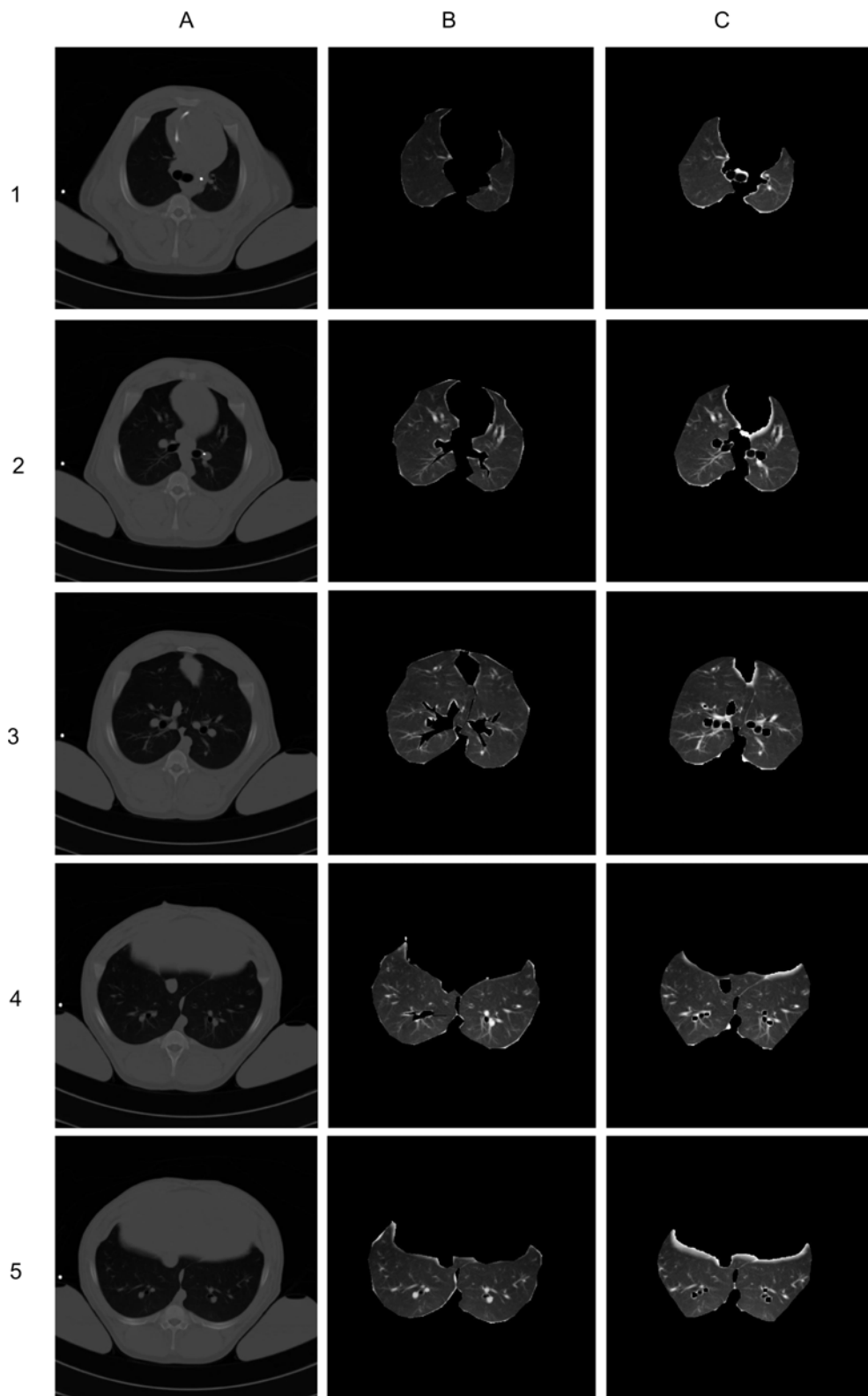
Figure 7.4: *The figure compares the manual extraction of the lung area with the extraction from the algorithm of the five CT slices from the pig with experimental ARDS. The column of sub figures in A is the original images, column B is the manual extracted lung areas and column C is the algorithm extracted lung areas.*
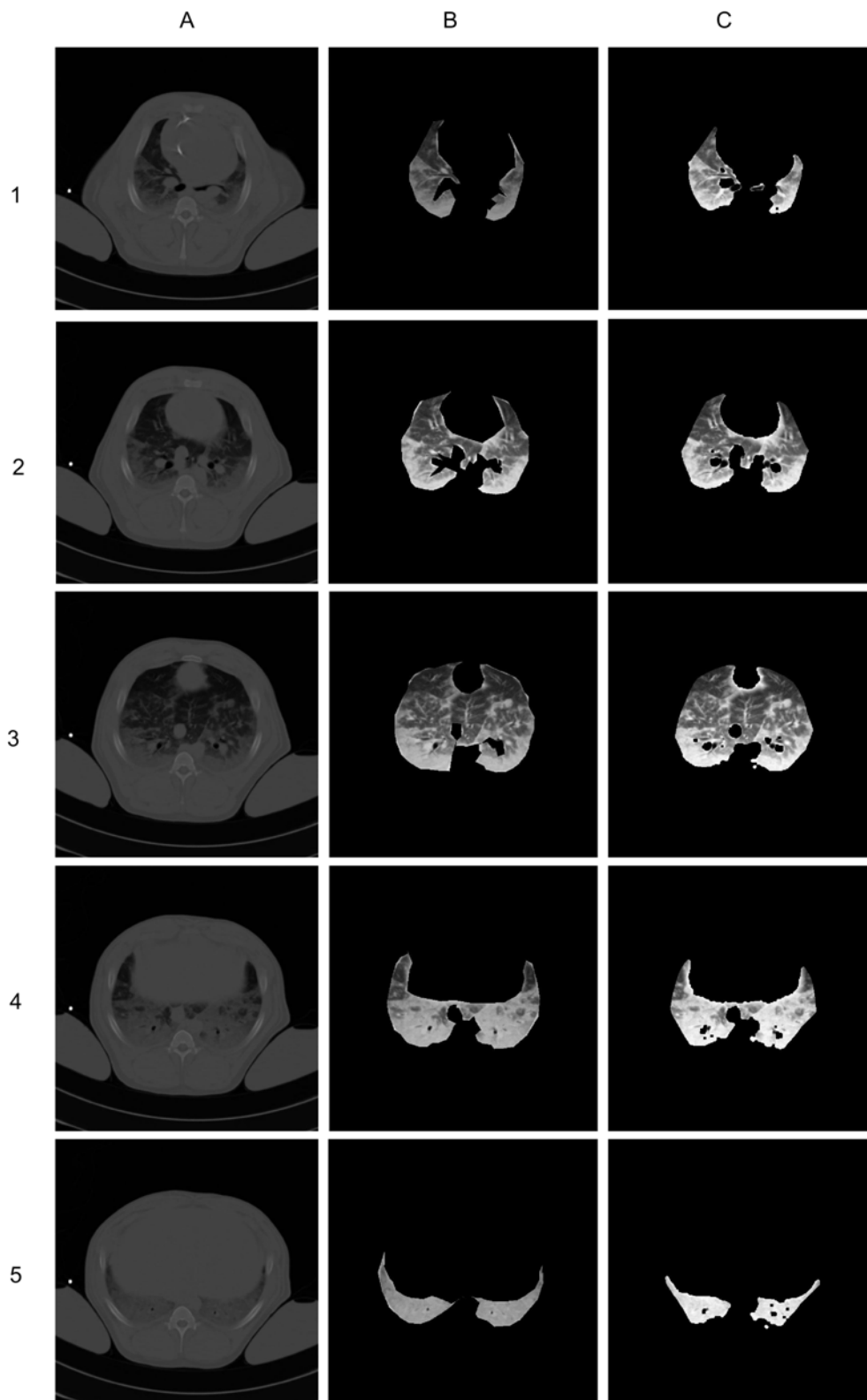
Figure 7.5: *The figure shows the difference in the manual and algorithm segmention of the lung area. The red dotted circles marks the difference in the manual and algorithm segmention process. The manual segmention which is the CT slices in the second column (figure B) illustrates a more sharp edges in the top of the lung area. The last column (figure C) is the algorithm segmented CT slice. This extracted lung area illustrates a more soft edge in the top of the lung. The first column (figure A) illustrates the original CT slices.*
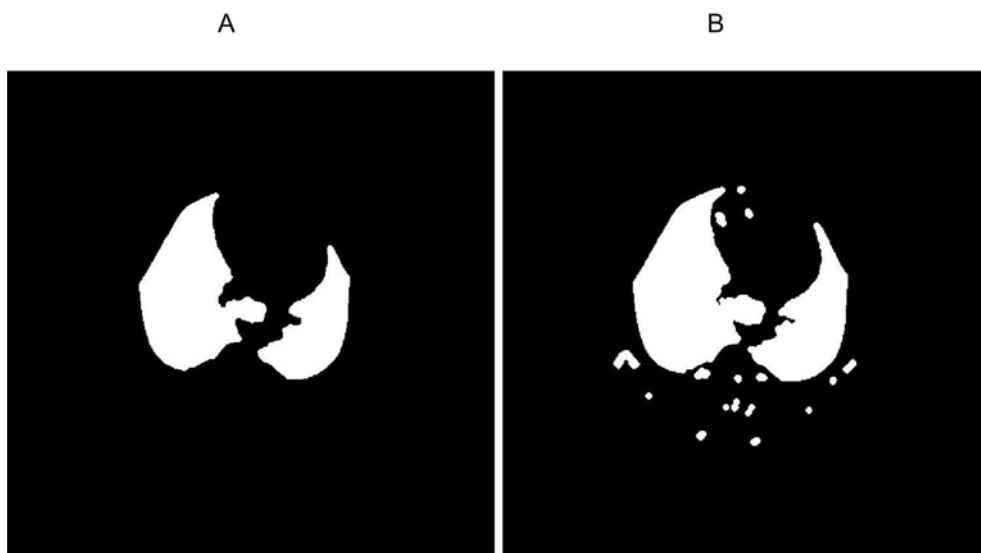
Figure 7.6: *The figure shows the two different masks from CT slice number one. Sub image A is the mask from the original algorithm. Sub image B is the mask from the modified algorithm, which is the original algorithm without the last erosion technique applied. As described in the text the last erosion technique tend towards softening the sharp edges of the top the lungs. However, it is considered that this softening of the sharp edges not will cause a large source of error than if it was left out.*
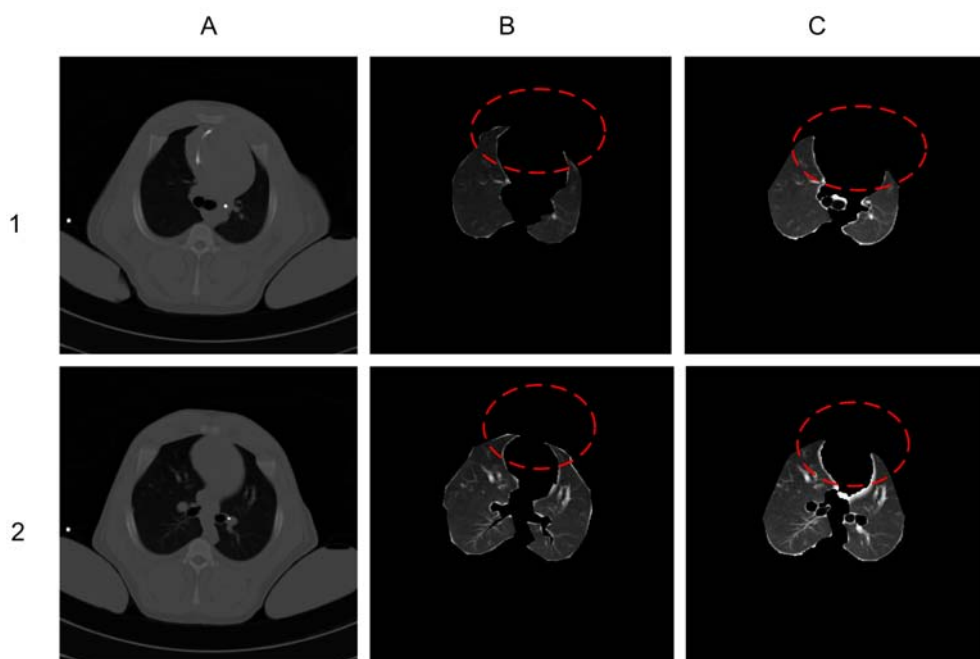
51

Figure 7.7: *The figure shows the difference in the manual and algorithm segmention of the lung area. The red dotted circles marks the difference in the manual and algorithm segmention process. The manual segmention which is the CT slices in the second column (B) illustrates how almost all of the large vessels is sorted out. The last column (C) is the algorithm segmented CT slice. This extracted lung area illustrates that not all of the large vessels is sorted out. The first column (A) illustrates the original CT slices.*
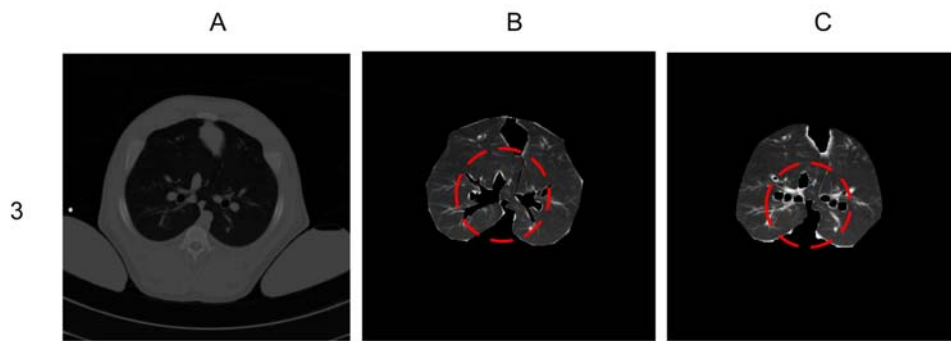
In the manual extracted lung area (figure 7.7B) it can be seen that all large vessels are sorted out. This is not the case in the lung area segmented by the algorithm (figure 7.7C). Not all vessels, especially not the small ones are sorted out. However, the small vessels are not always sorted out by manual segmentation either. As shown in figure 7.3 and in figure 7.4 almost all of the algorithm segmented area has no large vessels left. However, the small vessels still remain in both the manual and algorithm extracted area. The small vessels could be a possible source of error when segmenting the CT slices. This will affect the estimated value of collapsed tissue since the vessels consists of soft tissue and thereby covers the HU range of collapsed tissue, which can be seen in figure 5.2 on page 32.

Statistical comparison of extracted lung area

The algorithm has now been evaluated by eye by comparing the algorithm extracted lung area with the manually segmented lung area. However, this way of evaluating the algorithm is not sufficient. The distribution of open, collapsed and overdistended lung area now has to be estimated from both segmented lung areas. By evaluating and comparing these values it would be possible to determine whether there is a significant difference in the way the two metods segment the lung area.

The segmented lung areas from both the manual segmentation and the algorithm are recalculated as the percentage distribution of open, collapsed and overdistended lung area. This is done in the same way in both methods by recalculating the HU range, shown in figure 5.2 on page 32 as pixel values. All the extracted values are listed in table 7.2 which is divided into the three different lung compartments. Appropriate statistical methods also has to be applied in order to investigate the residuals between the obtained results. A common way of evaluating and comparing two measurement techniques is by using the Bland Altman plot. The Bland Altman plot is a statistical method for assessing agreement between two methods of measurement. In the Bland Altman method the differences between the values measured by two techniques are plotted against their averages. The plots can be seen in figure 7.8.

Image number	Open (Manual)	Open (Algorithm)	Difference	Sign
1 - Healthy	98.5%	97.1%	1.4%	+
2 - Healthy	97.1%	95.5%	1.6%	+
3 - Healthy	98.5%	98.5%	0%	
4 - Healthy	97.5%	97.4%	0.1%	+
5 - Healthy	98.0%	98.6%	0.6%	-
6 - OA	75.7%	80.8%	5.1%	-
7 - OA	88.6%	89.3%	0.7%	-
8 - OA	86.7%	88.2%	1.5%	-
9 - OA	68.1%	67.5%	0.6%	+
10 - OA	50.4%	45.5%	4.9%	+
Mean difference:	0.07%			
Image number	**Collapsed (Manual)**	**Collapsed (Algorithm)**	**Difference**	**Sign**
1 - Healthy	0.4%	1.2%	0.8%	-
2 - Healthy	0.4%	1.7%	1.3%	-
3 - Healthy	0.3%	0.6%	0.3%	-
4 - Healthy	2.0%	1.9%	0.1%	+
5 - Healthy	1.2%	0.9%	0.3%	+
6 - OA	24.2%	19.0%	5.2%	+
7 - OA	11.3%	10.0%	1.3%	+
8 - OA	13.1%	11.5%	1.6%	+
9 - OA	31.8%	32.4%	0.6%	-
10 - OA	49.6%	54.5%	4.9%	-
Mean difference:	0.06%			
Image number	**Overdistended (Manual)**	**Overdistended (Algorithm)**	**Difference**	**Sign**
1 - Healthy	1.0%	1.6%	0.6%	-
2 - Healthy	2.3%	2.8%	0.5%	-
3 - Healthy	1.2%	0.7%	0.5%	+
4 - Healthy	0.4%	0.5%	0.1%	-
5 - Healthy	0.8%	0.4%	0.4%	+
6 - OA	0.1%	0.9%	0.8%	-
7 - OA	0%	0.5%	0.5%	-
8 - OA	0.1%	0.1%	0%	
9 - OA	0.1%	0.1%	0%	
10 - OA	0%	0%	0%	
Mean difference:	-0.16%			

Table 7.2: Data from the algorithm and manual segmentation.
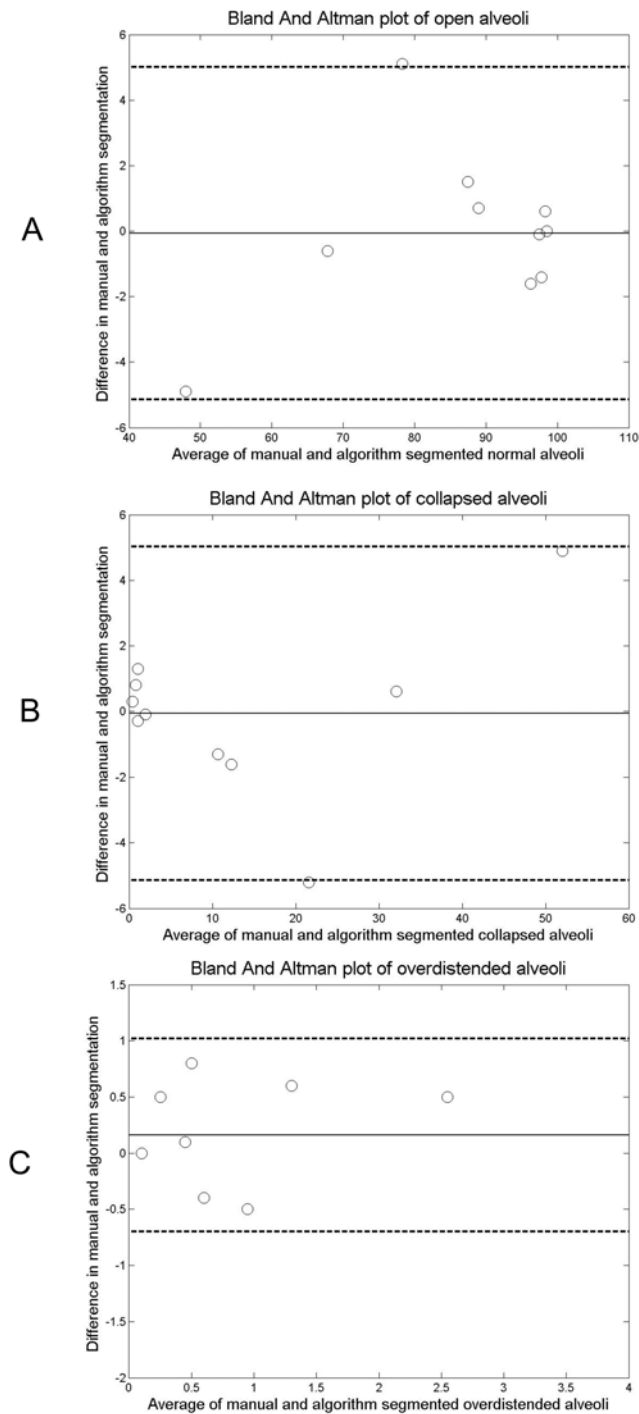
Figure 7.8: *The figure illustrates the Bland Altman plots comparing the extracted values from the algorithm and by manual segmentation. Sub figure A is the plot showing the open lung tissue. Sub figure B is the collapsed tissue and sub figure C is the overdistended lung tissue. The x-axes are the average value of the manually and algorithm segmented lung tissue. The y-axes are the difference between the manually and algorithm segmented lung tissue. The dotted lines are the limits of agreement which is twice the standard deviation of differences. The solid lines shows the mean difference. An inspection of the three plots shows that there is one point, in sub plot A and B, outside the standard deviation of differences.*

Horizontal lines are drawn at the mean difference, and at the mean difference plus and minus 2 times the standard deviation of the differences. An inspection of the three sub plots shows that almost all the plotted differences, except for one outlier, lies within the the 95 % confidence interval. The outlier in sub plot A and B turns out to be CT slice number 6, which can be seen in figure 7.4A. This is not in full accordance with the visual inspection when comparing the two different segmentation methods. An inspection of the segmentation from CT slice number 6 in figure 7.4A shows that there are some differences between the two segmented lung areas. However, the visual inspection of the two segmented lung area does not seem to cause such a significant difference that causes the observed outlier in the Bland Altman plot. The differences can probably be caused by a displacement in the two segmented lung areas. If this is the case the two segmented lung areas still tend to look alike, but the difference in the total percentage of the three lung compartments can be significantly different. Further inspection of this issue is carried out in the numerical comparison and analysis of the two methods.

Inspection of all three plots shows that there are no cases of a proportional error or cases where the variation of at least one method depends strongly on the magnitude of measurements. Furthermore, the plots shows no sign of bias except a small bias in plot C. The three different Bland Altman plots indicate that the algorithm is capable of an accurate segmentation of the lung area.

In order to evaluate the statistical significance of the differences between the manually and algorithm segmented lung area another statistical method has to be applied. Two different methods of testing the difference between paired observations from two populations is the Wilcoxon signed rank test and the paired sample t test. The Wilcoxon signed rank test is the nonparametric counterpart of the paired sample t test, and does thereby not assume normal distribution. In order to investigate whether the data are normally distributed the data in column 4 from table 7.2 on page 53 are plotted as histograms. The histograms can be seen in figure 7.9.
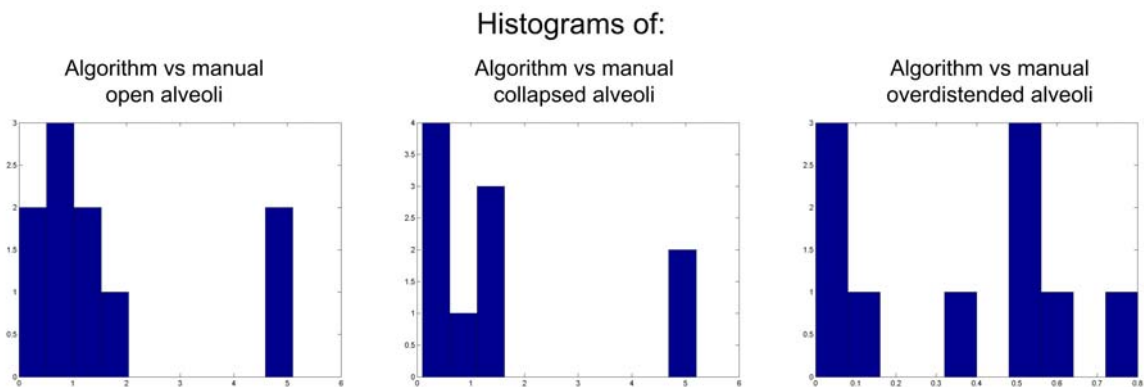
Figure 7.9: *The figure illustrates the histograms of the differences between the segmented areas from the manual segmentation and the algorithm segmentation. The figure is divided into open area (left sub figure), collapsed area (Sub figure in the middle) and overdistended area (right sub figure). As the histograms show there are no signs of normal distribution in either sub figure. Thus a non parametric statistical method as Wilcoxon signed rank test is applied.*

As the three different histograms shows the data are not normally distributed which means that the Wilcoxon signed rank test should be applied instead of the paired sample t test.

The steps involved in applying the Wilcoxon signed rank test are:

- Determine the difference for each sample pair.

- Arrange the absolute value of these differences in order, assigning a rank to each.

- Let T_+ = sum of the ranks having a positive value and T_- = sum of the ranks for the negative values.

- T_+, T_- or T = minimum of T_+ and T_- is used to determine a test of H_0 or H_1 using table look up.

The null hypothesis in this test is that the differences between the pairs of observations listed in table 7.2 is zero, which means that there is no difference in using the algorithm or the manual segmentation. Thus, a null hypothesis and the alternative hypothesis can be formulated:

- H_0: The population differences are centered at 0

- H_1: The population differences are not centered at 0

The null hypothesis is rejected at the significance level at $p \leq 0.05$. The test statistics of the Wilcoxon signed rank test can be seen in table 7.3. Based on the test statistics from the table it can be concluded that there is no significant difference in using the algorithm or the manual segmentation.

Open lung area - Algorithm vs. manual

Differences	N	Rank sum	Median dif.	95% conf.	P
Negative	4	21.5	0.1	-1.8 to 1.7	0.9336
Positive	5	23.5			
Zero	1				

Collapsed lung area - Algorithm vs. manual

Negative	5	27	0.0	-1.7 to 2.0	1.0000
Positive	5	28			
Zero	0				

Overdistended lung area - Algorithm vs. manual

Negative	5	22	-0.2	-0.5 to 0.2	0.2188
Positive	2	6			
Zero	3				

Table 7.3: Test statistic from the Wilcoxon signed rank test.

Numerical comparison of extracted lung area

The algorithm has now been evaluated by eye and by statistical methods. In order to investigate whether the manually and algorithm segmented lung areas represents the "same" areas a numerical analysis is applied. The concept of the numerical comparison is visualized in figure 7.10.
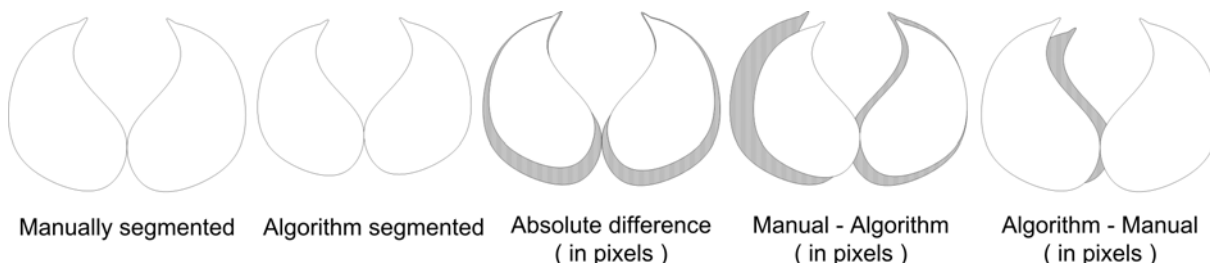

Figure 7.10: *The figure illustrates the principle of how the different numerical values are extracted. The total number of pixel are estimated from both the manually and algorithm segmented lung area. Those two estimated values are subtracted in order to investigate the difference in size of the two segmented lung area. The two last values are total pixel value of: the algorithm segmented area with subtracted manual segmented area. Total pixel value of: manual segmented area with subtracted algorithm segmented area. The grey area represents the numerical value.*

As the figure shows there are three different numerical values that will be estimated based on the total amount of pixels in the segmented lung areas. The total difference between the number of pixels in the manually and algorithm segmented lung areas, will indicate whether there is an agreement between the size of the two segmented lung areas. However, this value does not indicate whether the two segmented lung areas are located within the same position. In order to investigate this, the two segmented masks of the lung areas are subtracted from one another. The first test is where the extracted lung area from the algorithm is subtracted from the lung area segmented manually. The second test is where the lung area segmented manually is subtracted from the algorithm extracted lung area.

Table 7.4 contains all estimated values from the numerical analysis. In order to evaluate whether

Image number	Manuel (In pixel)	Algorithm (In pixel)	Difference	Difference in %	Manual - Algorithm	Algorithm - Manual
1	19259	19549	-290	1.4	2838	3128
2	29247	28105	+1142	4.0	4806	3664
3	40918	40175	+743	1.8	5132	4389
4	38866	36259	+2607	6.7	8013	5406
5	34843	32018	+2825	8.1	7506	4681
6	14145	14368	-223	1.6	3072	3295
7	24675	25698	-1023	4.0	3345	4368
8	39820	38204	+1616	4.1	4966	3350
9	24434	23237	+1503	4.8	4727	3224
10	11055	10036	+1019	9.2	3296	2277

Table 7.4: Data from the algorithm and manual segmentation.

there is a significant statistical difference between the residuals in table 7.4 column 4 a wilcoxon signed rank test is applied. Thus, a null hypothesis and the alternative hypothesis can be formulated:

- H_0: The population differences are centered at 0

- H_1: The population differences are not centered at 0

The null hypothesis is rejected at the significance level at $p \leq 0.05$. The result of the test is P = 0.0371 which means that there is a significant difference between the estimated pixels from the manually and algorithm extracted lung area.

As the values from the table in column 4 shows, the lung area segmented manually is in seven out of ten cases larger than the area segmented by the algorithm. In those cases where the algorithm segments a larger area than by manual segmentation are in CT slices number 1, 6 and 7. The number of pixels in the remaining CT slices number 2, 3, 4, 5, 8, 9 and 10 are larger in the manually segmented lung area than by the algorithm. In CT slices number 1 and 6 the differences are within a few hundred pixels. This is not the case in CT slice number 7 where the difference in pixel amount is above 1000. An inspection of CT slice number 7 in figure 7.4 shows that in the manual segmentation a more "rough" segmentation of the vessels has been applied than in the other manually segmented areas. In those cases where the manually segmented lung area is larger than by the algorithm it can be seen that the shape of the border in the algorithm segmented lung area has become more soften with no sharp edges. The significant difference between the total number of estimated pixels in the extracted and manually segmented lung area is posible because the two methods does not both segmented the lung area with the same errors.

7.5 Conclusion

During this chapter the image segmentation algorithm has been tested and validated. The validation of the algorithm encompasses both a visual, statistical and numerical test. The visual validation, which was a qualitative test was applied in order to investigate whether there are large differences in the way the two methods segments the lung area. The statistical method was applied in order to investigate whether there are significant differences in the way the two methods segment the lung area. The numerical test was applied in order to determine whether it is the "same" area that is extracted in both methods.

The test was carried out by letting a medical doctor experienced in using lung CT scans manual segment ten different lung areas from CT slices. These ten manual segmented lung areas was used as "optimal" references when comparing with the algorithm segmented lung area. As mentioned in the start of this chapter the optimal validation of the algorithm should eventually have included several experienced medical doctor instead of one. By using several experts instead of one it would have been possible to investigate the variance of the manually extracted lung areas and thereby have taken this into account when comparing the results. However, this validation strategy was not possible because of the time limit of the project.

The manual segmentation method is not without disadvantages. It is a very subjective method, which relies on the expert's knowledge, experience and awareness. In order to segment the lung

area in the most exact way the method needs a large number of fixpoints around the border of the lung area. By using an innumerable number of fixpoints it is most likely that the segmented lung area would represent the "true" lung area. These fixpoints marked by the expert have to be marked very accurately between the lung area and the surrounding tissue in order to avoid error sources. If the distance between the fixpoints is "too large" it could cause that some area close to the border are sorted out.

Another problem regarding the segmentation method, which both counts for the manual segmentation and the algorithm, is that when it comes to sorting out the small vessels in the lung area the two methods becomes inapplicable. The manual method allows marking of the large vessels but becomes inaplicable when it comes to sorting out the small vessels because of the size of the vessels, which are within a few pixel. This means that an accurate marking of this area is almost impossible. The algorithm is also inaplicable to sorting out these small vessels because of its insufficient ability to differentiate between collapsed tissue in the lung area and the small vessels. The consequence of keeping the small vessels in the segmented lung area is that they constitute a possible source of error when segmenting the CT slices. This will affect the estimated value of collapsed tissue since the vessels consists of soft tissue and thereby covers the HU range of collapsed tissue. Since both the manual segmentation and the algorithm are not capable of sorting out all vessels no reference of correct segmentation is acchieved. This makes it very difficult to determine to what extent the source of error is significant.

The visual comparison af the algorithm and manually segmented lung areas showed that in general the two different segmented lung areas agree well. However, there are some sub areas in the segmented lung areas that differs from the two segmentation methods. Especially in the way the top of the lung areas is segmented. In the manually segmented lung area the border in the top of the lung area is more like a clear cut with a sharp edge. This is not the case in the CT slices segmented by the algorithm. As described in the test results this issue could be due to the erosion technique applied when the final mask was developed. The erosion technique always tends towards softening sharp edges. One could argue that the final erosion technique should be left out in the algorithm in order to avoid this softening of the edges. However, by leaving out this erosion technique the small artifacts surrounding the lung area will not be removed. The source of error is considered to be in a larger scale if the last erosion tecnique was left out, which also was shown in a visual example in the test.

During the test it has also been shown that there is a significant difference between the total number of estimated pixels in the extracted and manually segmented lung area. It is assumed that this difference in the total number of pixels not necessarily means that the algorithm cannot segment the "real" lung area. If this difference in pixels should have been within an acceptable range it would have included that both methods should have segmented the lung area with the same errors.

Throughout the development of the algorithm several different techniques in classical image analysis and processing have been applied. Among those are erosion and dilation techniques and Otsu's threshold method. Most of the settings and values of the applied methods and techniques were obtained by trial and error. The examples used in the development of the algorithm showed that the different developed masks used in the algorithm could segment the lung area from CT slices in an accurate and effective way. Throughout this chapter examples of CT slices from another pig were analysed. The different trial and error settings obtained in the development process of the algorithm proved to be appropriate settings in the examples used in this test.

To summarize the results from the different applied tests: There is a significant difference between the total number of estimated pixels in the extracted and manually segmented lung area. The algorithm is not capable of correct segmentation of "sharp edges" in the top of the lung area, which is due to the last applied erosion technique. The algorithm is furthermore not capable of sorting out all vessels in the lung area because of its insufficient ability to differentiate between collapsed tissue in the lung area and the small vessels. Both of these issues could cause wrong estimates of the total lung area. However, these possible wrong estimates are still considered to be within an acceptable range. Thus, it can be concluded that the algorithm can be generalized and thereby applied in all remaining CT slices with the same obtained trial and error settings.

During this part of the project the CT slices has been used to gain information regarding the alveolar states of the lung. The subsequent part of this project describes how the remaining PV curves from the data materials are analyzed in order to obtain knowledge of the lung mechanics.

Part IV

Modelling the alveolar states based on static PV curves

Chapter 8

Model based on alveoli compartments

The main purpose of this report is to investigate whether there is a relationship between the alveolar states extracted from CT slices and the alveolar states simulated by the model based on alveoli compartments. During the previous part the image segmentation algorithm has been presented and validated which is intended to extract alveolar states from CT slices. This part of the report describes how the model based on alveoli compartments, which has been introduced in the Introduction and Analysis part, can be used to simulate the distribution of alveolar states based on the static PV curves. As mentioned in the Introduction and Analysis part the information obtained from the simulations of alveolar states could be usefull in clinical practice because an optimal compromise between optimizing gas exchange and avoiding overdistension and atelectasis could be obtained. In order to understand and afterwords use the model to fit to static PV data and simulate the alveolar states the model should be described in physiological and mathematical terms. Thus, this chapter describes the model and its parameters and how it is capable of simulating the alveolar states.

8.1 Alveoli states and gas exchange

In 2005 Smith et al. presented a compartment model of the lungs based on a physiological interpretation of lung function. The model, which is entended to use in clinical practice, was built on the assumption of alveoli beeing in three different states, overdistended, normal or collapsed, which are the same different states previously extracted from the CT slices. A schematic wiev of how the model links the relationship between lung mechanic and gas exchange can be seen in figure 8.1. The collapsed alveoli is included in the pulmonary shunt fraction (f_s) which is equal to the total fraction of cardiac output flowing through the pulmonary circulation but not involved in the gas exchange. Overdistended alveoli (V_d) can press the pulmonary capillaries together and thereby cause a limiting perfusion to that region of the lung. The overdistended alveoli are therefore added to the total dead space volume that encompasses open alveoli that are not perfused. [Despopoulos and Silbernagl, 2003]. The open alveoli account for the remaining alveoli that are both ventilated and perfused. [Smith et al., 2005]
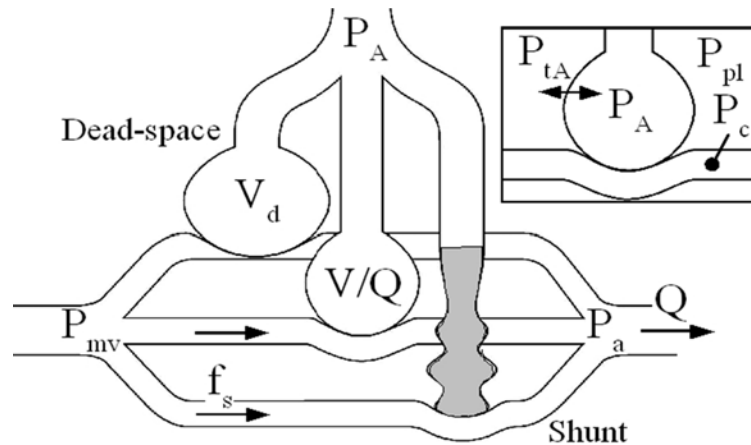
Figure 8.1: *The figure illustrates a schematic wiev of the alveoli beeing in three different states, overdistended (V_d), normal (V/Q) or collapsed (f_s). The small sub figure shows the pressure that acts on 1 alveoli. [Smith et al., 2005]*

8.2 Hydrostatic effect

The hydrostatic effect on pleural pressures which is the weight of the lungs and blood pressing down is also built into the model and can be explained by the schematic view in figure 8.2 Due to hydrostatic effect the pleural pressures (P_{Pl0}) decreases higher in the lungs and therefore over distension generally occurs first at the top of the lungs. Alveoli collapse, however typically occurs first at the bottom of the lungs where the pleural pressure acting on the outside of the alveoli, is highest.
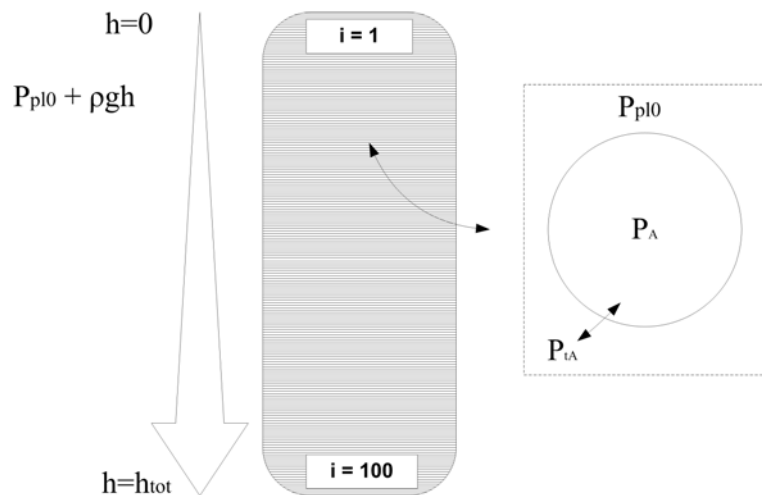

Figure 8.2: *A schematic view of the hydrostatic effect on pleural pressures.*

8.3 Alveolar PV relationship

In order to calculate the volume in the lungs the model uses a PV relationship assigned to each individual alveoli. Each alveoli in the model are asumed to have the same maximum volume and uses the same PV relationship which is illustrated in figure 8.3. This allows the volume
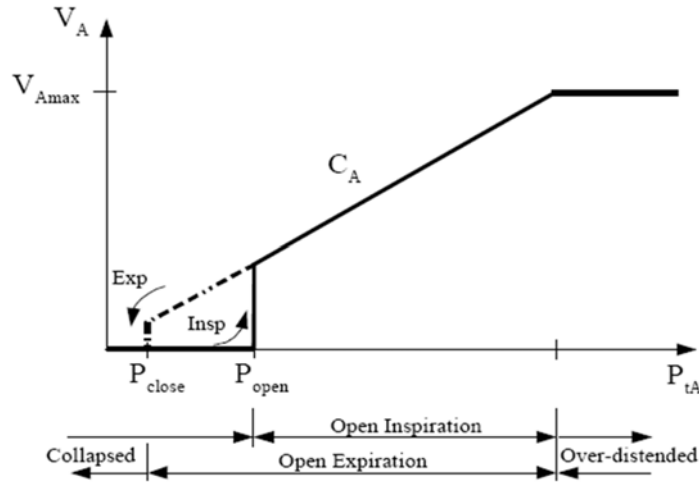
Figure 8.3: *The figure illustrates the PV relationship used in the model. P_{open} is the pressure above which the alveole will open during inflation. P_{close} is the pressure below which the alveoli will close during deflation. C_A is the compliance of the alveoli which are open. V_{Amax} is the maximum alveoli volume at which the alveoli becomes overdistended. [Smith et al., 2005]*

and state of each alveoli to be determined depending on the trans alveoli pressure ($P_{tA,i}$) that acts across the alveoli wall. The trans alveoli pressure at a certain height (h_{tot}) in the lungs is equal to the difference in pressure across the alveoli wall which can be calculated by using the following equation:

$$P_{tA,i} = P_A - (P_{Pl0} + \rho \cdot g \cdot h_{tot}) \tag{8.1}$$

Where P_A is the pressure in all the open alveoli, P_{Pl0} is the pleural pressure at the top of the lung, ρ is the density in the lungs, h_{tot} is the height of the lung and g is the gravity.

At a given pressure the total volume of the lung can be calculated by adding the volumes of all the alveoli. The static PV curve can be determined by calculating the total lung volume at a range of pressures.

The PV relationship for one alveoli during inspiration is defined as:

$$V_{A,i}(P_{tA.i}) = \begin{cases} 0, & P_{tA,i} < P_{open} \\ \\ f(P_{tA}) & P_{open} < P_{tA.i} < \frac{V_{Amax}}{C_A} \\ \\ V_{Amax} & \frac{V_{Amax}}{C_A} < P_{tA,i} \end{cases} \tag{8.2}$$

where f(P_{tA}) is the PV relationship in the normal open alveoli. This function is defined in the following equation and assumed to be linear:

$$f(P_{tA}) = P_{tA} \cdot C_A \tag{8.3}$$

The inspiratory PV curve can then be explained by using the above mentioned equations and figure 8.3. If $P_{tA.i}$ is less than P_{open} then the volume is equal to zero and the state of the alveolus

is collapsed. This means that if total value inside the enclosed brackets in equation 8.1 is higher than the pressure in the open alveoli, the alveolus will collapse. If $P_{tA.i}$ increases above P_{open} the linear PV relationship in equation 8.3 is applied. If the volume increase greater than V_{Amax} the alveolus becomes overdistended which means that a further increase in pressure not will cause an increase in volume. The parameter setting of P_{open} and V_{Amax} defines the limit at which the alveoli collapses or becomes overdistended. P_{open} is further described in section 8.5. V_{Amax} is defined as:

$$V_{Amax} = V_{max}/N_A \qquad (8.4)$$

Where V_{max} is the total lung volume and N_A is the total number of alveoli. Thus V_{Amax} depends on the defined maximum lung volume and the total number of alveoli. V_{max} and N_A are further described in the Model parameter section.

The model simulation of expiration only uses the alveoli that are opened during inspiration. The expiration can also be explained by figure 8.3. If the trans alveoli pressure of one alveoli at end-expiration is above P_{close} but less than P_{open} it remains closed. If the alveoli is open it will not close until the pressure decreases beneath P_{close}. [Smith et al., 2005]

8.4   Lung PV relationship

The total lung volume under any given airway pressure can be calculated in the following manner:

$$V_L(P_A) = V_{offset} + \sum_{i=1}^{N_c} V_{A,i}(P_{tA,i}) \cdot \frac{N_A}{N_c} \qquad (8.5)$$

where V_{offset} is the volume of the lungs when all alveoli are collapsed. N_C is the number of compartments the lung is divided in. N_A is the total number of alveoli. [Smith et al., 2005]

8.5   Model parameters

The model includes a number of parameters which have been introduced and described during the previous sections. The parameters are summarized in table 8.1 where normal healthy human values also are shown. N_A equal to 300 milion is specified by Despopoulus [Despopoulos and Silbernagl, 2003]. P_{open} and P_{close} are equally defined at 0 cmH2O [Smith et al., 2005]. V_{max} at 5 L is specified by Despopoulus [Despopoulos and Silbernagl, 2003] h_{tot} equal to 0.16 cm, g equal to 9.82 m/s^2 and ρ equal to 300 kg/m^3 have been specified by Gattinoni and coworkers [Gattinoni et al., 1993]. V_{offset} equal to 0 L, P_{p10} equal to -5 and C equal to 0.1 L/cmH$_2$O is specified by Despopoulus [Despopoulos and Silbernagl, 2003]. During the test of the model applied by Smith and coworkers the parameters used in the model were either predefined or adjusted in order to fit the model to the PV data. The predefined parameters encompasses: N_A, N_C, P_{open}, P_{close}, V_{max}/N_A, h_{tot} and g A curve fitting technique was applied in order to adjust 5 different parameters of the model to fit the static PV curves from patients. The best result was achieved by adjusting the following 5 parameters: V_{offset} (0.1 L), V_{max} (1.08 L), P_{p10} (8.6 cmH$_2$O), C_A (0.1 L/cmH$_2$O) and ρ (445 kg/m^3). The resulting curve fit was compared to the sigmoid function fit using data from an ARDS patient which was obtained from a graph in an earlier study by Venegas and coworkers. [Venegas et al., 1998] The result of fitting the sigmoid function and alveoli model, which can be seen in figure 8.4, showed that they achieved an almost equivalent fit to the experimental data from an ARDS patient. Figure 8.4 also shows the dynamic distribution of open, collapsed and overdistended alveoli along the static PV curve.

Number	Parameter	Normal value	Description
1	N_A	$300 \cdot 10^6$	Total amount of alveoli
2	P_{open}	0 cmH2O	Opening pressure
3	P_{close}	0 cmH2O	Closing pressure
4	V_{max}	5 L	Maximum lung volume
5	h_{tot}	0.16 m	Height of the lungs
6	V_{offset}	0 L	Lung volume offset
7	P_{p10}	-5 cmH$_2$O	Pleural pressure
8	C_A	0.1 L/cmH$_2$O	Compliance
9	ρ	300 kg/m^3	Density
10	g	9.81ms^{-2}	Gravity

Table 8.1: Model parameters with normal values.

At low pressures all the alveoli are collapsed. When the pressure increases during inflation an increasing amount of alveoli open. When the point of maximum gradient on the PV curve has been reached all alveoli are open. Above the point of maximum gradient the alveoli starts to become overdistended. [Smith et al., 2005]
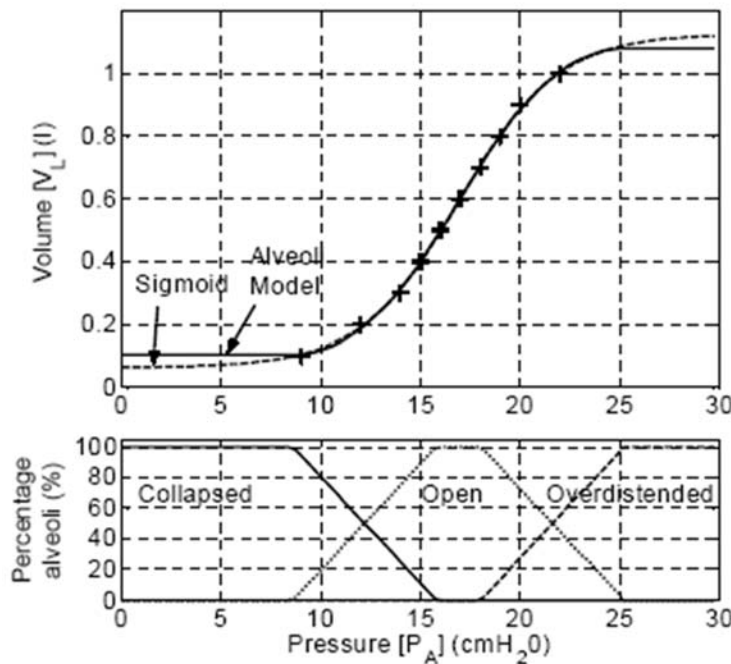

Figure 8.4: *The figure illustrates fitting of the sigmoid function (dashed line) and the alveoli model (solid line) to experimentally measured patient data (+) from Venegas et al. (top). The distribution of alveoli in the three states is calculated by the alveoli model and illustrated in the bottom figure [Smith et al., 2005]*

8.6 Conclusion

This chapter has presented the model based on alveoli compartments. The model can in contrast to the compliance obtained from the PV curve or where to locate the different inflection provide information regarding the continuous progress of the alveoli state. This information may be

advantageous in clinical practice when trying to find the optimal compromise between optimizing gas exchange and avoiding overdistension and atelectasis. In order to extract information regarding the continuous progress of the alveoli state from those static PV curves used in this study the model will be applied. This means that the distribution of the alveoli states is both extracted from the CT scans as described in Image Analysis and Processing in part III and simulated from the resulting fit using the model. This makes it possible to investigate whether there are an agreement between the extracted values of the alveolar states from the CT scans and the simulated alveolar states from the model. Before fitting the model on the static PV curves and simulating the alveolar states the model has to be adjusted to the specific data used in this study. This implies that a further analysis of how the parameters in the model affects the model simulations and PV curves has to be applied. Based on this analysis it will be posible to determine which parameters should be predefined in the model and which parameters should be used in the model simulations to obtain the best fit to PV data. Thus, the following chapter will contain a parameter sensitivity analysis.

Chapter 9

Parameter sensitivity analysis

The model has now been described in physiological and mathematical terms. In order to fit the model to PV data from each pig and thereby simulate the alveolar states as open, collapsed and overdistended alveoli the role of each parameter in the model should be investigated Thus, the different parameters used in the model, which were introduced in the previously chapter, has to be further investigated in order to both understand how each parameter affects the simulation but also to identify how the parameters should be adjusted in order to fit to PV data. In order to obtain an understanding of each parameter the sensitivity of all the parameters has to be investigated and analyzed. This analysis will make it possible to determine which parameters that should be predefined in the model simulation or used to obtain the best fit to PV data. Thus, the first section in this chapter contains the parameter sensitivity analysis. The second section compares the results of the sensitivity analysis and discusses which parameters should be adjusted to fit to PV data. The last section defines the predefined parameters with physiological values and the parameters used to obtain the best fit.

9.1   Parameter sensitivity analysis

The purpose of the parameter sensitivity analysis is to gain a better understanding of how each parameter affects the model simulation of PV curves. This is important when trying to find the optimal parameters for fitting to PV data. The parameter sensitivity analysis will indicate whether two or more parameter affects the model simulation in the same way. As described in the previous chapter the best fit of the model to the PV data used in the study by Smith et al. was obtained by adjusting the 5 following model parameters: lung volume offset, maximum lung volume, compliance, pleural pressure and density. However, these 5 parameters are not necesarily the same to adjust when trying to find the best fit of the model to the PV data used in this study. In an attempt to find the most relevant parameters the sensitivity of all the parameters described the previous chapter and listed in table 8.1 will be analyzed. During this parameter sensitivity analysis the parameter from 1-9 will be varied and simulated. Parameter number 10 (gravity) is irrelevant to vary and will therefore not be simulated. The simulation of the static PV curve and the alveolar states in this parameter sensitivity analysis will consist of different scenarioes. The actual parameter will be varied and simulated with three different settings. One setting as normal value defined in table 8.1 and the two other settings as values as either lower and upper limits of the clinical physiological range. Thus, all the values of the parameters in table 8.1 have been applied in the simulations, except the actual parameter that has to be analyzed. The following subsections describes the sensitivity of the actual parameter.

Number of alveoli

The human lungs contains about 300 million alveoli. [Despopoulos and Silbernagl, 2003], which also is the initial setting listed in table 8.1. Thus, 300 milion will be the first model simulation. A large study in 2003 by Hyde et. al. estimated the total amount of alveoli from rat lungs and rhesus monkey lungs. The number of alveoli in the rat lung ranged from 17,3 million to 24,6 million with a mean of 20,1 million. The average number of alveoli in the monkey ranged from 48,8 million to 67,1 million with a mean of 57,7 million. [Hyde et al., 2003] To my knowledge, now study has investigated the total amount of alveoli in pigs. However, a study by Ressmeyer and coworkers in 2006 demonstrated by comparison of precision-cut lung slices of human lungs and guinea pig that pig lungs are a more appropriate model for human airway than lungs from rats or mice. [Ressmeyer et al., 2006] Based on the asumption that the anatomy and physiology of a pig lung and a human lung are the same, the value of the parameter at 300 million will be applied in the final model simulation. However, in order to investigate whether a lower or higher setting of this parameter will affect the model simulation a simulation of both 200 million and 400 million alveoli will be applied. The simulations are performed for a pressure range of 0-40 cmH$_2$O Figure 9.1 shows the results of simulating the static PV curves and inflation alveolar states for total amount of alveoli: 200, 300 and 400 million alveoli. From the static PV curves it can be identified that an increase in the total amount of alveoli causes a more steep PV curve and a higher maximum lung volume. This is in full accordance with equation 8.4 defined in the previous chapter. If the number of alveoli increases the total lung volume will also increase. The resulting three sub figures illustrating the alveolar states shows that the varying total amount of alveoli does not affect the distribution of open, collapsed or overdistendend alveoli. The figure shows that a correct setting of total amount of alveoli is important when trying to simulate the static PV curve. However, as mentioned previously no study has investigated the total amount of alveoli in pigs. Thus, the value of the parameter at 300 million, which is equal to a human lung, will be predefined in the final model simulation.
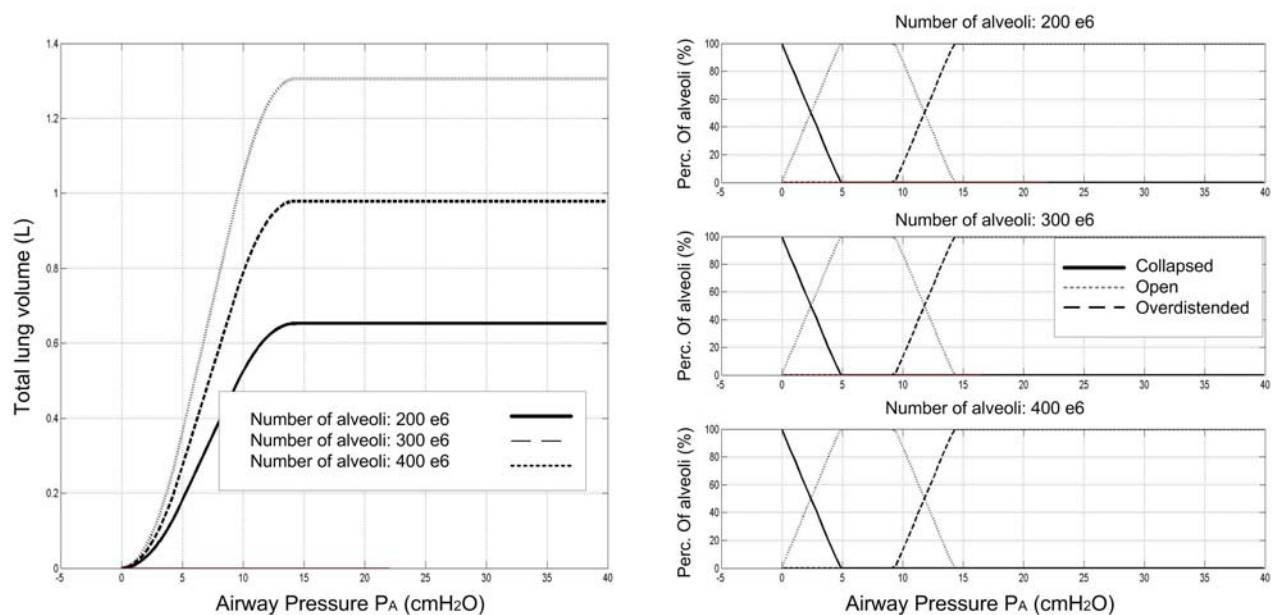

Figure 9.1: *The figure illustrates the model simulation of the static PV curve (left) and the corresponding simulation of alveolar states (right). The three different simulations represent three different applied settings of the total amount of alveoli*

Opening Pressure

The opening pressure can be considered as the pressure at which most of the collapsed units open up and may be recruited [Gattinoni et al., 1987]. Thus, a high opening pressure may result in an increase in the total amount of collapsed alveoli and a decrease in the total amount of open and overdistended alveoli. The first sensitivity simulation of the opening pressure is a pressure at 0 cmH$_2$O, which is the same as the initial value listed in table 8.1. It is likely that the opening pressure is above a pressure at 0 cmH$_2$O in ARDS patients. Thus, a simulation of an opening pressure at both 5 and 10 cmH$_2$O will be applied. The simulations are performed for a pressure range of 0-40 cmH$_2$O

Figure 9.2 shows the results of simulating the static PV curves and inflation alveolar states for varying the opening pressure at: 0, 5 and 10 cmH$_2$O. The deflation curve in each simulation are the same because of a constant applied closing pressure across all simulations. From the static PV curves it can be identified that an increase in the opening pressure causes a more steep inflation curve. The simulation with the opening pressure at 0 cmH$_2$O which is considered the normal opening pressure shows that the PV curve has a normal smooth shape. The simulation with the opening pressure at 10 cmH$_2$O, however shows a non normal physiological curve. The inflation curve is very steep and is almost linear and the corners on the curve are edged This indicates that the model is incapable of simulating such high values of opening pressures. As described previously a higher opening pressure causes an increase in the total amount of collapsed alveoli and a decrease in the total amount of open and overdistended alveoli, which can be seen in the resulting three sub figures illustrating the alveolar states. This is in full acordance with the conceptual clinical wiew that a PEEP setting should be adjusted based on the opening pressure which often has been regarded as the lower inflection point [Gattinoni et al., 1987].
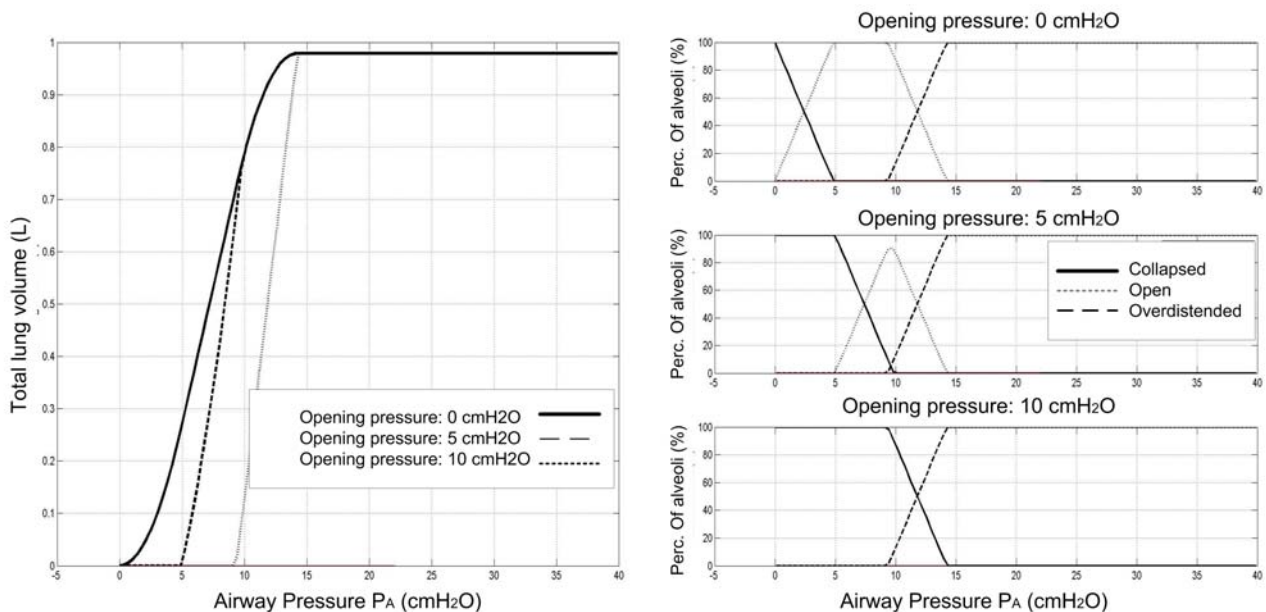

Figure 9.2: *The figure illustrates the model simulation of the static PV curve (left) and the corresponding simulation of alveolar states (right). The three different simulations represent three different applied settings of the opening pressure*

Closing Pressure

In order to simulate different settings of the closing pressure the opening pressure has to be increased to a higher value than the initial setting at 0 cmH$_2$O. This is necesary because the opening pressure has to be higher than the closing pressure when simulating different settings of the closing pressures. The initial setting of the opening pressure in this sensitivity analysis will be 10 cmH$_2$O. The different settings of the closing pressure will be 0, 5 and 8 cmH$_2$O, which means that the closing pressure in each simulation will be below the opening pressure. The simulation of the alveolar states is in this simulation different from the other simulations. In this simulation the alveolar states is simulated based on the deflation not the inflation curve. The simulations are performed for a pressure range of 0-40 cmH$_2$O.

Figure 9.3 shows the results of simulating the static PV curves and deflation alveolar states for varying the closing pressure at: 0, 5 and 8 cmH$_2$O. From the static PV curves it can be identified that an increase in the closing pressure causes a more steep deflation PV curve. The inflation curves in each simulation are the same because of the same applied opening pressure. The deflation curves becomes more equal to the inflation curves as the closing pressure increases close to the opening pressure. These applied simulations of varying the closing pressure indicates non normal physiological curve equal to those simulations with varying the opening pressure. The deflation curve is very steep and is almost linear and the corners on the curve are edged which indicates that the model is incapable of simulating such high values of closing pressures.
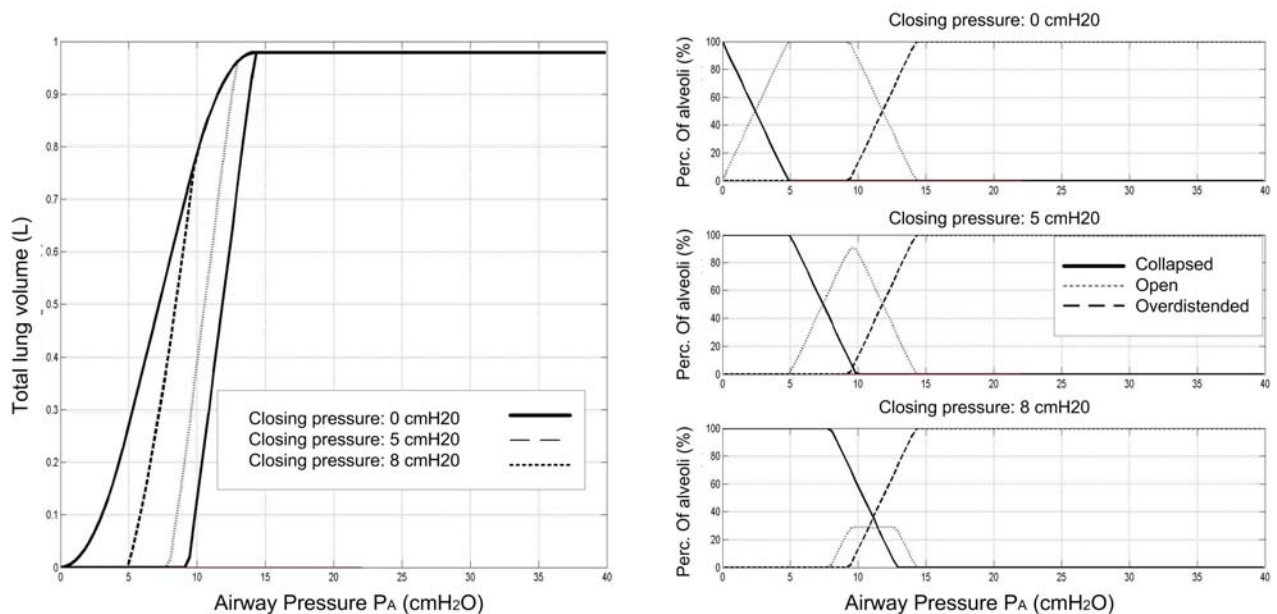

Figure 9.3: *The figure illustrates the model simulation of the static PV curve (left) and the corresponding simulation of alveolar states (right). The three different simulations represent three different applied settings of the closing pressure*

Maximum lung volume

The maximum lung volume corresponds to the total lung capacity. The normal range of lung capacity is between 2.5 L and 7 L [Despopoulos and Silbernagl, 2003]. 5 litres is the normal human value defined in table 8.1. In order to investigate a lower limit at the maximum lung

volume 0.5 and 3 L will be applied which probably are more equal to the maximum lung volume in pigs. The simulations are performed for a pressure range of 0-60 cmH$_2$O.

Figure 9.4 shows the results of simulating the static PV curves and inflation alveolar states for varying the maximum lung volume at: 0.5, 3 and 5 litres. The static PV curve shows that an increase in the maximum lung volume up to 3 L causes an increase in the upper asymptote of the static PV curve which is in full acordance with the physiologiclal interpretation of the maximum lung volume. It can furthermore be identified that an decrease in the maximum lung volume causes a decrease in the range of open lung alveoli. This is also in full acordance with the interpretation of the maximum lung volume. As identified in the static PV curve a low maximum lung volume results in a low pressure range before the upper asymptote is reached. This means that the range of open alveoli also decreases. Furthermore, an increase in the maximum lung volume also increases the pressure at which the alveoli begin to become overdistended.
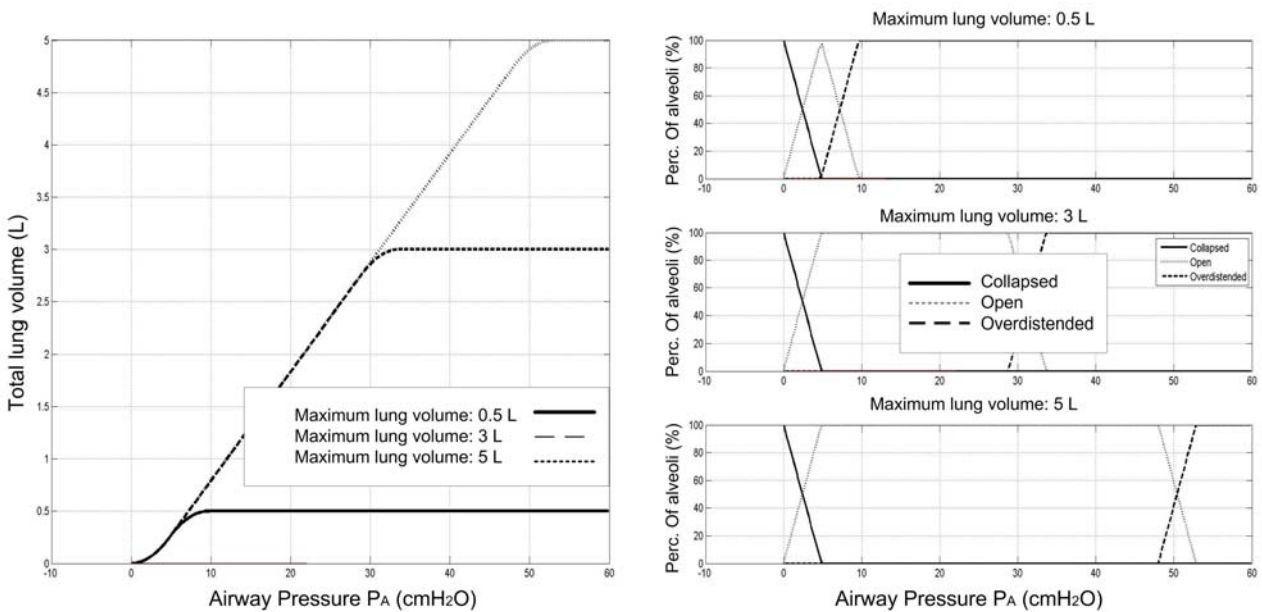

Figure 9.4: *The figure illustrates the model simulation of the static PV curve (left) and the corresponding simulation of alveolar states (right). The three different simulations represent three different applied settings of the maximum lung volume*

Lung height

The first applied setting of the lung height is the initial setting at 0.16 cm listed in table 8.1. This value is equal to the height of a normal human lung [Gattinoni et al., 1993]. However, the data used in this study is not from human subjects but from pigs. This means that values below 0.16 cm also has to be applied in the model simulation in order to simulate the height of a normal pig lung. Thus a value of 0.10 and 0.04 cm are simulated. The simulations are performed for a pressure range of 0-40 cmH$_2$O

Figure 9.5 shows the results of simulating the static PV curves and inflation alveolar states for varying the lung height at: 0.16, 0.10 and 0.04 cm. The static PV curve shows that an decrease in the lung height causes a more steep and linear PV curve. It can furthermore be

identified that an decrease in the lung height causes a precipitious decrease in the number of collapsed alveoli, a precipitious increase and decrease in the number of open alveoli and a precipitious increase in the number of overdistended alveoli. The steep static PV curve obtained when decreasing the lung height can be explained by equation 8.3 in the previous chapter. The range of trans alveoli pressure that acts across the alveoli wall decreases when the lung height is changed to a lower value.
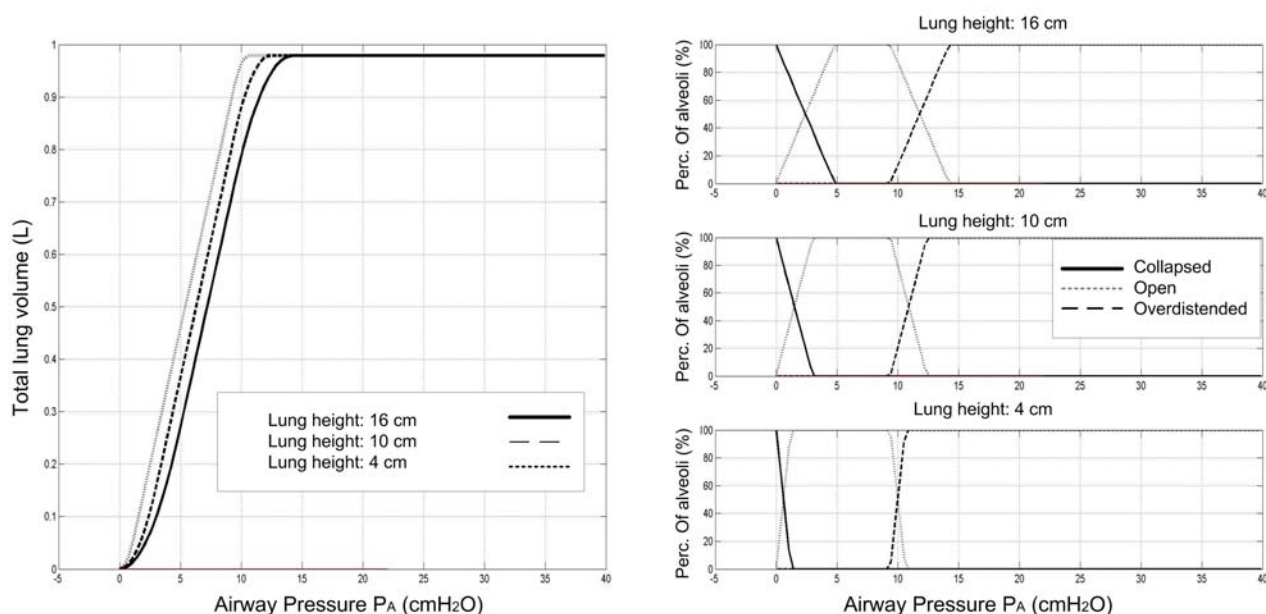

Figure 9.5: *The figure illustrates the model simulation of the static PV curve (left) and the corresponding simulation of alveolar states (right). The three different simulations represent three different applied settings of the lung height*

Offset lung volume

Offset lung volume has no physiological interpretation and due to that no normal value. When no normal value can be identified the initial setting is 0 L,which also is the initial setting listed in table 8.1. The two other settings are -1 L and 1 L, which allows an investigation of the effect in both a negative and positive direction. The simulations are performed for a pressure range of 0-40 cmH$_2$O.

Figure 9.6 shows the results of simulating the static PV curves and inflation alveolar states for varying the offset lung volume at: -1, 0, 1 L. The static PV curve shows as expected a vertical shift of the entire PV curve as the offset lung volume increases. The shape of the PV curve is preserved. The alveolar states are not affected by the changes in the offset lung volume which also can be seen in figure 9.6. The alveolar states are not affected because the entire static PV curve only has been shifted and not changed in shape or size. Thus, the offset volume may be applied to correct for any differences in volume scale between the data and the model when performing simulations and curve fitting.
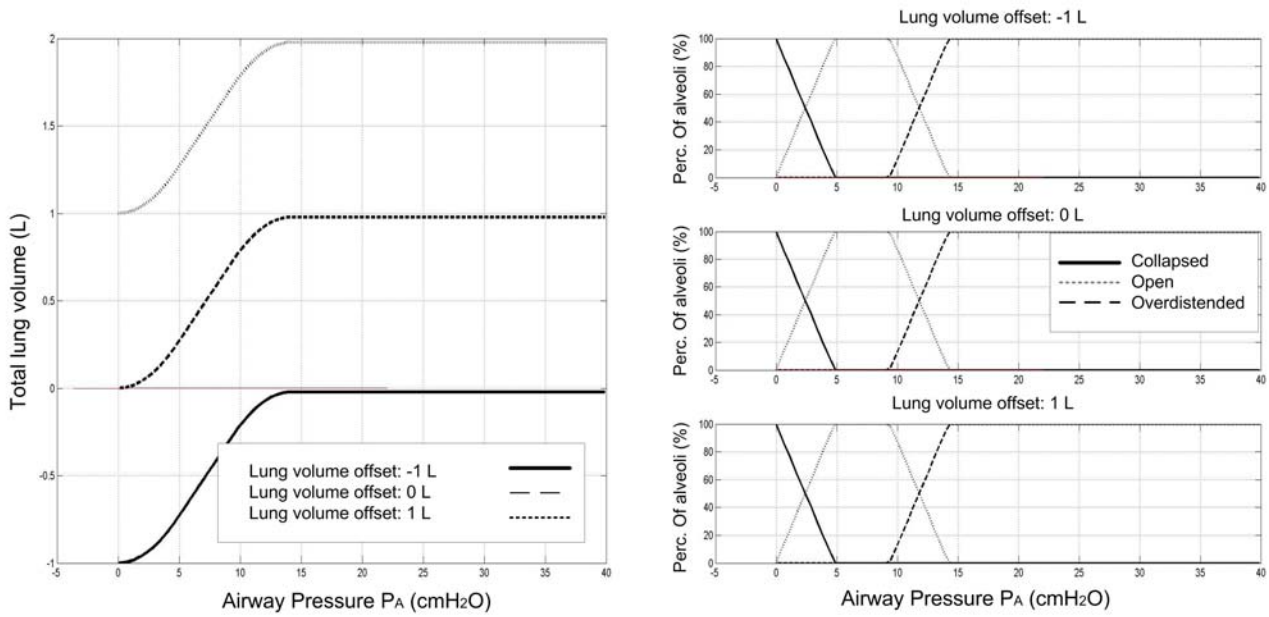
Figure 9.6: *The figure illustrates the model simulation of the static PV curve (left) and the corresponding simulation of alveolar states (right). The three different simulations represent three different applied settings of the offset lung volume.*

Pleural Pressure

The pleural pressure is the pressure surrounding the lung, within the pleural space and averages about -5 cmH2O during inspiration and up to 2 cmH2O during expiration [Despopoulos and Silbernagl, 2003]. The pleural pressure usually does not become above 5 cmH2O unless there is a very forcefull expiration requiring the use of expiratory muscles [Martini, 2004]. A pleural pressure setting at -5, 0 and 5 cmH2O is applied in the simulation. The simulations are performed for a pressure range of -5-35 cmH_2O.

Figure 9.7 shows the results of simulating the static PV curves and inflation alveolar states for varying the pleural pressure at: -5, 0 and 5 cmH2O. The static PV curve shows that an increase in the pleural pressure causes a shift to the right of the entire static PV curve which also was expected. The distribution of the open, collapsed and overdistended alveoli remains the same in all three simulation except for the shift to the right.
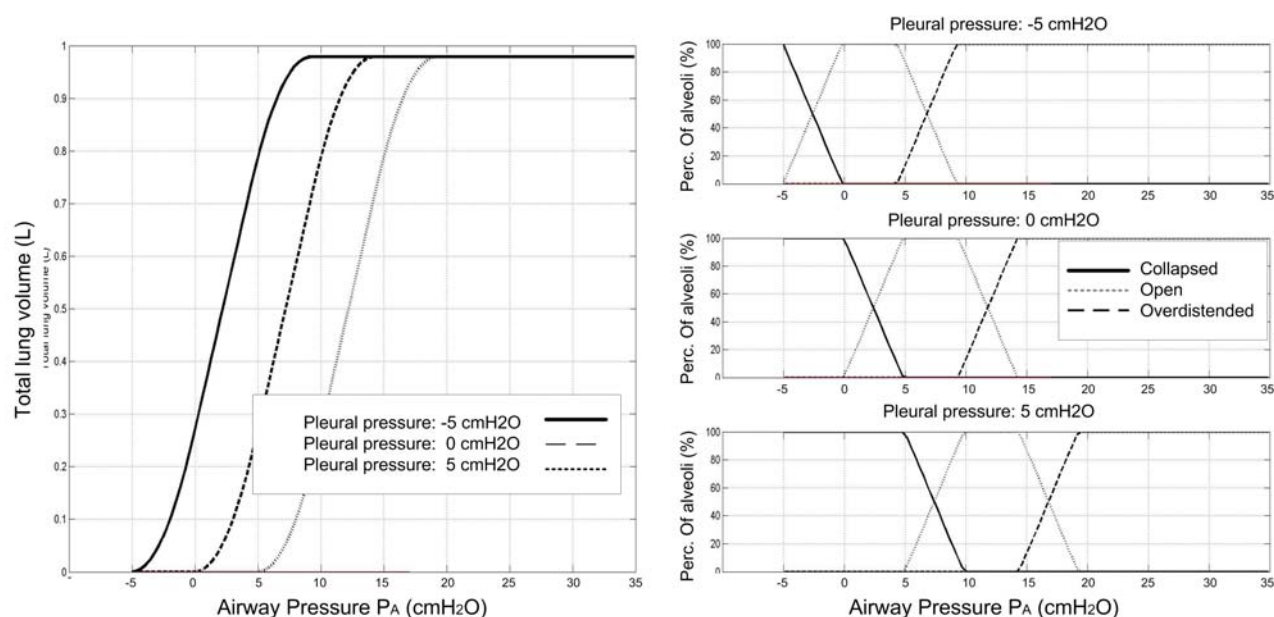
Figure 9.7: *The figure illustrates the model simulation of the static PV curve (left) and the corresponding simulation of alveolar states (right). The three different simulations represent three different applied settings of the pleural pressure.*

Compliance

The slope of the static PV curve represents the compliance of the lung. The normal lung compliance which is the steepest part of the static PV curve approximates 0.1 L/cmH_2O [Despopoulos and Silbernagl, 2003] The compliance used in the model does not represent the compliance of the lung but the compliance of a single alveoli. As previously described the model divides the lung into 300 million alveoli, which means that the normal compliance of the lungs at 0.1 L/cmH_2O can be calculated as the compliance representing one alveoli: 3.3^{-10} L/cmH_2O (0.1 L/cmH_2O / 300 · 10^6). The normal compliance of the lungs at 0.1 L/cmH_2O which also is the initial setting defined in table 8.1 will be the first simulation. Simulations above the normal value is considered not to be relevant since compliance always tend to decreases in the presence of lung disease. [Martini, 2004] Thus, a compliance setting at 0.06 (compliance for a single alveoli: 2.0^{-10} L/cmH_2O) and 0.03 L/cmH_2O (compliance for a single alveoli: 1.0^{-10} L/cmH_2O) are also simulated. These compliance values are considered to be more equal to those obtained in ALI/ARDS patients. The simulations are performed for a pressure range of 0-40 cmH_2O.

The result of simulating the static PV curve and inflation alveolar states for varying the compliance at: 0.1, 0.06 and 0.03 L/cmH_2O can be seen in figure 9.8. The static PV curve shows that an decrease in the compliance causes a flattering of the PV curve. This is in full accordance with the flattering PV curve and low compliance often obtained from a stiff lung as seen in ARDS patients. The alveolar states are affected by the changes in the compliance which also can be seen in figure 9.8. When the compliance is increased the range of pressure until maximum volume is reached becomes decreased, which means that a lung with a normal compliance does not need a high pressure to obtain a high lung volume. The decreased pressure range on the static PV curve

causes a low range where most alveoli are open and a lower pressure where the alveoli becomes overdistended.

Figure 9.8: *The figure illustrates the model simulation of the static PV curve (left) and the corresponding simulation of alveolar states (right). The three different simulations represent three different applied settings of the compliance.*

Density

A density of 300 kg/m^3 which also is the initial value listed in table 8.1, is the normal lung density of a healthy subject. This value can increase up to 800 kg/m^3 due to edema. [Gattinoni et al., 1993] Thus a density of 300, 550 and 800 kg/m^3 are simulated. The simulations are performed for a pressure range of 0-40 cmH$_2$O.

The result of simulating the static PV curve and inflation alveolar states for varying the density at: 300, 550 and 800 kg/m^3 can be seen in figure 9.9. The static PV curve shows that an increase in the density causes a flattening of the PV curve as seen with the compliance. This is also in full accordance with the flattening PV curve and the high density often obtained from patients with edema as seen in ARDS patients. The increased density causes a large pressure range until the maximum lung volume is reached. The steep static PV curve obtained when decreasing the density can be explained in the same way as for the lung height which is by equation 8.1 in the previous chapter. The range of trans alveoli pressure that acts across the alveoli wall decreases when the density is changed to a lower value. The simulation of the alveolar states shows that a density at 550 kg/m^3 causes a very small pressure range where all alveoli are open at the same time. This is not the case in the simulation with a density at 800 kg/m^3. In this simulation the distribution of open alveoli does not reach above 75%. A servere edema which is most likely when such a high density is present can physiological explain the alveolar states obtained in the simulations.
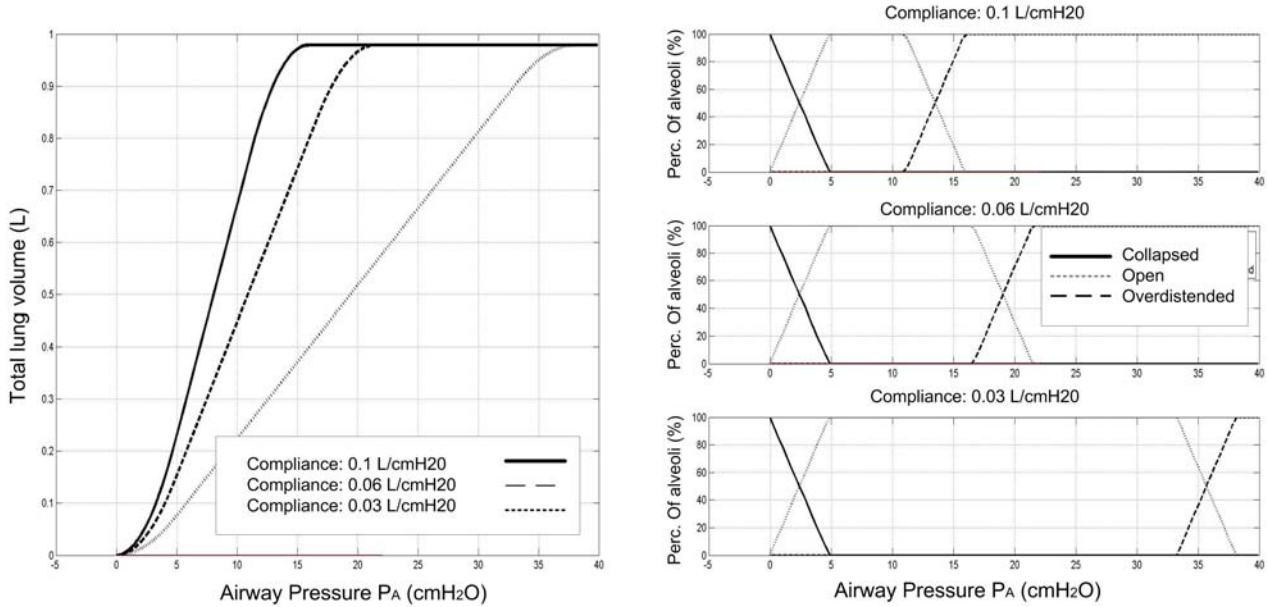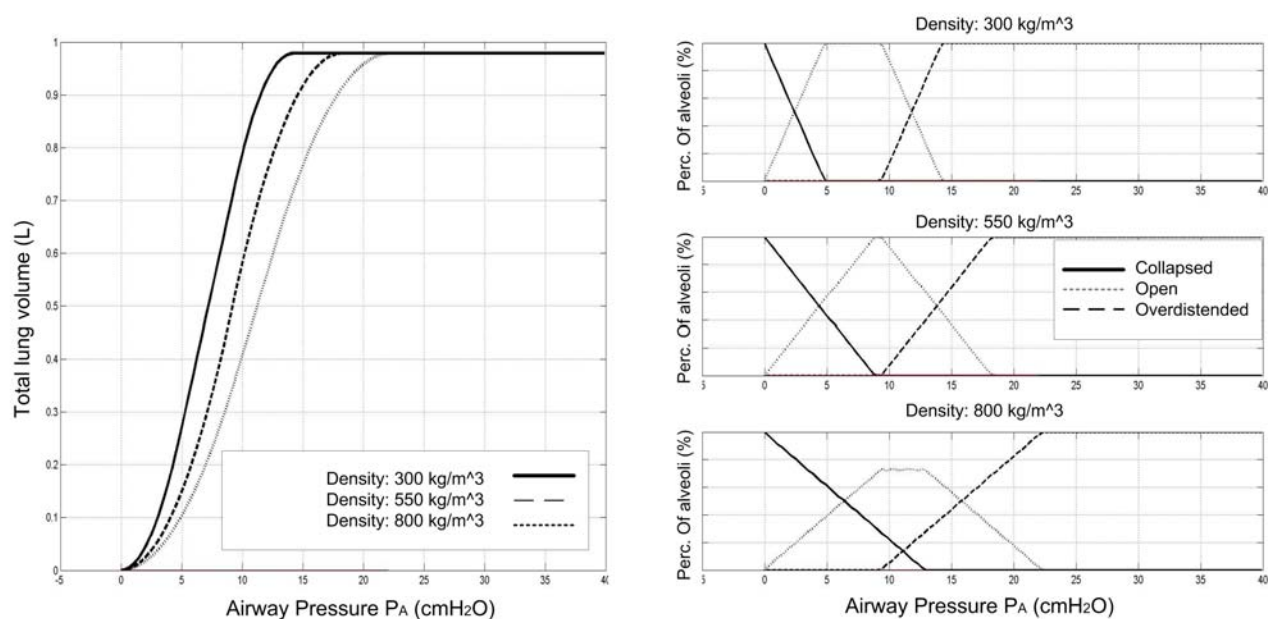
Figure 9.9: *The figure illustrates the model simulation of the static PV curve (left) and the corresponding simulation of alveolar states (right). The three different simulations represent three different applied settings of the density.*

9.2 Comparison of parameter sensitivities

During the previous subsections all the parameters in the model have been varied and simulated. The purpose of this analysis was to gain a better understanding of how each parameter affects the model simulation. The analysis should form the basis of which parameters should be used or predefined when trying to obtain the best fit of the model to PV data i.e. used to adjust the shape and size of the PV curve to fit to the measured PV data. A compromise has to be made between using enough or too many parameters when adjusting the size and shape of the PV curve to fit the model to the measured PV data. If too many parameters are used to obtain the best fit of the model to PV data it would be impossible to identify the model. If too few parameters are used it is most likely that it will cause a poor fit of the model to the PV data. In order to determine which of the described parameters should be predefined or used the effect of all the parameters should be compared. A complete comparison and overwiev of how the parameters affect the size and shape of the static PV curve can be seen in figure 9.10.

From figure 9.10 it can be identified that the shape and size of the static PV curve can be adjusted by changing the settings of the different parameters. Offset lung volume shifts the entire static PV curve in an vertical direction. Maximum lung volume increase the upper asymptote of the static PV curve. Opening and closing pressures shift the lower part of the static PV curve which accounts for the hysteresis. Pleural pressure shifts the entire static PV curve in either right or left direction. The number of alveoli increases the upper part of the static PV curve in a vertical direction. Both height of the lungs, compliance and density changes the shape of the static PV curve in a right or left position. Compared to pleural pressure, the height of the lungs, compliance and density only changes the gradient of the curve, not the entire static PV curve. As the figure shows, the height of the lungs, the compliance and the density affects the shape and size of the static PV curve in a simmilar manner. This indicates that all three of these
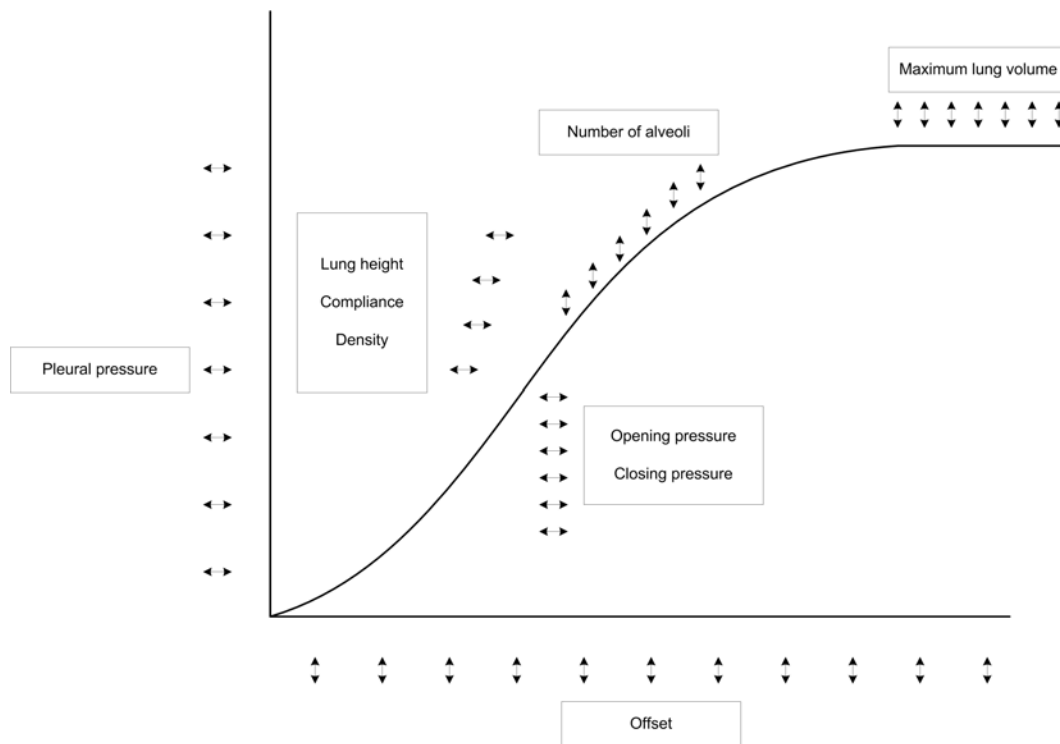
Figure 9.10: *The figure illustrates the effect of the parameters on the shape and size of the static PV curve. It can be identified that compliance, density and the height of the lung affects the shape of the PV curve in a simmilar manner.*

parameters may be used to fit the model to PV data in the same way. The problem of using two or more parameters that can adjust and vary the shape and size of the PV curve in the same way is that different simulation results of the alveolar states can be obtained depending on which parameter that has been adjusted.

The three different parameters has in spite of the almost equal influence on the shape and size of the PV curve not the same physiological interpretation. As described previously the height of the lungs is an allready known factor to some degree. This means that this parameter can be predefined in the model before applying the simulations. It is assumed that the height of the lungs in those pigs used in the data materials is equal to 0.10 cm.

Compliance is a parameter that may provide valuable information regarding the elastic properties of the respiratory system. In a diseased state as seen in ARDS, the compliance of the lung decreases significantly due to inflammation, swelling or edema. This means that the compliance obtained from a static PV curve tells something about the severity of the syndrome. [Maggiore et al., 2003b] Density of the lung also indicates whether it may be an ARDS patient. A density of 300 kg/m^3 as seen in a normal healthy subject does not affect the shape and size of the PV curve in an flattering way as seen in ARDS. A high density at 500-800 kg/m^3, which often can be seen in ARDS patients, causes the PV curve to flatten off. There is an physiological agreement between how the compliance and density affects the size and shape of the PV curve. In order to test whether two different results of simulating the alveolar states can be obtained, depending on which parameter that has be varied, the following sub test will be applied which encompass three different steps:

78

1. **Density simulation**. Simulation of the static PV curve and alveolar states with all predefined values of the parameters, with exception of the density. The parameter setting of density is 800 kg/m^3.

2. **Compliance simulation** Simulation of the static PV curve and alveolar states with all predefined values of the parameters, with exception of the compliance. The main purpose of this simulation is to fit the model to the obtained PV curve from the density simulation by varying compliance.

3. **Alveolar comparison** The simulated alveolar states from the density simulation and the compliance simulation are compared.

By applying the aforementioned sub test it will be possible to investigate whether the result of simulated alveolar states from the compliance simulation is equal to the simulated alveolar states obtained from the density simulation. If the result from the simulated alveolar states is equal, one of the two parameters can be predefined and one used to obtain the best fit of the model to PV data. If the two simulations of the alveolar states are unequal it is most likely because the two parameters provide different information of the alveolar states. Thus, both of the parameters should be used to obtain the best fit of the model to PV data.

The result of the sub test can be seen in figure 9.11. The two uppermost sub figure illustrates the static PV curve and alveolar states from the simulation with a density at 800 kg/m^3. The two lowest sub figures illustrates the the static PV curve and alveolar states from the compliance simulation. The purpose of this simulation is to vary the compliance value such as the best fit to the density simulation is obtained. The two static PV curves, which can be seen in the figure, are not completely identical which naturally may affect the comparison of the two curves. However, as the figure indicates there is obviously no match between the alveolar states from the two simulations. Thus, it can be concluded that density and compliance has different influence on the alveolar states. This means that both compliance and density should be used to obtain the best fit of the model to PV data i.e varied to adjust size and shape of the PV curve.
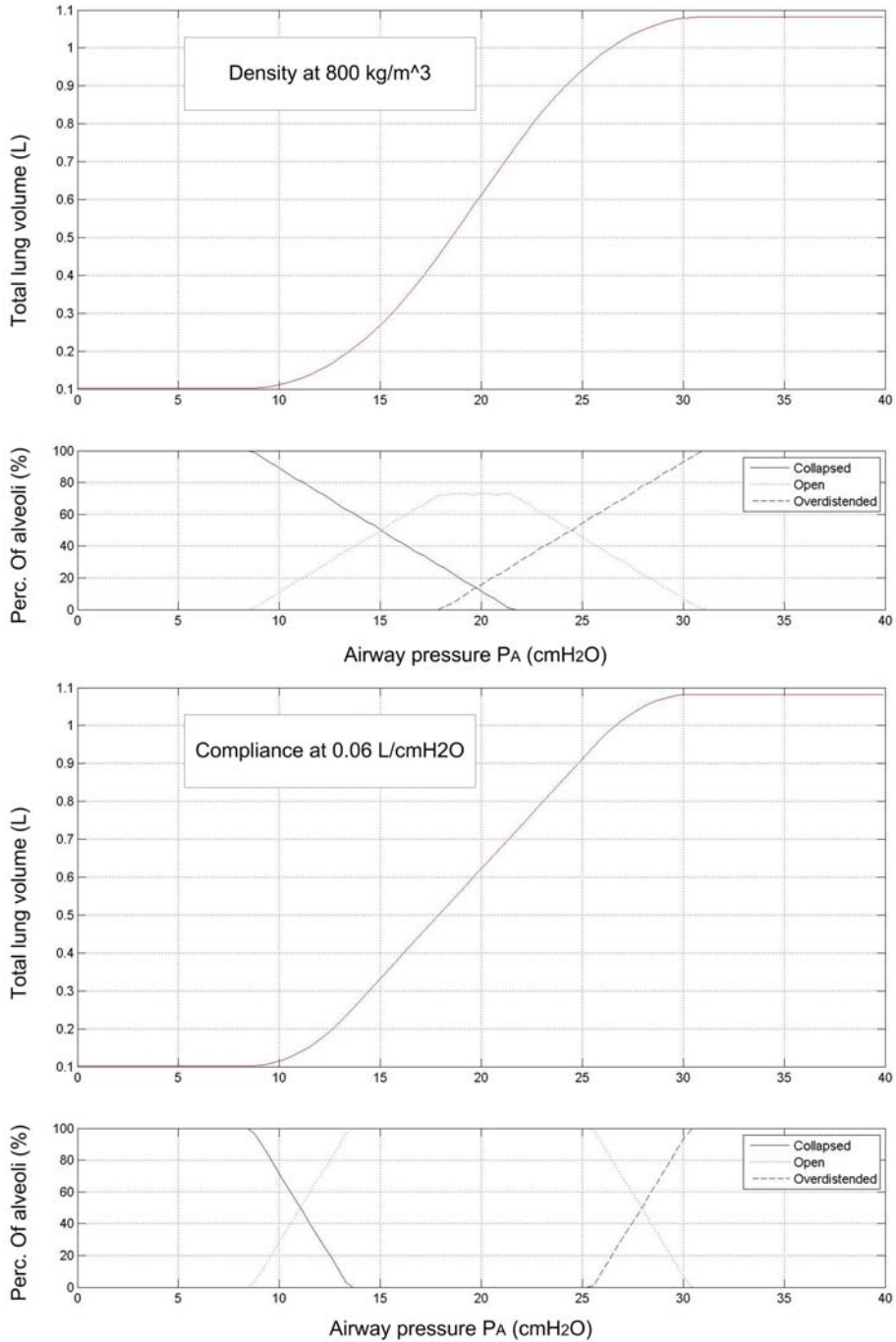
Figure 9.11: *The figure illustrates the effect of the parameters on the shape and size of the static PV curve. It can be identified that compliance, density and the height of the lung affects the shape of the PV curve in almost the same way.*

9.3 Definition of parameter settings

During the previous sub section the sensitivity of all parameters has been analyzed and described. The main purpose of this analysis was to determine which parameters should be used in order to obtain the best fit of the model to PV data i.e varied to adjust size and shape of the static PV curve. The analysis should also be used to determine which parameters should be predefined in the model before applying the different simulations. In the following the parameters are divided in predefined parameters with coherent value and parameters that will be used to obtain the best fit.

Definition	Parameter	Description	Predefined value
Predefined	N_A	Total amount of alveoli	$300 \cdot 10^6$
Predefined	V_{max}	Maximum lung volume	3 L
Predefined	h_{tot}	Height of the lungs	0.10 m
Predefined	g	Gravity	9.81ms^{-2}

Table 9.1: Model parameters divided as either predefined or adjustable. The predefined parameters are defined before the model simulation which means that these parameters cannot be varied and thereby used to obtain the best fit. The adjustable parameters are used during the simulation in order to obtain the best fit of the model to PV data.

Definition	Parameter	Description	start value
Adjustable	P_{open}	Opening pressure	0 cmH_2O
Adjustable	P_{close}	Closing pressure	0 cmH_2O
Adjustable	V_{offset}	Lung volume offset	0 L
Adjustable	P_{p10}	Pleural pressure	- 5 cmH_2O
Adjustable	C_A	Compliance	3.3^{-010} L/cmH_2O
Adjustable	ρ	Density	300 kg/m^3

Table 9.2: Model parameters divided as either predefined or adjustable. The predefined parameters are defined before the model simulation which means that these parameters cannot be varied and thereby used to obtain the best fit. The adjustable parameters are used during the simulation in order to obtain the best fit of the model to PV data.

9.4 Conclusion

The aim of this chapter has been to investigate the sensitivity of the model parameter values within the clinical ranges and to gain a better understanding of how each parameter affects the model simulation of the static PV curves and alveolar states. The parameter sensitivity test has been performed for: number of alveoli, opening pressure, closing pressure maximum lung volume, height of the lungs, offset volume pleural pressure compliance and density. The remaining model parameters are predefined and thereby kept constant in the model simulations. The different parameters have been shown to act physiological and to simulate changes of the static PV curve in all directions, which indicates potential for fitting the model to the static PV curves from the pigs. The parameter sensitivity test of density and compliance showed that these two parameters affects the shape of the static PV curve in a similar way, but provide different information of the alveolar states. Thus, both density and compliance are used to obtain the best fit of the model to PV data. The model may now be applied to simulate the alveolar states from the static

PV data. The investigation and test of the relationship between the alveolar states extracted from the CT scans and the simulated alveolar states from the model is described in the following chapter.

Part V

Relationship between CT scans and the model

Chapter 10

Finding relationship between CT scans and the model

The model has now been described both in physiological and mathematical terms. The different parameters used in the model has also been investigated in order to both understand how each parameter affects the simulation but also to identify how the parameters should be applied in order to fit the model to PV data. This part of the report contains the investigation and test of the relationship between the alveolar states extracted from the CT scans and the simulated alveolar states from the model. The first part of this chapter contains a test strategy describing the hypothesis of the test and how the test is carried out. The second part of this chapter contains the results obtained from the test.

10.1 Test strategy

The main purpose of this test is to investigate the relationship between the alveolar states extracted from the CT scans and the simulated alveolar states from the model. Before investigating this relationship it is important to define what to investigate and how to do it.

Hypothesis

Since the model is intended to be used in clinical practice it would be highly interesting to investigate whether the model can "answer" relevant clinical questions. In order to formulate these questions, the controversies and problems regarding how to find optimal ventilator settings, described in the Introduction and Analysis part are summarized and discussed and based on this the questions are formulated.

The static PV curve may provide valuable information regarding how to find the optimal PEEP setting which is crucial in ALI/ARDS patients. PEEP must be high enough to avoid collapse during expiration and to increase Peak Inspiratory Pressure (PIP) so that collapsed alveoli are recruited. At the same time high PIP must be avoided since it may cause barotrauma and volutrauma.

In clinical practice mechanical ventilation settings, including PEEP, are often determined by trial and error using different rules due to difficulty in understanding the interaction between ventilator and the specific patients' lung mechanics. Hence, ventilator support may often be influenced by the intuition and experience of the clinical staff. In spite of the valuable information the static PV curve can provide regarding how to find the optimal PEEP setting it is still a common issue that there is no consensus of how the curve should be interpreted and applied. If the model can simulate the recruitment of alveoli and following overdistension up the static PV

curve and thereby provide an answer of how to find these optimal PEEP settings it would be highly usable in clinical practice. This simulation will also allow the model to find an optimal pressure range. That is the range of pressures that define the best compromise between optimizing gas exchange and avoiding VILI.

The optimal pressure range can be defined as the pressure range between the minimum and maximum pressure, where there is a minimum of collapsed and overdistended alveoli. This can also be explained by the following equation:

$$OP_{Range} = min(min(\%C. + \%O.)) - max(min(\%C. + \%O.)) \tag{10.1}$$

Where: OP_{Range} is the optimal pressure range, C is synonym for Collapsed alveoli and O is synonym for Overdistended alveoli, min(min(% C + % O.)) is the minimum pressure where there is a minimum distribution of collapsed alveoli. max(min(% C + % O.)) is the maximum pressure where there is a minimum distribution of overdistended alveoli.

Thus, the first questions can be formulated:

- Can the model identify the optimal pressure range?

However, this question only answer if the model can find a certain pressure range. It would also be interesting to investigate whether the model can simulate the continous recruitment of alveoli and overdistension that occurs along the static PV curve. As described in section 2.2 on page 20 Pelosi and coworkers demonstrated in an experimental animal study where lung damage was performed by inducing OA that recruitment is a continuous process that occurs along the entire inspiratory limb of the PV curve of the respiratory system. [Pelosi et al., 2001] Thus, in order to investigate whether the model can simulate the continous process that occurs along the static PV curve the following question can be formulated:

- Can the model identify the progress of collapsed alveoli that may occur along the static PV curve?

Only one question is formulated because there is no progres of alveoli becoming overdistended due to the lack of overdistension in the lungs in the data for this study. The progress of open alveoli is not relevant because it is the same as for collapsed alveoli only with opposite sign.

All these different questions are assumed highly relevant in clinical practice since they may answer questions that cannot be obtained from evaluating the static PV curve by visual inspection alone. A graphical interpretation of these formulated questions can be seen in figure 10.1.
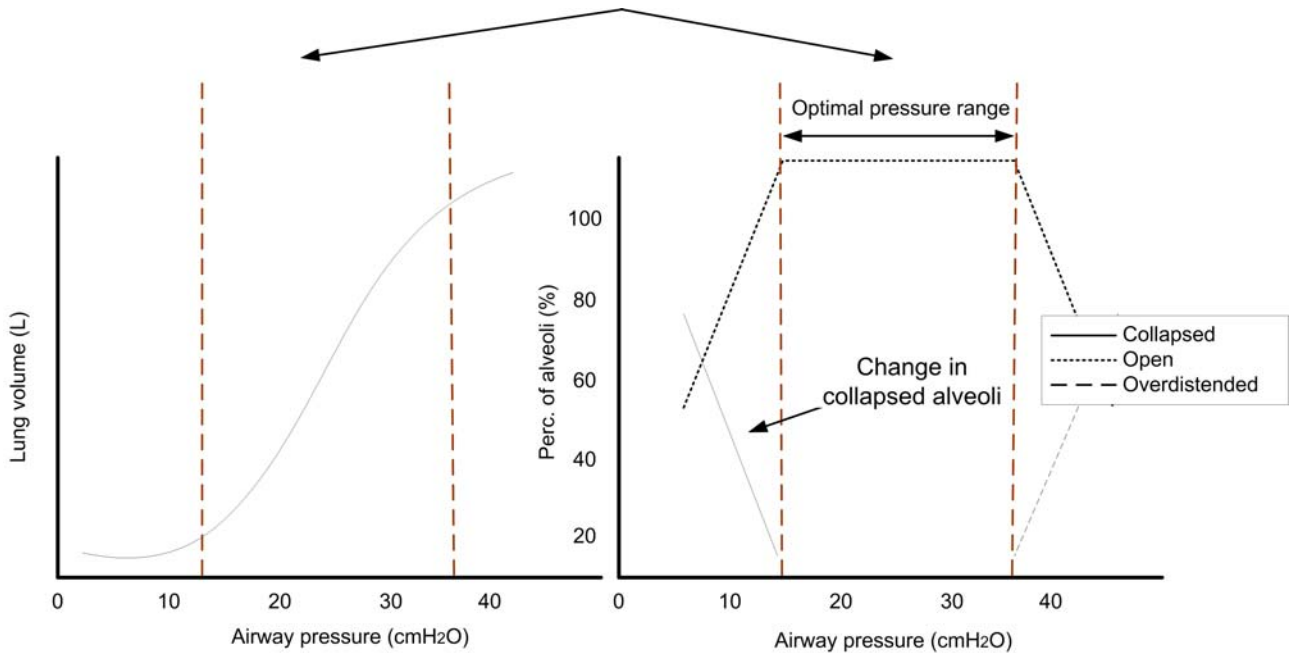
Figure 10.1:   *The figure illustrates the concept of the different formulated questions.*

Test settings

Before the test the image segmentation algorithm has to be applied on the CT slices and the model has to be fitted to the static PV data. The image segmentation algorithm is applied on every CT slice, and the distribution of open, collapsed and overdistended alveoli is estimated. These estimates are summed up and a complete percentage is obtained. In order to fit the model to PV data the model parameters has to be divided in predefined and adjustable parameters. Table 10.1 summarizes, based on the analysis performed in the previous chapter, the parameters used as either predefined or adjustable parameters.

Definition	Parameter	Description	Predefined value
Predefined	N_A	Total amount of alveoli	$300 \cdot 10^6$
Predefined	V_{max}	Maximum lung volume	3 L
Predefined	h_{tot}	Height of the lungs	0.10 m
Predefined	g	Gravity	$9.81 \mathrm{ms}^{-2}$
Adjustable	P_{open}	Opening pressure	0 cmH$_2$O
Adjustable	P_{close}	Closing pressure	0 cmH$_2$O
Adjustable	V_{offset}	Lung volume offset	0 L
Adjustable	P_{p10}	Pleural pressure	-5 cmH$_2$O
Adjustable	C_A	Compliance	3.3^{-010} L/cmH$_2$O
Adjustable	ρ	Density	300 kg/m^3

Table 10.1: Model parameters divided as either predefined or adjustable. The predefined parameters are defined before the model fitting which means that these parameters cannot be varied and thereby used to obtain the best fit. The adjustable parameters are used during the model fitting to obtain the best fit of the model to the PV data.

When the model has been fitted to PV data the simulations of the alveolar states are carried out. The same pressure range is used for model simulation as the pressure range given in the PV data. The following data used in the test can be defined.

Test data

Table 10.2 contains the data set used in the test. The table is divided into healthy pigs and in pigs with OA damaged lungs. A B and C refers to pig number 1, 2 and 3 respectively. When refering to each test case/number in the subsequent test sections it is the number in the first column in the table.

Number	Healthy/OA	PEEP (cmH_2O)	CT slices
1 - A	Healthy	5	600 (50 · 12)
2 - B	Healthy	5	600 (50 · 12)
3 - A	Healthy	10	600 (50 · 12)
4 - B	Healthy	10	600 (50 · 12)
5 - A	OA	5	600 (50 · 12)
6 - B	OA	5	600 (50 · 12)
7 - C	OA	5	600 (50 · 12)
8 - A	OA	10	600 (50 · 12)
9 - B	OA	10	600 (50 · 12)
10 - C	OA	10	600 (50 · 12)

Table 10.2: the table lists all data used in the test. A B and C refers to pig number 1, 2 and 3 respectively.

10.2 Test results

In order to investigate and answer the two formulated questions seperately, the test results are divided into two sub sections. Each sub section contains tables of measured and extracted values, how to analyze these values and the results of the test.

Test 1 - Optimal pressure range

The optimal pressure range from the simulated and the extracted alveolar states are obtained using equation 10.1. The simulated values of the optimal pressure range from the model and the extracted values from the CT scans can be seen in table 10.3. The values in the table are rounded to nearest integers. The values enclosed in brackets are the numerical values. The differences in the last column is the differences between the numerical values. A graphical comparison of the results in table 10.3 can be seen in figure 10.2. As table 10.3 and figure 10.2 shows there are no relationship between the optimal pressure range obtained from the simulations and those estimated from the CT scans. Based on the comparison seen in figure 10.2 it can be concluded that there is no reasson for analyzing the result by a statistical method. In order to investigate why there is no relationship a further graphical inspection of the results is carried out.

Number	Model (cmH$_2$O)	CT (cmH$_2$O)	Difference (cmH$_2$O)
1 - A	9-33 (24)	15-33 (18)	+6
2 - B	7-28 (21)	13-28 (15)	+6
3 - A	14-43 (29)	28-43 (15)	+14
4 - B	11-30 (19)	11-30 (19)	+0
5 - A	14-38 (24)	31-38 (7)	+17
6 - B	24-34 (10)	27-34 (7)	+3
7 - C	9-26 (17)	22-26 (4)	+13
8 - A	15-46 (31)	31-46 (15)	+16
9- B	12-40 (28)	27-40 (13)	+15
10- C	12-39 (27)	30-39 (9)	+18

Table 10.3: the table lists the results from the simulated values of the optimal pressure range from the model and the extracted values from the CT scans of the optimal pressure range. The values enclosed in brackets are the numerical difference in pressure.
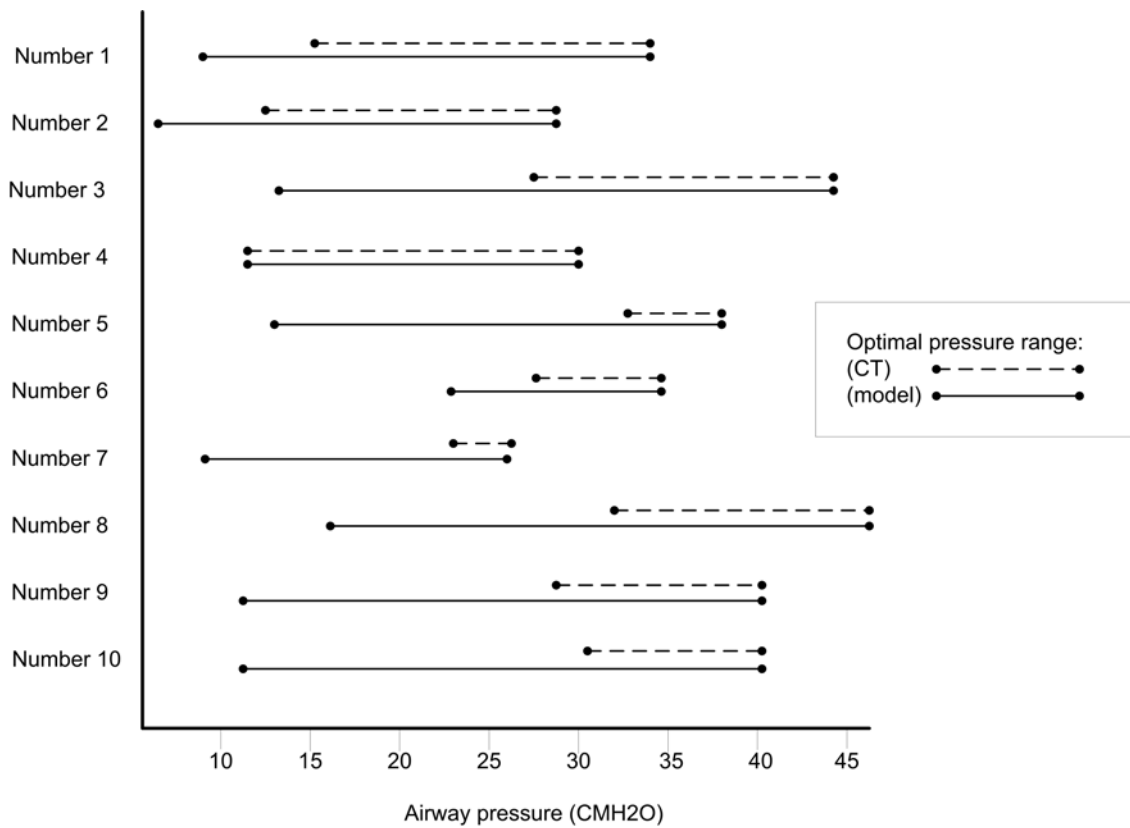

Figure 10.2: *The figure compares the results from table 10.3 which is the optimal pressure range.*

The first inspection of table 10.3 shows that the optimal pressure ranges obtained from the simulations is larger than the optimal pressure ranges from the CT scans. The table also shows that the maximum pressures in the optimal pressure ranges are the same for the model and CT scans which is due to the lack of overdistension in the data materials. The results obtained from pig number 4 and number 6 can be considered the "best" overall result i.e the relationship between the optimal pressure range from the simulations and the extracted optimal pressure range from the CT scans seems to agree well. A graphical result of the simulations obtained from pig number 4 and number 6 can be seen in figure 10.3 and figure 10.4.
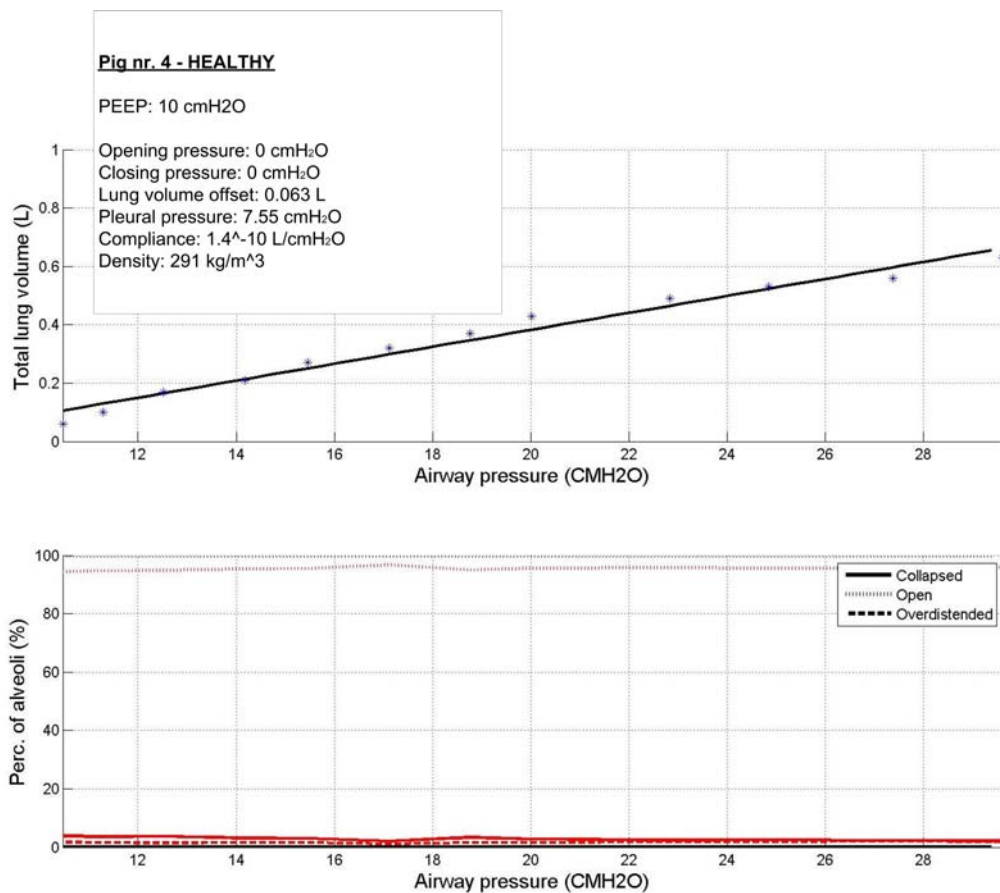

Figure 10.3: *The figure illustrates the simulation of the alveolar states from pig number 4. The first subfigure illustrates the best fit of the model and the static PV data. the second subfigure illustrates the simulated alveolar states (black lines) and the extracted alveolar states from the CT scans (red lines). The inserted subfigure lists the parameter values used to obtain the best fit.*

An inspection of case number 4 in figure 10.3 shows that the simulated alveolar states agrees with the extracted alveolar states from the CT scans. The simulated distribution of open alveoli is 100% along the entire pressure range. The extracted alveolar states from the CT scans are allmost equal distributed along the entire pressure range. However, the distribution of open alveoli never reaches 100 % as well as the distribution of collapsed alveoli never reaches 0 %.

It can furthemore be identified that along the entire static PV curve a small distribution of overdistended alveoli from the extracted CT scans are present. The continous distribution of collapsed alveoli, from the image segmentation algorithm, along the entire static PV curve that never reaches 0% and the continous distribution of overdistended alveoli indicates some sort of error in the image segmentation algorithm. The continous distribution of collapsed alveoli may be due to the problems regarding blood vessels which has been described in chapter 7.4 on page 48.
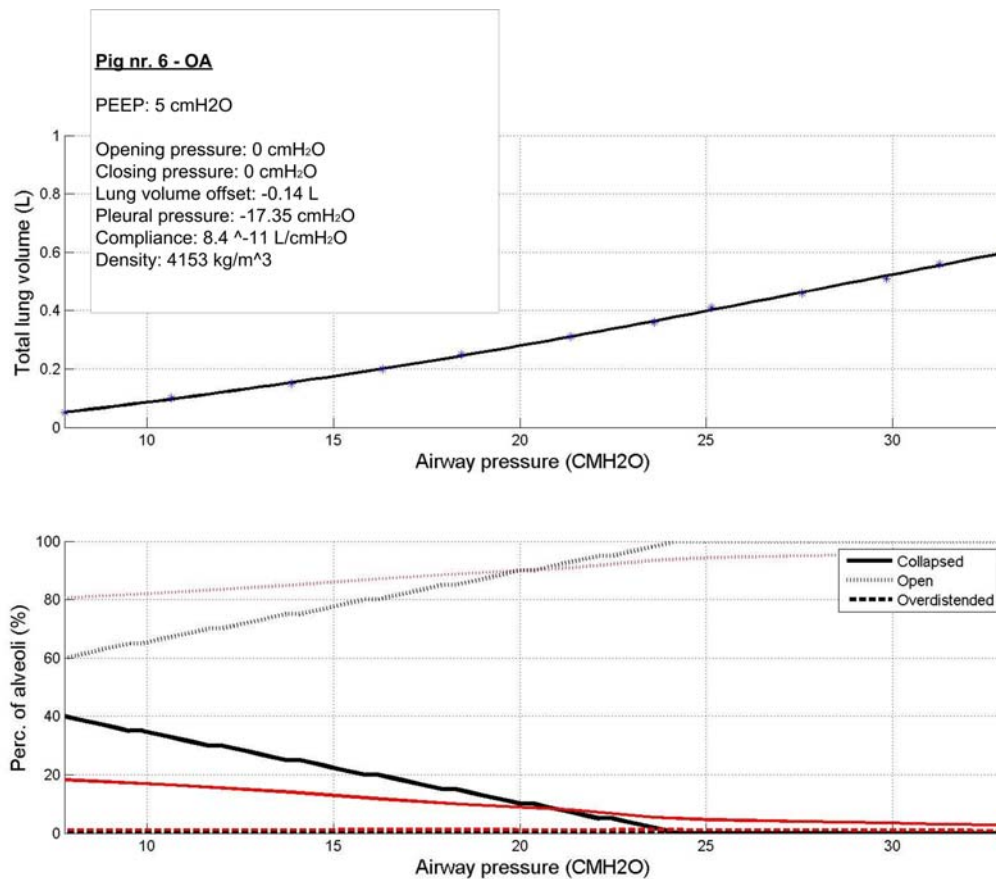

Figure 10.4: *The figure illustrates the simulation of the alveolar states from pig number 6. The first subfigure illustrates the best fit of the model and the static PV data. the second subfigure illustrates the simulated alveolar states (black lines) and the extracted alveolar states from the CT scans (red lines). The inserted subfigure lists the parameter values used to obtain the best fit.*

The simulated and extracted alveolar states from pig number 6 looks quite different from the simulated and extracted alveolar states from pig number 4. The figure shows a weak increase and decrease in the distribution of open and collapsed alveoli respectively which occurs along the entire pressure range. This occurs in both the simulated and extracted alveolar states. As seen in the figure from number 4 and seen in the figure from number 6 the continous distribution of collapsed and overdistended alveoli, from the image segmentation algorithm, along the entire static PV curve does not reach 0%. In fact, this problem is seen in all 10 CT extractions, which can be seen in appendix B

As shown by the results in table 10.3 number 10 yields the "worst" overall result which can be seen in figure 10.5. The simulation of the alveolar states shows that at a pressure at 12 cmH_2O all alveoli are open which also means that there are no collapsed alveoli. The extracted alveolar states shows that the recruitment occurs along the entire static PV curve. The optimal minimum pressure obtained from the CT scans where a steady level of collapsed alveoli is reached is 30 cmH_2O. This minimum pressure is considered very high even for a pig with OA damaged lungs.

Based on the evaluation of the results in table 10.3 and the visual results it can be concluded that there is no relationship between the optimal pressure range obtained from the model simulations and the CT scans.
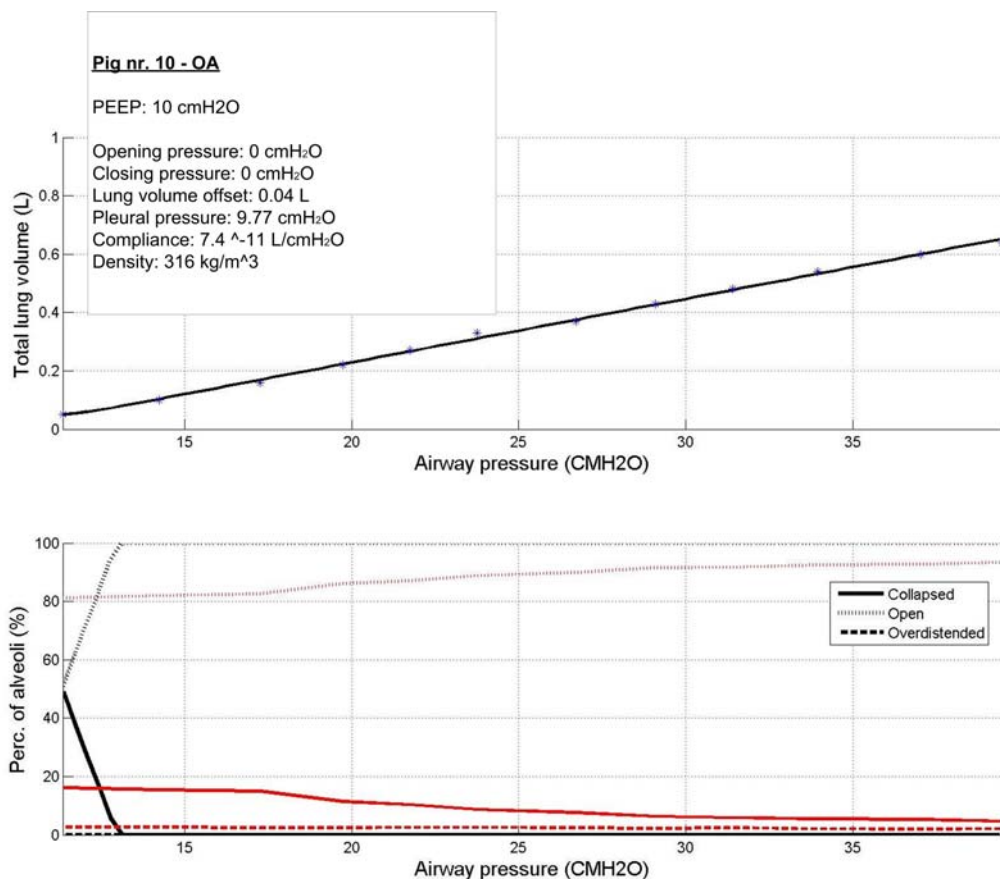

Figure 10.5: *The figure illustrates the simulation of the alveolar states from pig number 7. The first subfigure illustrates the best fit of the model and the static PV data. the second subfigure illustrates the simulated alveolar states (black lines) and the extracted alveolar states from the CT scans (red lines). The inserted subfigure lists the parameter values used to obtain the best fit.*

Test 2 - Progress of collapsed alveoli

Test 2 is a test of whether there is a relationship between the continous distribution of collapsed alveoli that may occur along the static PV curve. The results of the progress of collapsed alveoli which can be seen in table 10.4 are obtained in the following manner: The progress of collapsed

alveoli is equal to the slope or gradient of the line representing the distribution of collapsed alveoli. In the model simulations, the line is always linear which means that the result is the slope of the linear line. If the distribution of collapsed alveoli is equal to 0 along the entire static PV curve the resulting progress of collapsed alveoli is also equal to 0. The collapsed alveoli extracted from the CT scans is not distributed linearly for any of the pigs. In order to calculate a slope representing the progress of collapsed alveoli from the CT scans a linear line is drawn from the start- and end point of the collapsed distribution in which the slope is calculated. As

Number	Model ($\%/\text{cmH}_2\text{O}$)	CT ($\%/\text{cmH}_2\text{O}$)	Difference ($\%/\text{cmH}_2\text{O}$)
1 - A	0	-0.2	0.2
2 - B	0	-0.11	0.11
3 - A	0	-0.3	0.3
4 - B	0	-0.03	0.03
5 - A	0	-0.76	0.76
6 - B	-2.5	-0.69	1.81
7 - C	-25.9	-0.3	25.6
8 - A	0	-0.17	0.17
9 - B	0	-0.14	0.14
10 - C	-20.8	0.4	20.4

Table 10.4: The table lists the results of the progress of collapsed alveoli obtained from the model and CT scans.

the result in table 10.4 shows the progress of collapsed alveoli obtained from the model and CT scans in number 1, 2, 3, 4, 8 and 9 tend to agree. (complete overview of all ten plots can be seen in appendix B) It can be seen that the values from the model in these cases are 0 which means that along the entire static PV curve there are no distribution of collapsed alveoli. The progress of collapsed alveoli in these cases tend to agree because no development in the progress of collapsed alveoli in the CT scans occurs as well. In order to evaluate whether there is a relationship between the progress of collapsed alveoli from the model and CT scans one must evaluate the remaining simulations/extractions which are number 5, 6, 7 and 10. In these cases either the simulations or the CT scans shows development in the progress of collapsed alveoli. Number 7 and 10 indicates the overall "worst" results. The simulation from pig number 10 has previously been discussed and can be seen in figure 10.5. The simulation from pig number 7 can be seen in figure 10.6 As both figures shows the progress of collapsed alveoli from the simulations and extracted from the CT scans does not seems to agree. The progress of collapsed alveoli from the simulation in number 7 and 10 decreases from 50 % to 0 % within 2-3 cmH_2O. This sudden change in the distribution of collapsed alveoli does not occur in the extracted values from the CT scans. The distribution of collapsed and open alveoli from the CT scans along the entire static PV curve is in accordance with results obtained by Pelosi and coworkers. They showed that recruitment is a continuous process that occurs along the entire inspiratory limb of the PV curve of the respiratory system [Pelosi et al., 2001]. It can be concluded that the model is not capable of simulating this continous progress of the alveolar states as seen in the CT scans, which can be considered as a major limitation of the model.
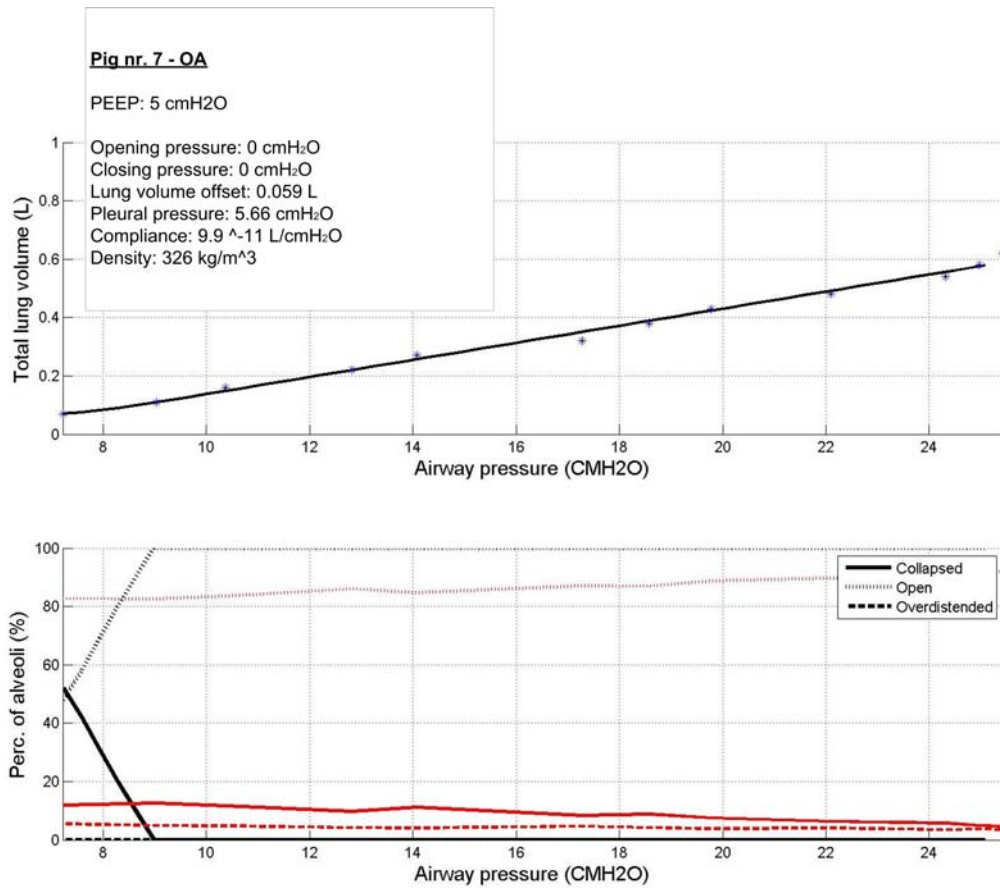
Figure 10.6: *The figure illustrates the simulation of the alveolar states from pig number 6. The first subfigure illustrates the best fit of the model and the static PV data. the second subfigure illustrates the simulated alveolar states (black lines) and the extracted alveolar states from the CT scans (red lines). The inserted subfigure lists the parameter values used to obtain the best fit.*

Parameters used to obtain best fit.

The parameters used to obtain the best fit of the model to PV data encompass as described previously: opening pressure, closing pressure, lung volume offset, pleural pressure, compliance and density. The range of values obtained for these parameters during fit of the model to PV data can be seen in table 10.5. As the table shows not all values of the parameters lies within the normal physiological range.

Number	Opening pressure (cmH_2O)	Closing pressure (cmH_2O)	Lung volume offset (L)	Pleural pressure (cmH_2O)	Compliance (L/cmH2O)	Density (kg/m_3)
1	0	0	0.08	5.7	7.0^{-11}	313
2	0	0	0.05	3.88	9.4^{-11}	298
3	0	0	-0.04	1.19	5.5^{-11}	293
4	0	0	0.06	7.55	1.4^{-10}	291
5	0	0	-0.01	8.62	7.8^{-11}	320
6	0	0	-0.14	-17.35	8.4^{-11}	4153
7	0	0	0.06	5.7	9.9^{-11}	326
8	0	0	-0.03	6.36	6.1^{-11}	314
9	0	0	0.01	8.25	7.0^{-11}	318
10	0	0	0.04	9.77	7.4^{-11}	316

Table 10.5: The different parameter values obtained to fit model to PV data.

The opening pressure and closing pressure are always equal to 0 cmH_2O. These two parameters have not been predefined but used to fit data. However, they have not been changed in order to obtain the best fit. It is most likely that the opening and closing pressures are higher than 0 cmH_2O, especially in patients with ALI/ARDS because of the damaged lung area. The lung volume offset, which has no physiological interpretation, are allmost equal to 0 in each of the ten simulations. This parameter may be applied to correct for any differences in the volume scale between the PV data and the model. The pleural pressure varies between 1.19 to 9.77 cmH_2O. The pleural pressure usually does not become positive unless there is a very forcefull expiration requiring the use of expiratory muscles [Despopoulos and Silbernagl, 2003]. Thus, the obtained values for this parameter seem to lie outside the normal physiological range. The normal compliance of the lung is 0.1 L/cmH_2O [Despopoulos and Silbernagl, 2003]. The compliance listed in the table represents the compliance of the individual alveolus. In order to recalculate the compliance representing a single alveolus into lung compliance, one has to multiply alveoli compliance with the total amount of alveoli in the lungs which is defined as 300 milion. Thus, a recalculation of the highest and lowest value of the alveoli compliance into lung compliance yield: 1.4^{-10} L/cmH_2O equals a lung compliance at 0.04 L/cmH_2O (1.4^{-10} $L/cmH_2O \cdot 300 \cdot 10^6$). 9.9^{-11} L/cmH_2O equals a lung compliance at 0.03 L/cmH_2O (9.9^{-11} $L/cmH_2O \cdot 300 \cdot 10^6$). This range from 0.03 L/cmH_2O to 0.04 L/cmH_2O can be considered relatively low. However, lung compliance as low as 0.02 L/cmH_2O can be seen in ARDS patients [Lumb, 2005] Thus it can be concluded that the obtained values of compliance seems to lie between normal physiological values and values close to ARDS patients.

The density varies between 291 and 326 kg/m^3 in nine out of ten simulations which are close to the normal value at 300 kg/m^3 in healthy subjects. It was expected that density was higher in those cases where OA was induced. Thus, it seems like this parameter does not reflect whether it is a healthy subject or a patient with ARDS. The only simulations with a non normal value of density is from pig number 6. The graphical result from simulation number 6 has allready be shown in figure 10.4. As the figure shows, the distribution of the simulated alveolar states are quite different from all the remaining simulations. The distribution of open and collapsed alveoli in pig number 6 tend to look like the actual extracted distribution of open and collapsed alveoli from the algorithm. However, there is a more significant increase and decrease in the simulated distribution of open, collapsed and overdistended alveoli than in the extracted distribution of the open, collapsed and overdistended alveoli. The upper sub figure showing the static PV curve, indicates that the model seems to fit PV data relatively accurate. Indeed more accurate than in the remaining figures. However, this is not in accordance with the obtained non normal physiological parameter values of pleural pressure and density. The only explanation of this result can be the shape and size of the static PV curve. Compared to the remaining 9 static PV curves, which can be seen in appendix B, this static PV curve seems to reflect the true shape of a static PV curve with a lower inflection point. The remaining 9 static PV curves tends to be more edged and linear. Thus, it seems like the model cannot simulate the true shape of a static PV curve, as the simulation of the true shape of the static PV curve results in non normal physiological values. The model's lack of ability to simulate the true shape of the static PV curve can be considered as another major limitation.

10.3 Conclusion

The purpose of this chapter has been to investigate the relationship between the alveolar states extracted from the CT scans and the simulated alveolar states from the model. Result from the first test showed that there is no relationship between the optimal pressure range identified by the model and extracted from the CT scans. Result from the second test showed that there is no relationship between the progression of collapsed alveoli along the entire static PV curve identified by the model and extracted from the CT scans. It has furthermore been shown that not all of the obtained values of the parameters used to obtain the best fit of the model to PV data were within the normal physiological range. It has also been shown that the model has a lack of ability to simulate the true shape of the static PV curve which may be considered as a major limitation.

Part VI

Closure

Chapter 11

Closure

In the following chapter the important points and results described in the previous chapters will be summarized and dicussed. Furthermore, potential arease of future work are suggested. Finally the conclusion of the project will answer the problem statement formulated in chapter 3, which is: How is the relationship between model simulations from the model based on alveoli compartments and the number of open, collapsed and overdistended alveoli from CT scans?

11.1 Summary

Finding the optimal settings for the ventilatior is normally a simple task. However, in patients with Acute Lung Injury (ALI) and Acute Respiratory Distress Syndrome (ARDS) finding these settings is a more complex task. Lung regions of these patients are often collapsed or overdistended and are therefore not participating in gas exchange. In order to improve gas exchange, prevent further overdistension and recruit the collapsed alveoli, a correct PEEP setting of the ventilator must be selected. Finding appropriate PEEP settings is, however considered very complex, since too low PEEP may cause atelectrauma and too high PEEP may increase PIP which may cause barotrauma and volutrauma The main concern regarding ventilator treatment of these patient groups are therefore to find an accurate balance between appropriate gas exchange and preventing VILI. A way of obtaining information regarding how to find the most appropriate ventilator settings is by evaluating the pressure volume curve. However, in spite of the valuable information the static PV curve can provide it is still a common issue that there is no consensus of how the curve should be interpreted and applied. The evaluation is therefore very often performed by eye which is both unprecise and highly subjective. Another common issue is that the static PV curve is unable to provide information regarding the amount of open, collapsed and overdistended alveoli. As described in chapter 2 in the Introduction and Analysis Part several approaches have been taken to model the static PV curve in order to find a more objective and precise PEEP setting when adjusting the ventilator. However, only a few of these models which are the model based on alveoli compartments and the models based on opening and closing pressures can simulate changes in open, collapsed and overdistended alvoli which could be considered of major concern when trying to avoid VILI. Of these models only the model based on alveoli compartments have been developed with the aim of application in clinical practice and is based on physiological parameters.

The aim of this study is to investigate whether there is a relationship between simulations of the alveolar states from the model based on alveoli compartments and morphological findings of open, collapsed and overdistended alveoli from CT scans. The data materials used in this study for testing this relationship encompasses both CT scans and coherent static PV curves. Both

CT scans and PV curves has been obtained from three different pigs. Four different sequences of examinations from two pigs, and two different sequences of examinations from one pig. The different sequences encompasses measurement with a PEEP setting of 5 or 10 cmH2O and with or without experimental ARDS induced by injection of oleic acid.

An image segmentation algorithm developed by using classical image analysis and processing is presented. The algorithm extracts the lung area from CT scans and estimates the distribution of open, collapsed and overdistended alveoli based on Hounsfield Units (HU). The validation of the algorithm has been carried out by comparing the algorithm segmented lung area with manually extracted lung area extracted by a medical doctor experienced in using lung CT scans. The algorithm extracted lung area showed to agree well both visually, statistically and numerically with the manually segmented lung area.

The model based on alveoli compartments is used to simulate the alveolar states from the 10 different static PV curves obtained from 3 pigs, having either healthy- or OA damaged lungs. The image segmentation algorithm is applied on all the coherent CT scans and the distribution of the alveolar states is extracted. The test of whether there is a relationship betweeen simulations of alveolar states from the model and morphological findings of open, collapsed and overdistended alveoli from CT scans is divided into two subtests. Result from the first test showed that there is no relationship between the optimal pressure range identified by the model and extracted from the CT scans. Result from the second test showed that there is no relationship between the progression of collapsed alveoli along the entire static PV curve identified by the model and extracted from the CT scans. It has furthermore been shown that not all of the obtained values of the parameters used to obtain the best fit of the model to PV data were within the normal physiological range. It has also been shown that the model has a lack of ability to simulate the true shape of the static PV curve which may be considered as a major limitation.

11.2 Discussion and perspectives

During both development and validation of the image segmentation algorithm, analysis of the model including the parameter sensitivity analysis, the subsequent fit of model to PV data and the results of the test several questions and problems have arisen. These questions and problems will be discussed in this section. Furthermore, potential areas of future work are suggested.

The presented image segmentation algorithm is as mentioned capable of extracting the full lung areas in CT slices and based on this calculate the percentage distribution of collapsed, normal and overdistended lung area. During the design of the algorithm several different known image processing techniques and methods were applied. Finding the optimal settings of the applied methods has mostly been based on trials and errors on several different CT slices. However, the obtained trial and error settings proved out in the test of the algorithm to be generaliable and thereby applied in all remaining CT slices. In spite of the good agreement between the algorithm segmented lung area and the manually segmented lung area the algorithm did however prove to have several disadvantages. When it comes to sorting out the small vessels in the lung area the algorithm becomes less acceptable due to its insufficient ability to differentiate between collapsed tissue in the lung area and the small vessels. The consequence of keeping the small vessels in the segmented lung area is that they constitute a possible source of error when segmenting the CT slices. This will affect the estimated value of collapsed tissue since the vessels consist of soft tissue and thereby covers the HU range of collapsed tissue. Since both the manual segmentation

and the algorithm was not capable of sorting out all vessels no reference of correct segmentation has been achieved which made it difficult to determine to what extent the source of error was significant.

Result from the first test showed that there is no relationship between how the model simulates and the algorithm based on CT scans identifies the optimal pressure range. From all ten plots of the compared alveolar states, it can be seen that the extracted distribution of collapsed alveoli never reaches 0 %, even at high pressures above 30 cmH$_2$O. This is obviously an error in the algorithm, which probably could be due to the aforementioned blood vessels. An inspection of all plots, which can be seen in the figures in B, shows that the distribution of collapsed alveoli extracted from the algorithm in plot number 1, 2, 3 and 4 is allmost equally distributed along the entire static PV curve. Theese four plots are from the pigs without OA induced. It is most likely that this equally distribution of collapsed alveoli in the lungs from these pigs does not reflect the real amount of collapsed tissue. This steady distribution of collapsed alveoli may represent the source of error related to the blood vessels.

Future works could eventually deals with improving the image segmentation algorithm in such a way that the vessels are sorted out. In 1994 Sonka and coworkers presented an automated method for segmentation of airway trees from three dimensional sets of CT images. The method was based on a combination of conventional three dimensional seeded region growing used to identify large airways, knowledge based two dimensional segmentation of individual CT slices to identify probable locations of smaller diameter airways and merging of airway regions from the two and three dimensional sets of airway trees. The method proved out to be very effective in the segmentation of airway trees and in the construction of the final airway tree. [Sonka et al., 1994] Especially the knowledge based two dimensional segmentation of the smaller airways used in the method by Sonka and coworkers could in a future study be applied as a part of the image segmentation algorithm.

Another disadvantage of the algorithm is the way it softens certain borders especially at the top of the lung area. As described in the test results, this issue could be due to the erosion technique applied when the final mask was developed. The constant distribution along the entire static PV curve of overdistended alveoli extracted from the algorithm, which can be seen in all plots in appendix B, may be caused by this error segmentation at the top of the lung area. Future works could eventually deals with leaving out several of these erosion operators and instead use recognition patterns of certain problematic areas in the CT scan.

During the validation of the algorithm the manually segmented lung area was segmented by a medical doctor experienced in using lung CT scans. These manually segmented lung areas were used as "optimal" references when comparing with the algorithm segmented lung areas. However, this way of obtaining a reference of optimal segmentation can be questioned in several ways. The manual segmentation method is not without disadvantages. It is a very subjective method, which relies on the expert's knowledge, experience and awareness. In order to segment the lung area in the most exactly way the method needs a large number of fixpoints around the border of the lung area. These fixpoint marked by the expert has to be marked very accurate between the lung area and the surrounding tissue. in order to segment the the "true" lung area. If a small amount of fixpoints are used it could cause a cut off of some area close to the border. However this very subjective method as a manual segmentation is, can be compensated by letting more than one medical doctor segment the CT scans. By using several experts instead of one it would have been possible to investigate the variance of the manual extracted lung area and

thereby have taken this into account when comparing the results.

The results from the second test show that there is no relationship between how the model simulates and the algorithm based on CT scans identifies the distribution of collapsed alveoli. In seven out of ten plots the simulated progress of collapsed alveoli is equal to 0 %/cmH$_2$O along the entire static PV curve. (pig number 1, 2, 3, 4, 5, 8 and 9). In the plots from pig number 7 and 10 it can be seen that the simulated distribution of collapsed alveoli is starting from approximately 50 % in the beginning of the pressure range and decreased to 0 % within a range of 2-3 cmH$_2$O. This is clearly not the case in the distribution of collapsed alveoli extracted from the CT scans. The distribution of collapsed alveoli from the CT scans tend to decrease over a longer pressure range. The plot from pig number 6 is the only one showing the same gradient of the distribution of collapsed alveoli i.e. recruitment over the entire static PV curve. What probably is the most interesting in pig number 6 is the non normal physiological values of the parameters used to obtain the best fit. Especially density at 4153 kg/m^3 and pleural pressure at -17.35 cmH$_2$O are considered to be above and beyond normal physiological values. In spite of these non normal values the fit of the model to PV data in this case seems to fit accurately compared to the nine remaining model fits. An inspection of the different plots in the parameter sensitivity analysis shows that pleural pressure affects the shape of the static PV curve by shifting it in a horizontal direction. The shifting in a horizontal direction is also seen in the resulting simulated alveolar states. This means that the non normal value of pleural pressure probably not is causing the significant change in the alveolar states. On the other hand, an inspection of density in the parameter sensitivity analysis shows to affect the alveolar states in a way that flattens the progression of open, collapsed and overdistended alveoli. In fact this way of flattening the simulated alveolar states, is only seen in the sensitivity analysis of density and the height of the lungs. Density and the height of the lungs are both described in equation 8.1 at page 65, which means that this equation is the only part in the model that accounts for the flattering effects of the alveolar states as seen in the simulations The non normal value of density obtained in the case with pig number 7, is approximately ten times to large compared to the normal value. This indicates that the hydrostatic effect described in this equation may be a factor ten too small. Future works could eventually deals with a more specific analyze of this part of the model.

11.3   Conclusion

An image segmentation algorithm that extracts the lung area from CT scans and estimates the distribution of open, collapsed and overdistended alveoli based on Hounsfield Units (HU) has been developed. The validation of the algorithm was carried out by comparing the algorithm segmented lung area with manually extracted lung area extracted by a medical doctor experienced in using lung CT scans. The algorithm extracted lung area showed out to agree well both visually, statistically and numerically with the manually segmented lung area. The model based on alveoli compartments was used to simulate the alveolar states from 10 different static PV curves obtained from 3 pigs, having either healthy lungs or OA damaged lungs. The image segmentation algorithm was applied on all the coherent CT scans and the distribution of the alveolar states was extracted. The test of whether there is a relationship betweeen simulations of alveolar states from the model and morphological findings of open, collapsed and overdistended alveoli from CT scans were divided into two subtests. Results from the first test showed that there is no relationship between the optimal pressure range identified by the model and extracted from the CT scans. Results from the second test showed that there is no relationship between the progression of collapsed alveoli along the entire static PV curve identified by the model and

extracted from the CT scans. It has furthermore been shown that not all of the obtained values of the parameters used to obtain the best fit of the model to PV data were within the normal physiological ranges. It has also been shown that the model has a lack of ability to simulate the true shape of the static PV curve. Future work could deal with a more specific analysis and whether to improve the equation describing the hydrostatic effect in the model. Future work could also deal with improving the image segmentation algorithm when it comes to sorting out vessels in the lungs.

Bibliography

Amato, M., Barbas, C., Medeiros, D., Magaldi, R., Schettino, G., Lorenzi-Fihlo, G., Kairalla, R., Deheinzelin, D., Munoz, C., Oliveira, R., Takagaki, T., and Carvalho, C. (1998a). Effect of protective-ventilation strategy on mortality in the acute respiratory distress syndrome. *New England Journal Medicine*, 338:347–354.

Amato, M., Barbas, C., Medeiros, D., Magaldi, R., Schettino, G., Lorenzi-Filho, G., Kairalla, R., Deheinzelin, D., Munoz, C., R.Oliveira, Takagaki, T., and Carvalho, C. (1998b). Effect of a protective-ventilation strategy on mortality in the acute respiratory distress syndrome. *US Government Printing Office, DHEW Publication*, 338:347–354.

Austin, J., Müller, N., Friedman, P., Hansell, D., Naidich, D., Remy-Jardin, M., Webb, W., and Zerhouni, E. (1996). Glossary of terms for ct of the lungs: recommendations of the nomenclature committee of the fleischner society. *Radiology*, 200:327–331.

Bein, T., Kuhr, L., Bele, S., Ploner, F., Keyl, C., and Taeger, K. (2002). Lung recruitment maneuver in patients with cerebral injury: effects on intracranial pressure and cerebral metabolism. *Intensive Care Med.*, 28:554–558.

Bernard, G., Artigas, A., Brigham, K., Carlet, J., Falke, K., and Hudson, L. (1994). The american-european consensus conference on ards. definitions, mechanisms, relevant outcomes, and clinical trial coordination. *Am J Respir Crit Care Med*, 149:818–824.

Bogaard, J., Overbeek, S., Verbraak, A., Vons, C., Folgering, H., van der Mark, T., Roos, C., and Sterk, P. (1995). Pressure-volume analysis of the lung with an exponential and linear-exponential model in asthma and copd. *Eur Respir J*, 8:1525–1531.

Bond, D. and Froese, A. (1993). Volume recruitment maneuvers are less deleterious than persistent low lung volumes in the atelectasisprone rabbit lung during high-frequency oscillation. *Critical Care Medicine*, 21:402–412.

Bond, D., McAloon, J., and Froese, A. (1994). Sustained inflations improve respiratory compliance during high-frequency oscillatory ventilation but not during large tidal volume positive-pressure ventilation in rabbits. *Critical Care Medicine*, 22:1269–1277.

Bone, R. (1976). Diagnosis of causes for acute respiratory distress by pressure-volume curves. *Chest*, 70:740–746.

Brismar, B., Hedenstierna, G., Lundquist, H., Strandberg, A., Svensson, L., and Tockics, T. (1985). Pulmonary densities during anesthesia with muscolar relaxation. a proposal of atelectasis. *Anesthesiology*, 62:422–428.

Broccard, A., Shapiro, R., Schmitz, L., Adams, A., Nahum, A., and Marini, J. (2000). Prone positioning attenuates and redistributes ventilator-induced lung injury in dogs. *Crit Care Med.*, 28:295–303.

Cakar, N., Akinci, O., Tugrul, S., Ozcan, P., Esen, F., Eraksoy, H., Cagatay, A., Telci, L., and Nahum, A. (2002). Recruitment maneuver: does it promote bacterial translocation? *Crit Care Med.*, 30:2103–2106.

Cakar, N., van der Kloot, T., and Nahum, M. Y. A. A. A. (2000). Oxygenation response to a recruitment maneuver during supine and prone positions in an oleic acid-induced lung injury model. *Journal Respiratory Critical Care Medicine*, 161:1949–1956.

Carroll, G., Tuman, K., Braverman, B., Logas, W., Wool, N., and Ivankovic, A. (1988). Minimal end-expiratory pressure (peep) may be best peep. *Chest*, 93:1020–1025.

Chase, J. G., Yuta, T., Mulligan, K. J., Shaw, G. M., and Horn, B. (2006). A novel mechanical lung model of pulmonary diseases to assist with teaching and training. *BMC Pulmonary Medicine*, 6:21.

Claxton, B., Morgan, P., Mckeague, H., Mulpur, A., and Berridge, J. (2003). Alveolar recruitment strategy improves arterial oxygenation after cardiopulmonary bypass. *Anaesthesia*, 58:111–116.

Crotti, S., Mascheroni, D., Caironi, P., Pelosi, P., Ronzoni, G., Mondino, M., Marini, J., and Gattinoni, L. (2001). Recruitment and derecruitment during acute respiratory failure: a clinical study. *Am J Respir Crit Care Med*, 164:131–140.

Dale, P. J., Matthews, L. F., and Schroter, R. C. (1980). Finite element analysis of lung alveolus. *Journal of Biomechanics*, 13:865–873.

Dambrosio, E. R. A. M. and Servillo, G. (1995). Titration of tidal volume and induced hypercapnia in acute respiratory distress syndrome. *Am J Respir Crit Care Med*, 152:121–128.

Dambrosio, M., Roupie, E., Mollet, J., Anglade, M., Vasile, N., and Brochard, F. L. L. (1997). Effects of positive end-expiratory pressure and different tidal volumes on alveolar recruitment and hyperinflation. *Anesthesiology.*, 87:495–503.

Desai, S. R., Wells, A. U., Rubens, M. B., Evans, T. W., and Hansell, D. M. (1999). Acute respiratory distress syndrome: Ct abnormalities at long-termfollow-up. *Radiology*, 210:29–35.

Despopoulos, A. and Silbernagl, S. (2003). *Color Altas of Physiology.* Thieme.

Dreyfuss, D., Basset, G., Soler, P., and Gy, G. S. (1985). positive-pressure hyperventilation with high inflation pressures produces pulmonary microvascular injury in rats. *American Review of Respiratory Disease*, 132:880–884.

Dreyfuss, D. and Saumon, G. (1998). Ventilator induced lung injury. *Am Journal Respiratory Crit Care Med*, 157:294Ũ323.

Dreyfuss, D., Soler, P., Basset, G., and Saumon, G. (1988). High inflation pressure pulmonary edema. respective effects of high airway pressure, high tidal volume, and positive end-expiratory pressure. *American Review of Respiratory Disease*, 137:1159–1164.

Dyhr, T., Laursen, N., and Larsson, A. (2002). Effects of lung recruitment maneuver and positive end-expiratory pressure on lung volume, respiratory mechanics and alveolar gas mixing in patients ventilated after cardiac surgery. *Acta Anaesthesiol Scand.*, 46:717–725.

Evans, B., Wachter, J., Wiener-Kronish, and Luce, J. (1988). Incidence of the adult respiratory distress syndrome in an urban population. *Am Rev Respir Dis*, 137:A469.

Frazer, D., Lindsley, W., Rosenberry, K., McKinney, W., Goldsmith, W., Reynolds, J., Tomblyn, S., and Afshari, A. (2004). Model predictions of the recruitment of lung units and the lung surface areavolume relationship during inflation. *Ann Biomed Eng*, 32:756–763.

Fujino, Y., Goddon, S., Dolhnikoff, M., Hess, D., Amato, M., and Kacmarek, R. (2001). Repetitive high-pressure recruitment maneuvers required to maximally recruit lung in sheep model of acute respiratory distress syndrome. *Crit Care Med.*, 29:1579–1586.

Funk, D., Graham, M., and Girling, L. (2004). A comparison of biologically variable ventilation to recruitment manoeuvres in a porcine model of acute lung injury. *Respir Res*, 5:22.

Gattinoni, L., Andrea, D., Pelosi, P., Vitale, P., Pesenti, G., and Fumagalli, R. (1993). Regional effects and mechanism of positive end-expiratory pressure in early adult respiratory distress syndrome. *Jama*, 269:2122–7.

Gattinoni, L., Caironi, P., Pelosi, P., and Goodman, L. R. (2001). What has computed tomography taught us about the acute respiratory distress syndrome. *American Journal Respiratory Critical Care Medicine*, 164:1701–1711.

Gattinoni, L., Pelosi, P., Crotti, S., and Valenza, F. (1995). Effects of positive end expiratory pressure on regional distribution of tidal volume and recruitment in adult respiratory distress syndrome. *Am J Respir Crit Care Med*, 151:1807–1814.

Gattinoni, L., Pesenti, A., Bombino, M., Baglioni, S., Rivolta, M., Rossi, F., Rossi, G., Fumagalli, R., Marcolin, R., and Mascheroni, D. (1988). Relationships between lung computed tomographic density, gas exchange, and peep in acute respiratory failure. *Anesthesiology*, 69:824–832.

Gattinoni, L., Pesenti, A., Rossi, L. A. A. F., and Bombino, M. (1987). Pressure-volume curve of total respiratory system in acute respiratory failure. computed tomographic scan study. *Am Rev Respir Dis*, 136:730–736.

Gattinoni, L., Presenti, A., and Torresin, A. (1986). Adult respiratory distress syndrome profiles by computed tomography. *J Thorac Imaging*, 1:25.

Gattiononi, L., Pesenti, A., Avalli, L., Ross, F., and Bomino, M. (1987). Pressurevolume curve of total respiratory system in acute respiratory failure: computed tomographic scan study. *American Review of Respiratory Disease*, 136:730–736.

Gibson, G., Pride, J., Davis, J., and Schroter., R. (1979). Exponential description of the static pressure-volume curve of normal and diseased lungs. *Am Rev Respir Dis*, 120:799–8111.

Gonzales, R. C., Woods, R. E., and Eddins, S. L. (2004). *Digital image processing using matlab*. Pearson.

Goodman, P. (2000). Radiographic findings in patients with acute respiratory distress syndrome. *Clin Chest Med.*, 21:419–433.

Grasso, S., Mascia, L., and del Turco, M. (2002). Effects of recruiting maneuvers in patients with acute respiratory distress syndrome ventilated with protective ventilatory strategy. *Anesthesiology*, 96:795–802.

Hall, J., Schmidt, G., and Wood, L. (1998). Acute hypoxemic respiratory failure. *Principles of Critical Care.*, pages 537–564.

Harman, E. M. and Walia, R. (2006). *Acute Respiratory Distress Syndrome.* `http://www.emedicine.com/med/topic70.htm`.

Harris, R., Hess, D., and Venegas, J. (2000). An objective analysis of the pressure-volume curve in the acute respiratory distress syndrome. *American Journal Respiratory Critical care medicine*, 161:432Ű439.

Harris, R. S. (2005). Pressure-volume curves of the respiratory system. *Respiratory care*, 50.

Heart, N. and Lung Institute, N. I. o. H. (1972). Respiratory distress syndromes: Task force report on problems. *US Government Printing Office, DHEW Publication*, 73-432:165–180.

Heller, H., Brandt, S., and Scuster, K.-D. (2002). Development of an algorithm for improving the description of the pulmonary pressure-volume curve. *J Appl Physiol*, 92:1770Ű1771.

Henzler, D., Orfao, S., Rossaint, R., and Kuhlen, R. (2003). Modification of a sigmoidal equation for the pulmonary pressure-volume curve for asymmetric data. *Journal Appl Physiol*, 95:2183–2184.

Hess, D. and Bigatello, L. (2002). Lung recruitment: the role of recruitment maneuvers. *Respiratory Care*, 47:308–317.

Hickling, K. (1997). Mechanical ventilation in ards: is the lung a promotor of multiple organ failure? *Journal Anesth*, 11:50–64.

Hickling, K. (1998). The pressure-volume curve is greatly modified by recruitment: a mathematical model of ards lungs. *American Journal Respiratory Critical care medicine*, 158:194–202.

Hickling, K. (2001). Best compliance during a decremental, but not incremental, positive end-expiratory pressure trial is related to open-lung positive end-expiratory pressure: a mathematical model of acute respiratory distress syndrome lungs. *American Journal Respiratory Critical care medicine*, 163:69–78.

Hyde, D., Tyler, N., Putney, L., Singh, P., and Gundersen, H. (2003). Total number and mean size of alveoli in mammalian lung estimated using fractionator sampling and unbiased estimates of the euler characteristic of alveolar openings. *Wiley Interscience, The Anatomical Record Part A: Discoveries in Molecular, Cellular, and Evolutionary Biology*, 277A:216–226.

Ichikado, K., Johkoh, T., and Ikezoe, J. (1997). Acute interstitial pneumonia: high-resolution ct findings correlated with pathology. *AJR Am J Roentgenol*, 168:333–338.

Ichikado, K., Suga, M., and Gushima, Y. (2000). Hyperoxia induced diffuse alveolar damage in pigs: correlation between thin-section ct and histopathologic findings. *Radiology*, 216:531–538.

Ingimarsson, J., Bjorklund, L., Larsson, A., and Werner, O. (2001a). The pressure at the lower inflexion point has no relation to airway collapse in surfactant-treated premature lambs. *Acta Anaesthesiologica Scandinavica*, 45:690–695.

Ingimarsson, J., Björklund, L., Larsson, A., and Werner, O. (2001b). The pressure at the lower inflexion point has no relation to airway collapse in surfactant-treated premature lambs. *Acta Anaesthesiologica Scandinavica*, 45:690–695.

Johannigman, J., Miller, S., Davis, B., Davis, K. J., Campbell, R., and Branson, R. (2003). Influence of low tidal volumes on gas exchange in acute respiratory distress syndrome and the role of recruitment maneuvers. *J Trauma.*, 54:320–325.

Kloot, T. V., Blanch, L., Youngblood, A., Weinert, C., Adams, A., Marini, J., Shapiro, R., and Nahum, A. (2000). Recruitment maneuvers in three experimental models of acute lung injury. effect on lung volume and gas exchange. *Am J Respir Crit Care Med.*, 161:1485–1494.

Kowe, R. and Schroter, R. C. (1986). Analysis of elastic and surface tension effects in the lung alveolus using finite element methods. *Journal of Biomechanics*, 19:541–549.

Lapinsky, S., Aubin, M., Mehta, S., Boiteau, P., and Slutsky, A. (1999). Safety and efficacy of a sustained inflation for alveolar recruitment in adults with respiratory failure. *Intensive Care Med.*, 25:1297–1301.

Lim, C., Jung, H., Koh, Y., Lee, J., Shim, T., Lee, S., Kim, W., Kim, D., and Kim, W. (2003). Effect of alveolar recruitment maneuver in early acute respiratory distress syndrome according to antiderecruitment strategy, etiological category of diffuse lung injury, and body position of the patient. *Crit Care Med.*, 31:411–418.

Lu, Q., Capderou, A., Cluzel, P., Mourgeon, E., Abdennour, L., Law-Koune, J., Grenier, C. S. A., Zelter, M., and Rouby, J. (2000). A computed tomographic scan assessment of endotracheal suctioning-induced bronchoconstriction in ventilated sheep. *Am J Respir Crit Care Med.*, 162:1898–1904.

Lu, Q. and Rouby, J.-J. (2000). Measurement of pressure-volume curves in patients on mechanical ventilation: methods and significance. *Critical Care*, 4:91–100.

Lu, Q., Vieira, S., and Richecoeur, J. (1999). A simple automated method for measuring pressure-volume curve during mechanical ventilation. *Am J Respir Crit Care Med*, 159:275–282.

Lumb, A. B. (2005). *Nunn's Applied Respiratory Physiology*. Elsevier, 6 edition.

MacIntyre, N. R. (2000). Mechanical ventilation strategies for lung protection. *Seminars in respiratory and critical care medicine*, 21.

Maggiore, S., Lellouche, F., Pigeot, J., Taille, S., Deye, N., Durrmeyer, X., Richard, J., Mancebo, J., Lemaire, F., and Brochard, L. (2003a). Prevention of endotracheal suctioning-induced alveolar derecruitment in acute lung injury. *American Journal Respiratory Critical Care Medicine*, 167:1215Ű1224.

Maggiore, S., Richard, J.-C., and Brochard, L. (2003b). What has been learnt from p/v curves in patients with acute lung injury/acute respiratory distress syndrome. *European Respiratory Journal*, 22:22–26.

Malbouisson, L. M., Muller, J. C., Constantin, J. M., Lu, Q., Puybasset, L., and Rouby, J.-J. (2001). Computed tomography assessment of positive end expiratory pressure induced alveolar recruitment in patients with acute respiratory distress syndrome. *Am J Respir Crit Care Med*, 163:1444–1450.

Markhorst, D. G., van Genderingen, H. R., and van Vught, A. J. (2004). Static pressure-volume curve characteristics are moderate estimators of optimal airway pressures in a mathematical model of (primary/pulmonary) acute respiratory distress syndrome. *Intensive Care Medicine*, pages 2086–2093.

Martini, F. H. (2004). *Fundamentals of anatomy and physiology.* Benjamin Cummings.

Matamis, D., Lemaire, F., and Harf, A. (1984a). Total respiratory pressure-volume curves in the adult respiratory distress syndrome. *Chest*, 86:58–66.

Matamis, D., Lemaire, F., Harf, A., Teisseire, B., and Brun-Buisson, C. (1984b). Redistribution of pulmonary blood flow induced by positive end-expiratory pressure and dopamine infusion in acute respiratory failure. *Chest*, 129:39–44.

Mathworks (2007). *Matlab newsgroup.* `http://www.mathworks.de/matlabcentral/newsreader/view_thread/153873`.

Matthews, F. L. and West, J. B. (1972). Finite element displacement analysis of a lung. *Journal of Biomechanics*, 5:591–600.

Mergoni, M., Martelli, A., Volpi, A., Primavera, S., Zuccoli, P., and Rossi., A. (1997). Impact of positive end-expiratory pressure on chest wall and lung pressure-volume curve in acute respiratory failure. *Am. J. Respir. Crit. Care Med.*, 156:846–854.

National-Heart-Lung-Institute (2007). *ARDS - Who is at risk?* `http://www.nhlbi.nih.gov/health/dci/Diseases/Ards/Ards_WhoIsAtRisk.html%`.

Pasenti, A., Tagliabue, P., Patroniti, N., and Fumagalli, R. (2001). Computerized tomography scan imaging in acute respiratory distress syndrome. *Intensive Care Med.*, 27:631–639.

Patroniti, N., Foti, G., Cortinovis, B., Maggioni, E., Bigatello, L., Cereda, M., and Pesenti, A. (2002). Sigh improves gas exchange and lung volume in patients with acute respiratory distress syndrome undergoing pressure support ventilation. *Anesthesiology*, 96:788Ű794.

Payán, D. R., Pedroza-Granados, J., and Domínguez-Cherit, G. (2001). Acute respiratory distress syndrome and ct scans. *RT magazine.*

Pelosi, P., Brazzi, L., and Gattinoni, L. (1999a). Diagnostic imaging in acute respiratory distress syndrome. *Current Opinion in Critical Care*, 5:9–16.

Pelosi, P., Cadringher, P., Bottino, N., Panigada, M., Carrieri, F., Riva, E., Lissoni, A., and Gattinoni, L. (1999b). Sigh in acute respiratory distress syndrome. *Am J Respir Crit Care Med.*, 159:872–880.

Pelosi, P., Goldner, M., McKibben, A., Adams, A., Eccher, G., Caironi, P., Losappio, S., Gattinoni, L., and Marini, J. (2001). Recruitment and derecruitment during acute respiratory failure: an experimental study. *Am J Respir Crit Care Med.*, 164:122–130.

Peruzzi, W., Franklin, M., and Shapiro, B. (1997). New concepts and therapies of adult respiratory distress syndrome. *J cardiothorac Vasc Anesth*, 11:771–786.

Piacentini, E., Villagrá, A., Aguilar, J. L., and Blanch, L. (2003). Clinical review: The implications of experimental and clinical studies of recruitment maneuvers in acute lung injury. *Crit Care.*, 8:115–121.

Puybasset, L., Cluzel, P., Chao, N., Slutsky, A., Coriat, P., Rouby, J., and Group, T. C. S. A. S. (1998). A computed tomography scan assessment of regional lung volume in acute lung injury. *Am J Respir Crit Care Med*, 158:1644–1655.

Puybasset, L., Rouby, J., Mourgeon, E., Cluzel, P., Souhil, Z., Law-Koune, J., Stewart, T., Devilliers, C., Lu, Q., and Roche, S. (1995). Factors influencing cardiopulmonary effects of inhaled nitric oxide in acute respiratory failure. *Am J Respir Crit Care Med.*, 152:318–328.

Rahn, H., Fenn, W., and Otis, A. (1946). The pressure-volume diagram of the thorax and the lung. *American Journal Phys.*, 146:161Ũ178.

Ressmeyer, A., Larsson, A., Vollmer, E., Dahlèn, S., Uhlig, S., and Martin, C. (2006). Characterisation of guinea pig precision-cut lung slices: comparison with human tissues. *European Respiratory Journal*, 28:603–11.

Richard, J., Maggiore, S., Jonson, B., Mancebo, J., Lemaire, F., and Brochard, L. (2001). Influence of tidal volume on alveolar recruitment. respective role of peep and a recruitment maneuver. *American Journal Respiratory Critical Care Medicine*, 163:1609–1613.

Rimensberger, P., Cox, P., Frndova, H., and Bryan, C. (1999). The open lung during small tidal volume ventilation: concepts of recruitment and 'optimal' positive end-expiratory pressure. *Crit Care Med.*, 27:1946–1952.

Rothen, H., Sporre, B., Engberg, G., Wegenius, G., Hogman, M., and Hedenstierra, G. (1995). Influence of gas composition on recurrence of atelectasis after a reexpansion maneuver during general anaesthesia. *Anaesthesiology*, 82:832–842.

Rotta, A. T. (2006). Lung-protective ventilation in pediatrics. *US Respiratory Care.*

Sandhar, B., Niblett, D. J., Argiras, E. P., Dunhill, M. S., and Sykes., M. K. (1988). Effects of positive end-expiratory pressure on hyaline membrane formation in a rabbit model of the neonatal respiratory distress syndrome. *Intensive Care Medicine*, 14:538–546.

Santos, C. C., Zhang, H., Liu, M., and Slutsky, A. S. (2005). Bench-to-bedside review: Biotrauma and modulation of the innate immune response. *Critical Care*, 9:280–286.

Servillo, G., Svantesson, C., and Beydon, L. (1997). Pressure volume curves in acute respiratory failure. automated low flow inflation versus occlusion. *Am J Respir Crit Care Med*, 155:1629–1636.

Simon, B., Christensen, G., Low, D., and einhardt, J. (2005). Computed tomography studies of lung mechanics. *Proc Am Thorac Soc*, 2:517–521.

Slutsky, A. (1999). Lung injury caused by mechanical ventilation. *Chest*, 116:9S–15S.

Smith, B. W., Rees, S. E., Tvorup, J., Christensen, C., and Andreassen, S. (2005). Modeling the influence of the pulmonary pressure-volume curve on gas exchange. *27th Annual International Conference of the IEEE Engineering in Medicine and Biology Society.*

Sonka, M., Sundaramoorthy, G., and Hoffman, E. (1994). Knowledge based segmentation of intrathoracic airways from multidimensional high resolution ct images. *Medical Imaging*, 2168:73–85.

Tagliabue, P., Gianatelli, F., and Vedovati, S. (1998). Lung ct scan in ards: are three sections representative of the entire lung? *Intensive Care Med.*, 24:s93.

Takeuchi, M., Goddon, S., Dolhnikoff, M., Shimaoka, M., Hess, D., Amato, M., and Kacmarek, R. (2002). Set positive end-expiratory pressure during protective ventilation affects lung injury. *Anesthesiology*, 97:682–92.

Takishima, T. and Mead, J. (1972). Tests of a model of pulmonary elasticity. *J Appl Physiol*, 33:576Ű581.

Tawhai, M., Hunter, P., Tschirren, J., Reinhardt, J., McLennan, G., and Hoffman, E. (2004). Ct-based geometry analysis and finite element models of the human and ovine bronchial tree. *J Appl Physiol*, 97:2310Ű2321.

Tawhai, M., Nash, M., Tschirren, J., Hoffman, E., and Hunter, P. (2005). An imagebased computational model of ovine lung mechanics and ventilation distribution. *Proc. SPIE*, 5746:84–91.

The ARDS foundation (2007). *XRAYS of Lungs affected with ARDS*. `http://www.ardsil.com/xray.htm`.

Tusman, G., Böhm, S., de Anda Vázquez, G., do Campo, J., and Lachmann, B. (1999). Alveolar recruitment strategy' improves arterial oxygenation during general anaesthesia. *Br J Anaesth.*, 82:8–13.

Tusman, G., Böhm, S., Melkun, F., Staltari, D., Quinzio, C., Nador, C., and Turchetto, E. (2002). Alveolar recruitment strategy increases arterial oxygenation during one-lung ventilation. *Ann Thorac Surg.*, 73:1204Ű1209.

Umamaheswara, G., Gallart, L., Law-Koune, J., Lu, Q., Cluzel, L. P. P., Coriat, P., and Rouby, J. (1997). Factors influencing the tracheal fluctation of inhaled nitric oxide in patients with acute lung injury. *Anesthesiology.*, 87:823–834.

Venegas, J., Harris, R., and Simon, B. (1998). A comprehensive equation for the pulmonary pressure volume curve. *American Journal Appl Physiol*, 84:389–395.

Venegas, J., Tsuzaki, K., Fox, B., Simon, B., and Hales, C. (1993). Regional coupling between chest wall and lung expansion during hfv, a positron imaging study. *J Appl Physiol*, 74:2242Ű2252.

Vieira, S., Puybasset, L., and Lu, Q. (1999a). A scanographic assessment of pulmonary morphology in acute lung injury. *Am J Respir Crit Care Med.*, 159:1612–1623.

Vieira, S. R. R., Puybasset, L., Lu, Q., Richecoeur, J., Cluzel, P., Coriat, P., and Rouby, J.-J. (1999b). A scanographic assessment of pulmonary morphology in acute lung injury. significance of the lower inflection point detected on the lung pressure-volume curve. *American Journal Respiratory Critical Care Medicine*, 159:1612–1623.

Vieira, S. R. R., Puybasset, L., Richecoeur, J., Lu, Q., Cluzel, P., Gusman, P. B., Coriat, P., and Rouby, J.-J. (1998). A lung computed tomographic assessment of positive end-expiratory pressure-induced lung overdistension. *American Journal Respiratory Critical Care Medicine*, 158:1571–1577.

Villagrá, A., Ochagavia, A., Vatua, S., Murias, G., Fernandez, M., López-Aguilar, J., Fernandez, R., and L., L. B. (2002). Recruitment maneuvers during lung protective ventilation in acute respiratory distress syndrome. *Am J Respir Crit Care Med.*, 165:165–170.

Villar, J. and Slutsky, A. (1989). The incidence of the adult respiratory distress syndrome. *Am Rev Respir Dis*, 140:814Ű816.

Webb, H. and Tierney, D. (1974). Experimental pulmonary edema due to intermittent positive pressure ventilation with high inflation pressures. protection by postive end-expiratory pressure. *American Review of Respiratory Disease*, 110:556–565.

West, J. B. (2003). *Pulmonary pathophysiology.* Lippincott Williams and Wilkins.

Zhao, Y., Rees, S. E., Kjærgaard, S., Smith, B. W., Larsson, A., and Andreassen, S. (2007). An automated method for measuring static pressureŨvolume curves of the respiratory system and its application in healthy lungs and after lung damage by oleic acid infusion. *Physiol. Meas.*, 28:235–247.

Part VII

Appendix

Appendix A

Nomenclature

ALI: Acute Lung Injury

ARDS: Acute Respiratory Distress Syndrome

Cinf/Clin: Higher compliance region at higher lung volumes

CLIN: Compliance with linear segment

Cstart/Cend: A low compliance region

CT: Computed Tomography

ICU: Intensive Care Unit

LIP: Lower Inflection Point

PEEP: Positive End Expiratory Pressure

PIP: Peak Inspiratory Pressure

FRC: Functional Residual Capacity

TCP: Threshold Closing Pressure

TLC: Total Lung Capacity

TOP: Threshold Opening Pressure

VILI: Ventilator Induced Lung Injury

UIP: Upper Inflection Point

ZEEP: Zero End Expiratory Pressure

WOB: Work Of Breathing

Appendix B

Simulation results

This appendix contain all the graphical results obtained from the simulation of the alveolar states and the extraction of the alveolar states from the CT scans. All the obtained parameter values resulting in the best fit of model to PV data are furthermore listed.
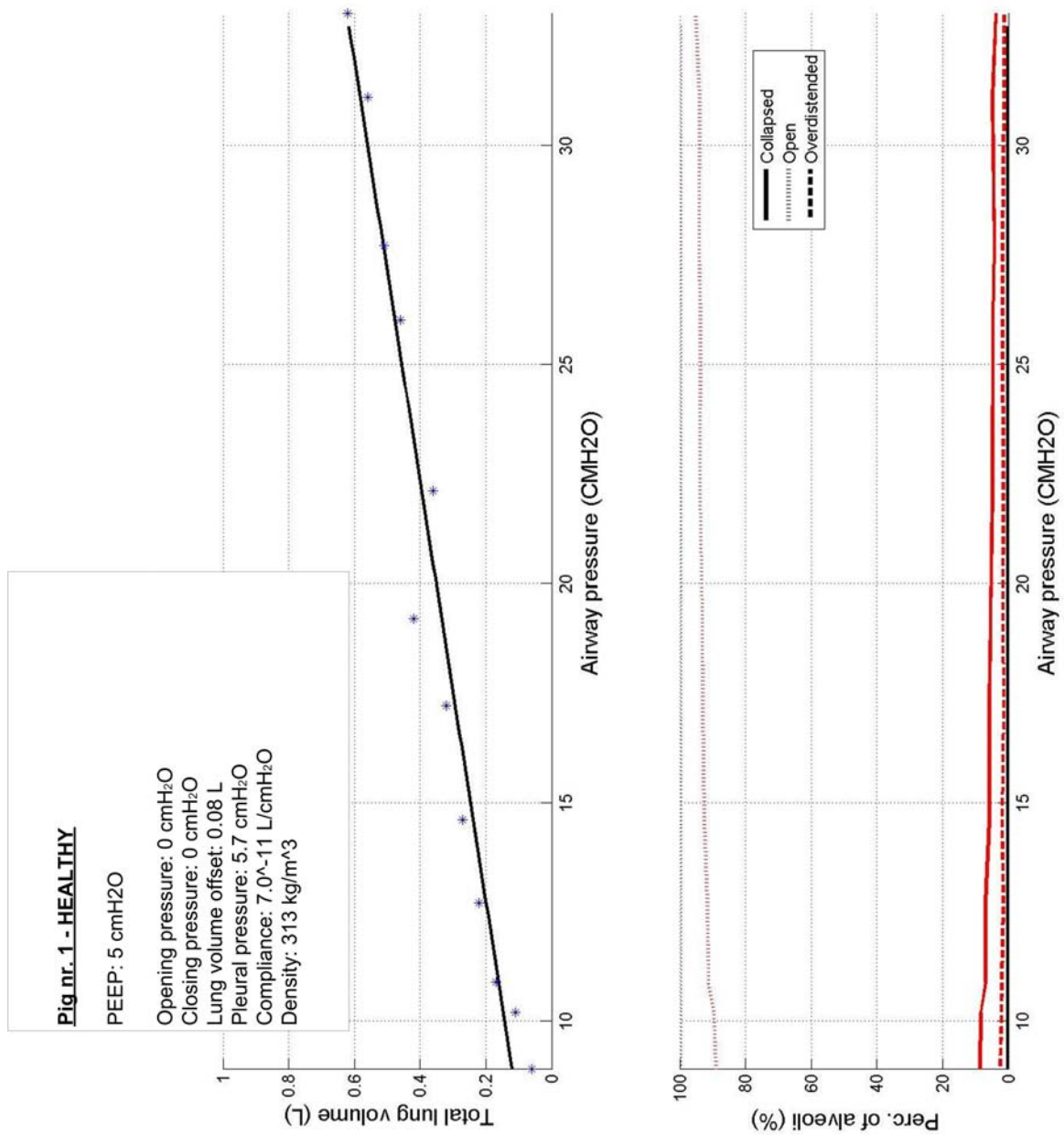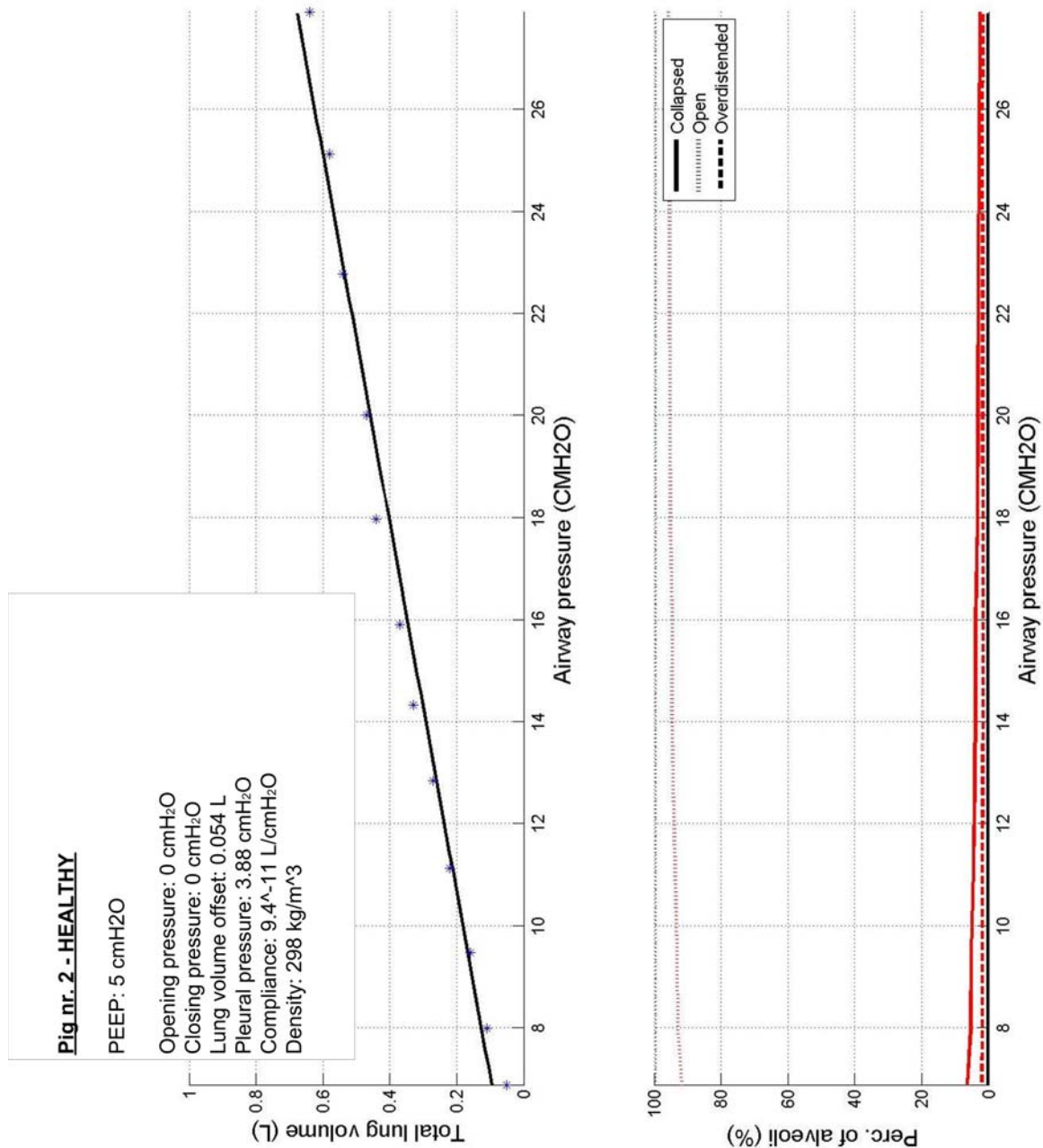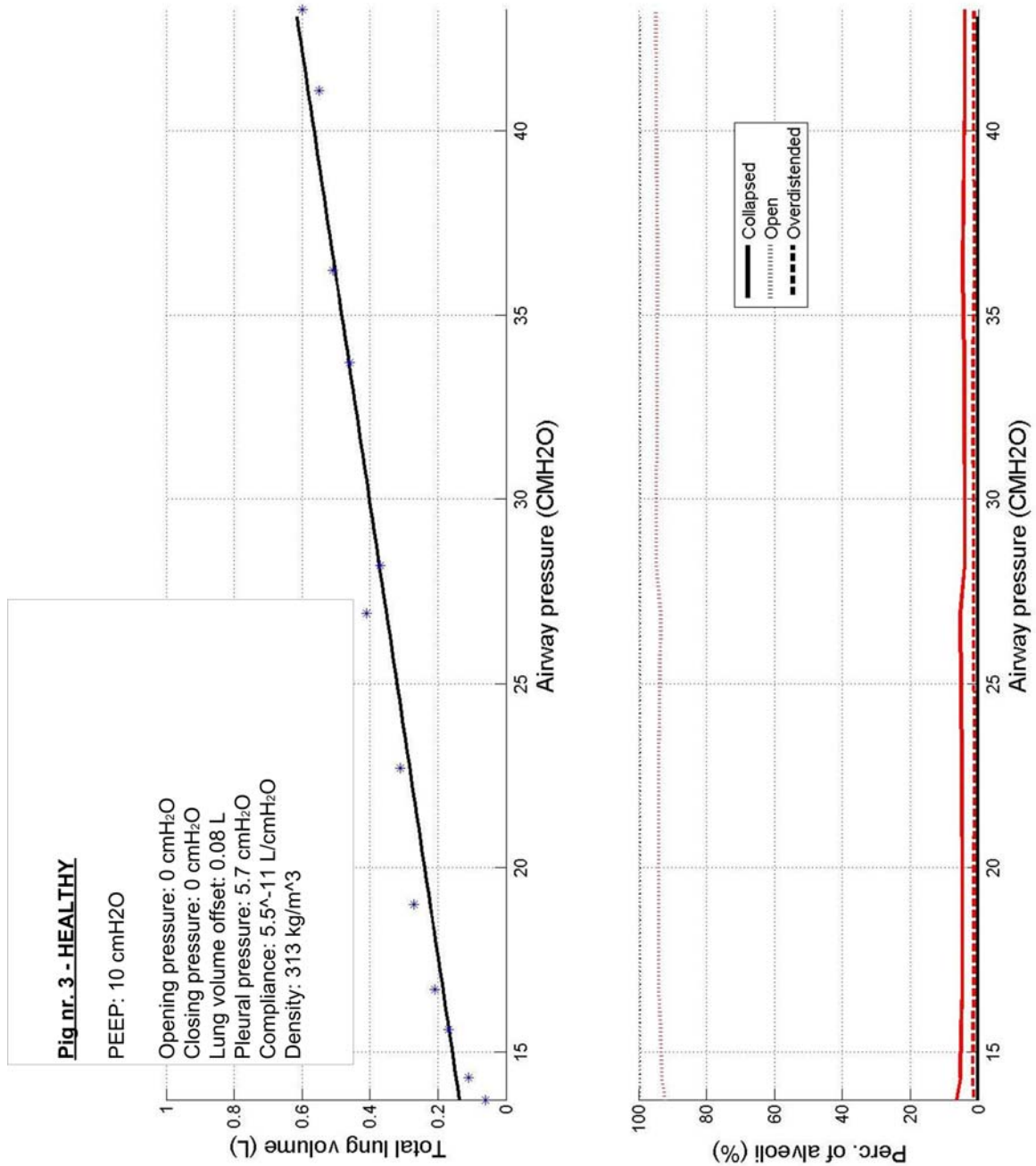
Figure B.1: *The figure illustrates the simulation of the alveolar states and the extraction of the alveolar states from pig number 1. The first subfigure illustrates the best fit of the model and the static PV data. the second subfigure illustrates the simulated alveolar states (black lines) and the extracted alveolar states from the CT scans (red lines).*
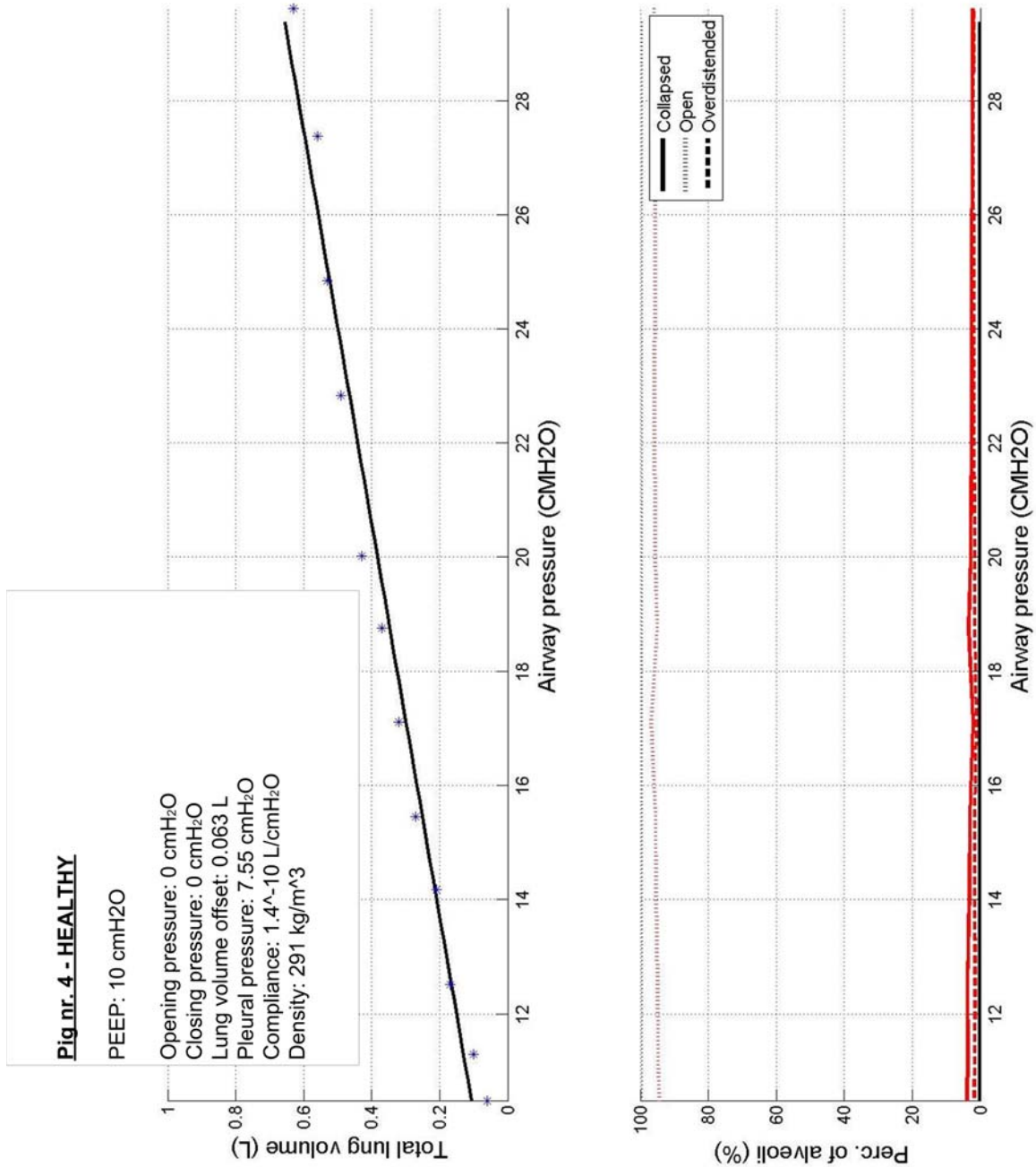
Figure B.2: *The figure illustrates the simulation of the alveolar states and the extraction of the alveolar states from pig number 2. The first subfigure illustrates the best fit of the model and the static PV data. the second subfigure illustrates the simulated alveolar states (black lines) and the extracted alveolar states from the CT scans (red lines).*
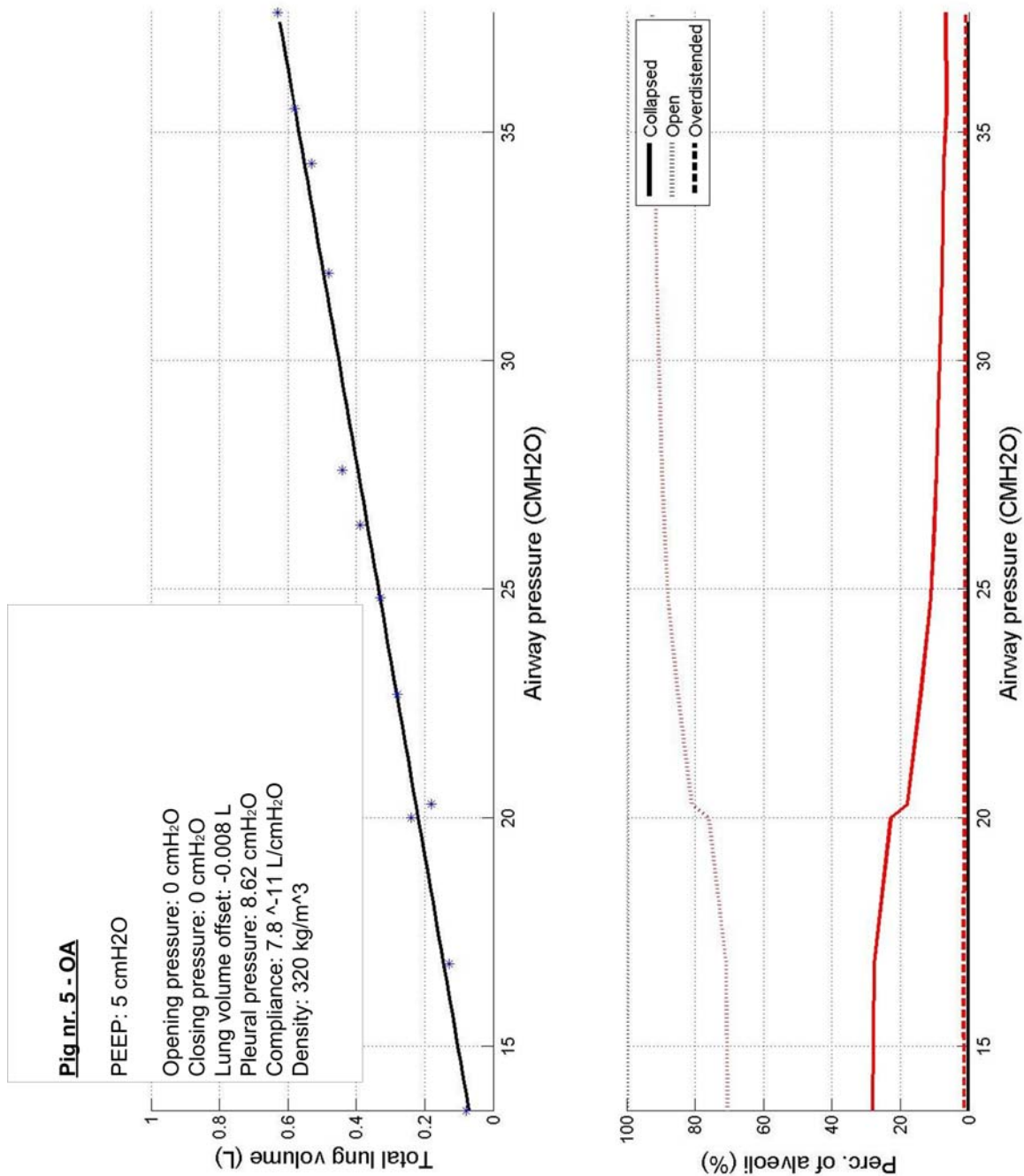
Figure B.3: *The figure illustrates the simulation of the alveolar states and the extraction of the alveolar states from pig number 3. The first subfigure illustrates the best fit of the model and the static PV data. the second subfigure illustrates the simulated alveolar states (black lines) and the extracted alveolar states from the CT scans (red lines).*
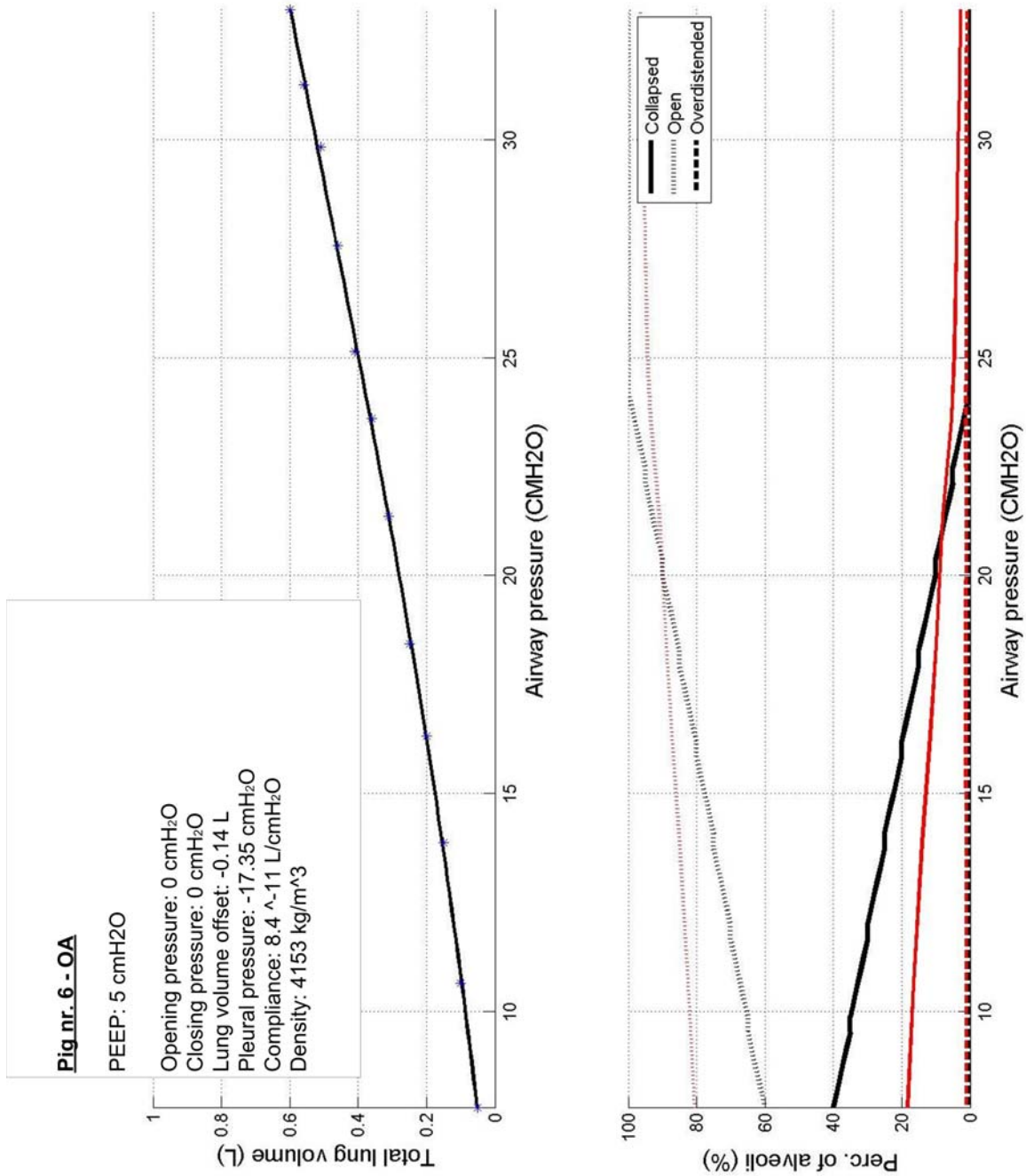
Figure B.4: *The figure illustrates the simulation of the alveolar states and the extraction of the alveolar states from pig number 4. The first subfigure illustrates the best fit of the model and the static PV data. the second subfigure illustrates the simulated alveolar states (black lines) and the extracted alveolar states from the CT scans (red lines).*

Figure B.5: *The figure illustrates the simulation of the alveolar states and the extraction of the alveolar states from pig number 5. The first subfigure illustrates the best fit of the model and the static PV data. the second subfigure illustrates the simulated alveolar states (black lines) and the extracted alveolar states from the CT scans (red lines).*
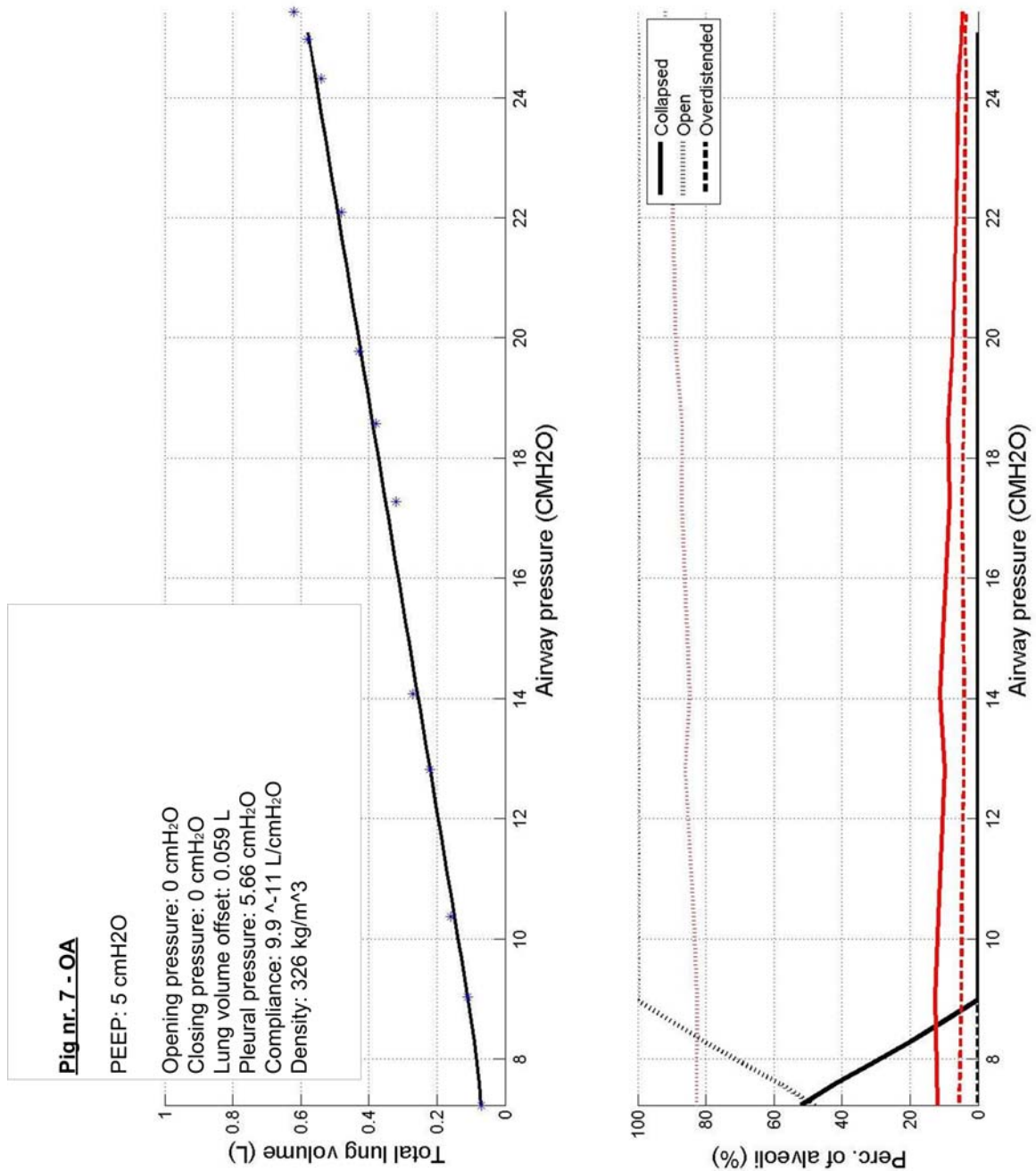
119

Figure B.6: *The figure illustrates the simulation of the alveolar states and the extraction of the alveolar states from pig number 6. The first subfigure illustrates the best fit of the model and the static PV data. the second subfigure illustrates the simulated alveolar states (black lines) and the extracted alveolar states from the CT scans (red lines).*
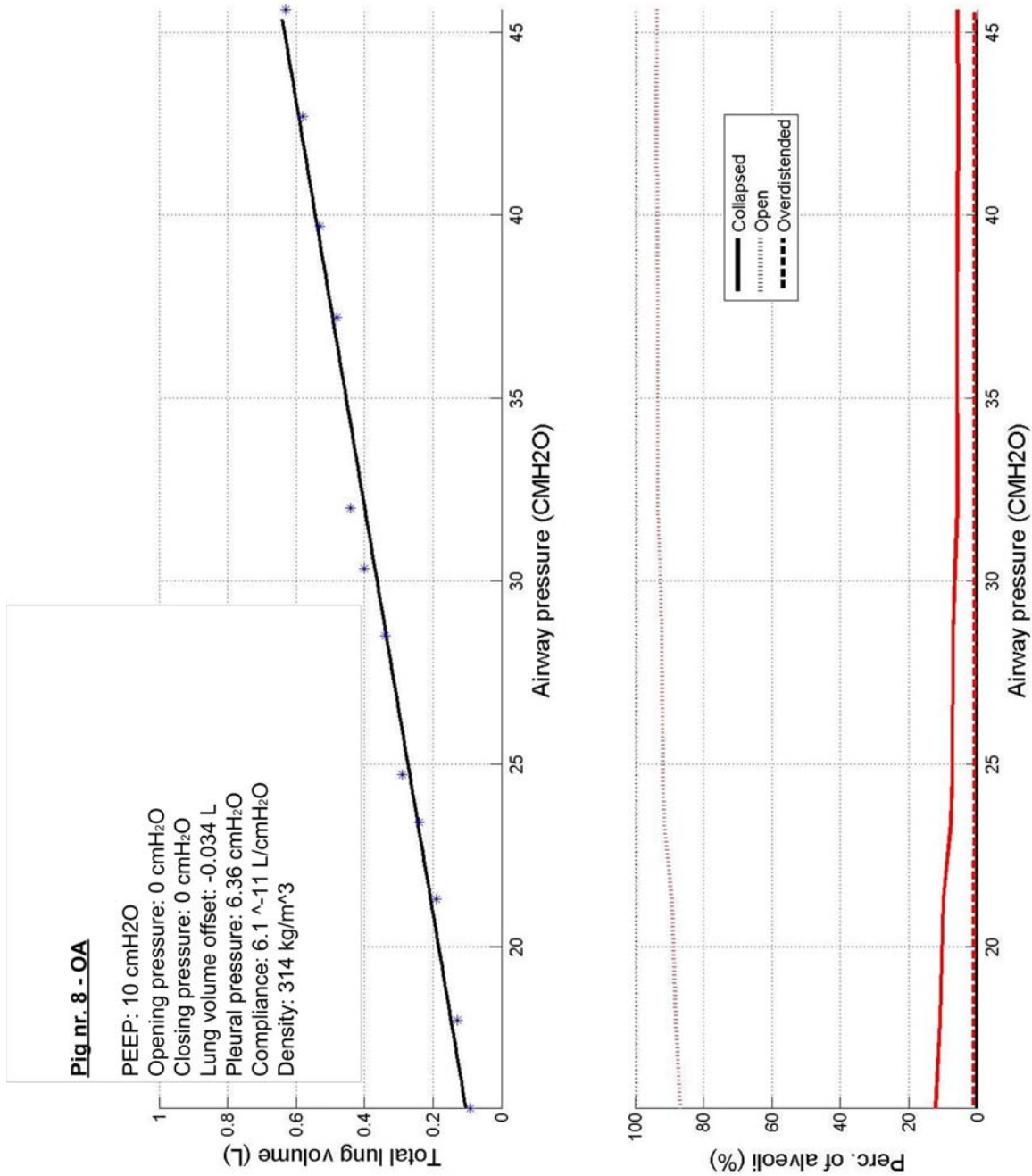
Figure B.7: *The figure illustrates the simulation of the alveolar states and the extraction of the alveolar states from pig number 7. The first subfigure illustrates the best fit of the model and the static PV data. the second subfigure illustrates the simulated alveolar states (black lines) and the extracted alveolar states from the CT scans (red lines).*

Figure B.8: *The figure illustrates the simulation of the alveolar states and the extraction of the alveolar states from pig number 8. The first subfigure illustrates the best fit of the model and the static PV data. the second subfigure illustrates the simulated alveolar states (black lines) and the extracted alveolar states from the CT scans (red lines).*
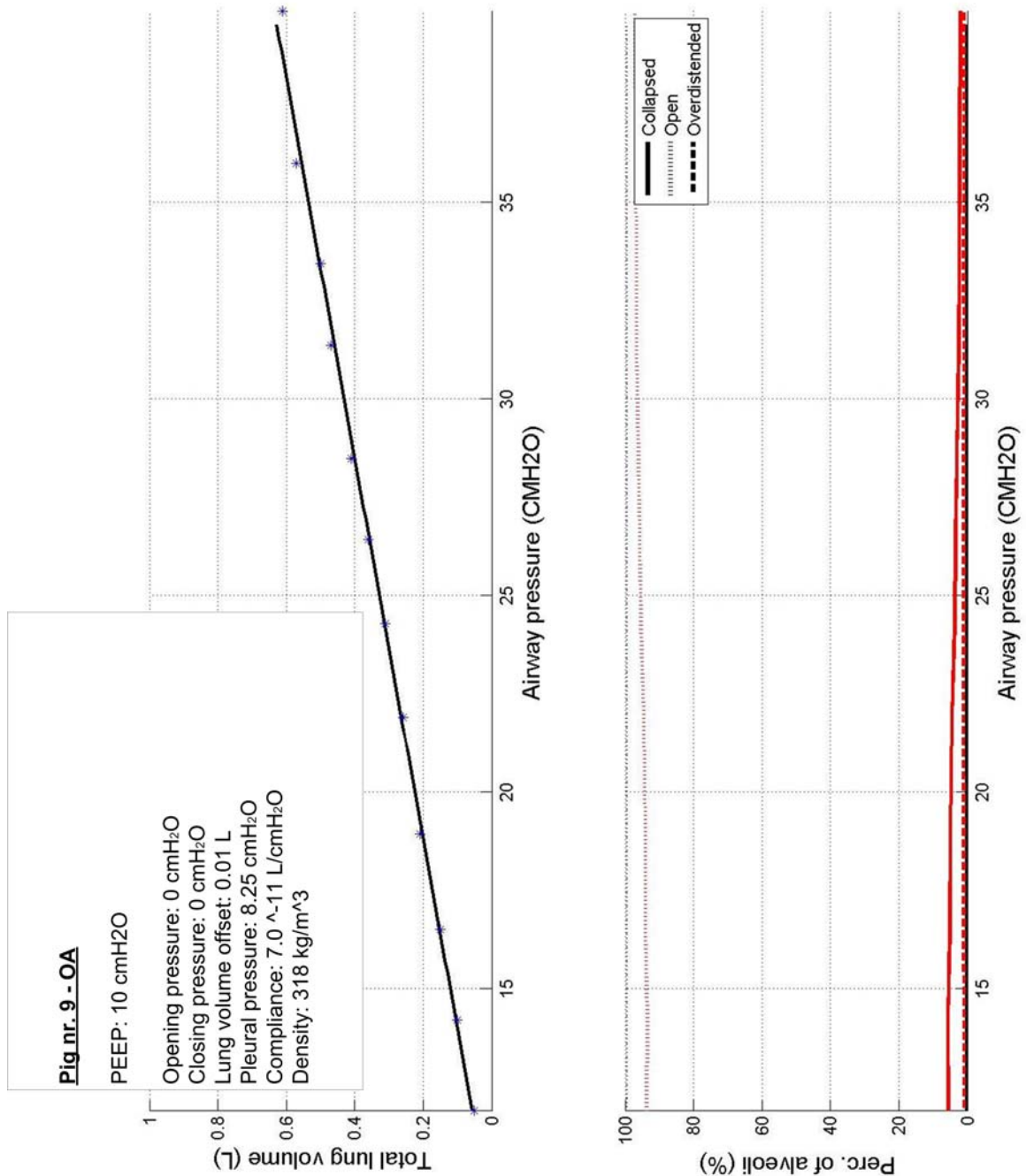
Figure B.9: *The figure illustrates the simulation of the alveolar states and the extraction of the alveolar states from pig number 9. The first subfigure illustrates the best fit of the model and the static PV data. the second subfigure illustrates the simulated alveolar states (black lines) and the extracted alveolar states from the CT scans (red lines).*
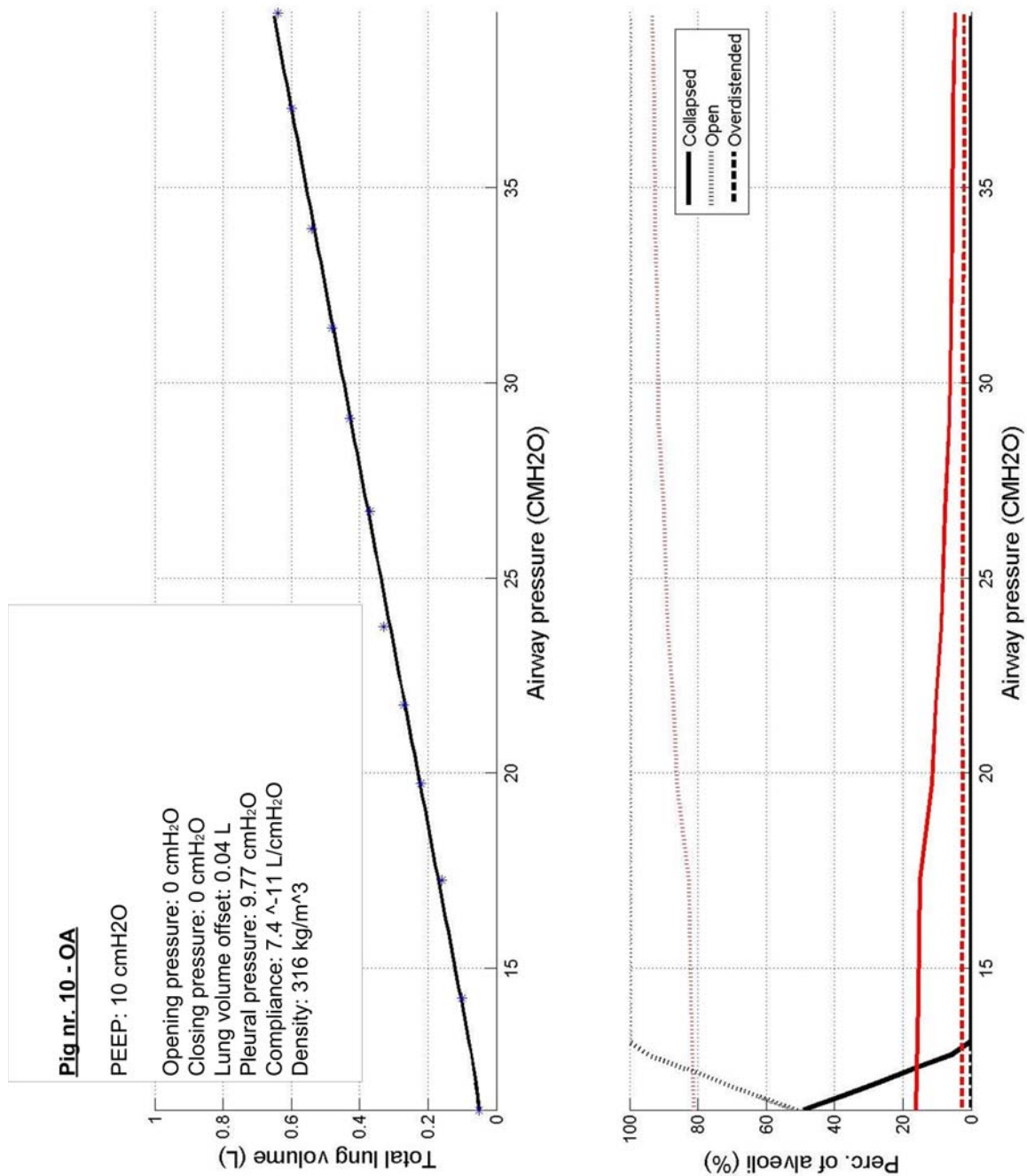
Figure B.10: *The figure illustrates the simulation of the alveolar states and the extraction of the alveolar states from pig number 10. The first subfigure illustrates the best fit of the model and the static PV data. the second subfigure illustrates the simulated alveolar states (black lines) and the extracted alveolar states from the CT scans (red lines).*